UNIVERSITÀ DEGLI STUDI DI PALERMO

Dottorato di Ricerca in Ingegneria Civile, Ambientale, dei Materiali

Indirizzo: Ingegneria delle Strutture

Dipartimento di Ingegneria Civile, Ambientale, Aerospaziale, dei Materiali

Settore Scientifico Disciplinare ICAR 09

Compressive response of concrete columns under service conditions strengthened by confining devices: from the local to the global behavior.

IL DOTTORE

Ing. Marco Filippo Ferrotto

IL COORDINATORE

Chiar.mo Prof. Antonina Pirrotta

TUTOR

Chiar.mo Prof. Ing. Maurizio Papia

Chiar.mo Prof. Ing. Liborio Cavaleri

EXTERNAL ADVISOR

Chiar.mo Prof. Ing. Oliver Fischer

CICLO XXX

ANNO CONSEGUIMENTO TITOLO 2018

ACKNOWLEDGEMENTS

The present thesis represents the conclusion of an important path of my work and of my professional growth. Many people deserve to be thanked for trusting in me and supporting the development of this research in these three years.

I feel like thanking firstly my advisor Prof. Liborio Cavaleri for his excellent guide and teaching without which I could never have accomplished my studies. He has always been available to listen and help me especially in the arduous moments. I would like to thank him also for the possibility he gave me to work with other research groups learning different approaches on the scientific research.

Special thanks to my advisor Prof. Maurizio Papia who gave me the opportunity to work with him that has been a benchmark for all my questions solving all my problems and clarifying doubts and uncertainties.

Acknowledgements are due to my external advisor Prof. Oliver Fischer who allowed me to spend several months at the Technische Universität München, in Germany. His financial support, essential to realize the experimental investigation in the laboratory of structures of his department has been utmost of importance for the development of one of the most important parts of my thesis.

During period spent at the Technische Universität München I was able to learn several innovative approaches to solve complex problems for the definition of experimental test procedures thanks to the precious teaching of Dr. Ing. Roland Niedermeier to which I am very grateful.

I would like to thank all the staff of the Department of Civil, Geo and Environmental Engineering, in particular the nice and willing secretary Anneliese Spitzauer to whom I owe her a lot, Wolfgang, Nichole, Thomas, Bernard and all the others laboratory technicians.

Another special acknowledgement is felt to Prof. Giuseppe Campione that has significantly contributed in the solution of several difficult issues with original advices.

I cannot forget the time I spent with my colleagues, Francesco, Gabriele, Alberto, Giovanni, Fabio, Nino, Salvo, Emma, Jennifer and Alessia with whom I shared a lot of beautiful moments.

Furthermore, I will never thank enough the support of my family that made possible this desired road. Thanks Mom, Dad, my sister Alessandra, Alberto, my brother Marcello and Cristina. To them I dedicate every single page of this thesis.

RINGRAZIAMENTI

Questa tesi rappresenta la fine di un importante percorso di lavoro e di crescita professionale. In questi tre anni tante persone meritano ringraziamenti per aver creduto in me ed avermi supportato nello sviluppo di questa ricerca.

Sento principalmente di dovere ringraziare il mio relatore Prof. Liborio Cavaleri per la sua eccellente guida e i preziosi insegnamenti senza i quali non avrei mai potuto completare i miei studi. Lo ringrazio per essere sempre stato disponibile ad ascoltarmi e aiutarmi specialmente nei momenti più complicati e per avermi dato la possibilità di lavorare anche con altri gruppi di ricerca, imparando diversi approcci per la risoluzione dei problemi scientifici.

Un particolare ringraziamento va al mio relatore Prof. Maurizio Papia per avermi dato la possibilità di lavorare con lui che è sempre stato per me un punto di riferimento e con cui ho potuto sempre confrontarmi per risolvere i problemi, chiarire i dubbi e le incertezze.

Ringrazio doverosamente il mio co-tutor Prof. Oliver Fischer per avermi dato la possibilità di passare diversi mesi in Germania alla Technische Universität München. Grazie al suo indispensabile sostegno economico è stato possibile realizzare nel laboratorio di strutture del Suo dipartimento la sperimentazione che si è rivelata una delle parti più significative della mia tesi.

Durante il periodo passato alla Technische Universität München ho avuto l'opportunità di imparare approcci innovativi per risolvere complessi problemi legati progettazione dei setup di prova grazie ai preziosi insegnamenti del Dr. Ing. Roland Niedermeier a cui sono molto grato.

Voglio inoltre ringraziare tutto lo staff del Dipartimento di Ingegneria Civile, Geotecnica e Ambientale, ed in particolare ringrazio la sempre gentile e disponibile segretaria Anneliese Spitzauer a cui devo molto, Wolfgang, Nichole, Thomas, Bernard e tutti gli altri tecnici del laboratorio.

Un sentito ringraziamento va anche al Prof. Giuseppe Campione per il suo importantissimo contributo nella risoluzione di molti argomenti complessi con consigli sempre originali.

Non dimentico il tempo passato con i miei colleghi Francesco, Gabriele, Alberto, Giovanni, Fabio, Nino, Salvo, Emma, Jennifer e Alessia, con cui ho condiviso tanti bei momenti.

Inoltre, non potrò mai ringraziare abbastanza la mia famiglia e il supporto che mi ha dato, rendendo possibile questo desiderato percorso. Grazie a mia madre, mio padre, Alberto, mia sorella Alessandra, mio fratello Marcello e Cristina. A loro dedico ogni singola pagina di questa tesi.

SUMMARY

Strengthening of existing concrete columns with *Fiber Reinforced Polymers* (FRP) or *Steel Jacketing* results generally in a satisfactory structural member improvement in terms of load and strain capacity. A reliable prediction of the capacity obtained by these reinforcement strategies requests a proper knowledge of the load-strain response of the confined concrete elements. However, so far, the available design methods and technical codes do not consider the effect of the possible presence of service loads at the moment of application of the reinforcement, and therefore, the compressive behavior of the confined concrete under preload is still unclear.

The goal of the present thesis is to identify the efficiency of the confinement action in terms of strength and deformational capacity of concrete columns subjected to different preloading levels and strengthened with FRP or Steel Jacketing. First, an overview of the state of the art is discussed before proposing a strategy research including experimental investigations in both cases of FRP and Steel confined medium scale concrete columns subjected to different preload levels. Then, the formulation of FE models to reproduce the physical process of the confined concrete after reinforcement previously interested by a fixed stress/strain state is defined comparing the numerical results with the experimental data. Further, analytical formulations supporting the prediction of the actual load-bearing capacity are developed on the basis of the experimental-numerical observations.

SOMMARIO

Il rinforzo di colonne in calcestruzzo armato tramite materiali polimerici fibrorinforzati (FRP) o tramite incamiciature in acciaio conferisce agli elementi strutturali degli edifici esistenti un elevato incremento di capacità portante e deformativa grazie alle proprietà dei materiali che svolgono la funzione di confinamento. Conoscere adeguatamente le proprietà meccaniche degli elementi in calcestruzzo confinato risulta di fondamentale importanza nell'ambito di un progetto di sistemi di rinforzo strutturale. Tuttavia, le normative attualmente vigenti non forniscono prescrizioni su come tenere in considerazione la presenza dei carichi di esercizio sugli elementi strutturali al momento dell'applicazione dei dispositivi di confinamento, e quindi il comportamento in compressione del calcestruzzo confinato in condizioni di precarico risulta ancora poco chiaro.

Lo scopo della presente tesi è quello di valutare il comportamento meccanico degli elementi in calcestruzzo soggetti a diversi livelli di precarico e confinati successivamente con FRP o incamiciatura in acciaio. e di investigare come questo stato di precarico influenza la risposta in compressione.

Dall'analisi dello stato dell'arte è stato possibile identificare il punto di partenza per le ricerche effettuate, che hanno previsto diverse indagini sperimentali condotte su colonne in media scala soggette a diversi livelli di precarico e successivamente rinforzate con incamiciatura in acciaio o con FRP. Lo studio ha previsto anche un approccio al problema tramite modellazione agli elementi finiti, indispensabile per la riproduzione del processo fisico, confrontando i risultati numerici con quelli ottenuti dalle sperimentazioni. Inoltre, sono stati proposti modelli analitici per la previsione della capacità, sviluppati sulla base delle osservazioni numerico-sperimentali.

CONTENTS

1. INTRODUCTION

For many years, repair and rehabilitation of existing structures have been a topic of ongoing studies stating the need to repair buildings that suffer damage and to restore, where possible, the load-bearing capacity, or the need to retrofit buildings subjected to variations in geometry or changes in their intended use, in agreement to actual codes.

The buildings that are more generally interested in retrofitting or improvement in bearing and deformational capacity date back to more than twenty/thirty years ago. Therefore, they were conceived in a period when technical codes neglected the importance of seismic actions and made it possible to design for satisfying only the gravitational loads[1].

This design philosophy was dropped when it was realized that in the case of a seismic event such buildings would not had adequate capacity to oppose to horizontal actions, with high probability of failure.

Actual codes assign fundamental importance to seismic actions, providing design criteria that allow to obtain a satisfactory seismic behavior and to express strength and ductility that guarantee the protection of things and persons[2].

[1] In the thirty years between 1974 and 2005, Italian legislation has known five Technical Standards for Construction. These are: Ministerial Decree of 30 May 1974, *Technical standards for the execution of works in normal and prestressed reinforced concrete and for metal structures*; Ministerial Decree of 27 July 1985, *Technical standards for the execution and testing of structures in normal and prestressed reinforced concrete and for metal structures*; Ministerial Decree of 20 November 1987, *Technical standards for the design, construction and testing of masonry buildings and for their consolidation*; Ministerial Decree of 9 January 1996, *Technical standards for the design, construction and testing of masonry buildings*.

[2] Ministerial Decree of 14 January 2008, published in the "Official Gazette", no. 29 of 4 February 2008 - Suppl. Ordinary no. 30. See also the *Circular on "New Technical Standards for Construction"* of February 2,2009 containing the *Instructions for the Application of the "New Technical Standards for Construction"* contained in the Ministerial Decree of January 14,2008, published in the "Official Gazette" no. 47 of February 26,2009 - Suppl. Ordinary No 27. In the latter Directive, it is stressed that "in view of the innovative nature of these standards, it was

Based on the need to work with efficient and rapid structural reinforcement techniques, research has increasingly focused on investigating strategies able to increase the load-bearing and deformational capacity to meet the requirements of the new regulatory codes.

Confinement is one of the most popular techniques proven to be efficient in restoring the original capacity of existing reinforced concrete columns of different kind of structures. Very different techniques are able to improve the structural capacity depending on the nature of the confinement devices and materials. Among the most known confinement techniques, there are "Concrete Jacketing", "Steel Jacketing", "FRP-Jacketing". Each of them is characterized by specific mechanical properties and produces an improvement in ductility and load-bearing capacity strongly depending on the interaction between column and applied confinement device.

Even though the effectiveness in improving the capacity of columns is widely demonstrated with a very large database of experimental works carried out under standardized laboratory prescriptions reproducing monotonic and cyclical behavior, there are several barriers that hindered the widespread use in practice. As reported in a recent review paper provided by Ma et al. (2017), these barriers include the lack of explicit design formulations, the necessity to know the long-term durability and to experiment the full scale behavior up to the collapse.

Generally, depending on the type and methods of application and implementation in situ, reinforcement interventions can give to the existing structures increasing of strength, ductility, stiffness. Localized improvement interventions can also be planned to improve the strength or deformational capacity of certain structural elements that are more vulnerable during a seismic event (Fig. 1.1).

A general guideline is to aim for a uniform distribution of strength and stiffness among members on any given floor in order to minimize the risk of loss of mechanical regularity in plan or in height.

Thus, a good strategy is the selective retrofitting of members that belong to the lateral load-resisting system in order to achieve similar relative drift ratios at yielding.

---

considered appropriate to issue the present explanatory circular which has sought to give priority, with a more widespread approach, to the most innovative and in some ways more complex arguments dealt with by the New Technical Standards".

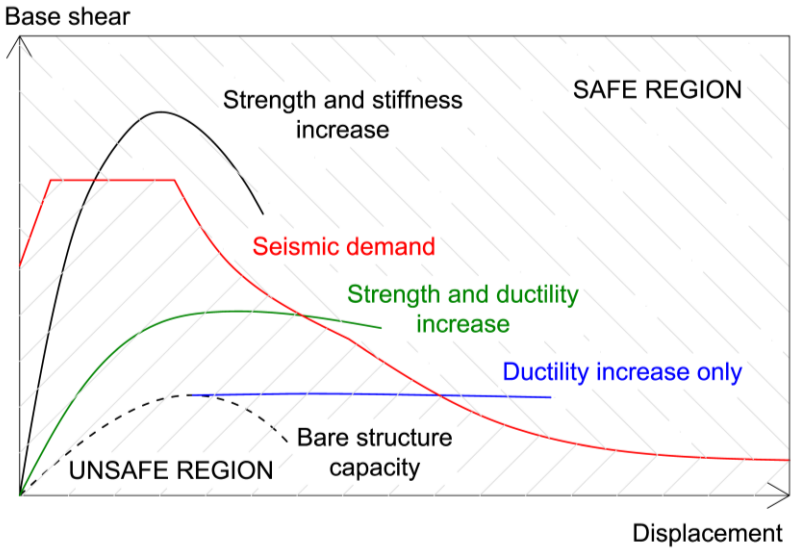

Figure 1.1. Improvement of structural capacity.

Regarding the effects of confinement reinforcement systems on the structural capacity, it is useful to define how the different techniques locally and/or globally modify the response of the reinforced structures. Below, strengthening techniques in object are briefly described highlighting the main aspect when applied on an existing structure.

Concrete Jacketing is a very widespread technique and widely analyzed. By using this confinement technique, load-bearing capacity of columns is improved because of an increasing of the original section too: a certain amount of longitudinal and transversal steel reinforcement is applied that provide also ductility increase (Ersoy et al., 1993, Takeuti et al., 2008, Minafò, 2015).

This intervention can modify the stiffness of a column and certainly modifies its mass, therefore it is necessary to foresee a careful design and control the eventual evolution of the structure fundamental period if it changes in a non-negligible way[3].

The confinement technique by the combined system of steel angles and battens, commonly known as Steel Jacketing provides considerable improvements in terms of both load-bearing and ductility, exploiting the

[3] It is worth noting that a modification of the reference period changes the seismic pseudo-acceleration and consequently the earthquake effects.

benefits of steel deformability. Depending on how the connections between the reinforced elements are made, substantial changes in the stiffness of the original structure occur, with relatively limited changes in the structural mass.

Strengthening with FRP Jackets is one of the most developed and discussed techniques in recent decades because, although it is able to provide a considerable increase in ductility and prevents premature failure of structural elements not adequately designed, presents several problems related to the global behavior of the structure. In fact, to achieve an overall improvement, confinement of columns only is insufficient but particular attention must be paid to the joints of the brittle elements (e. g. beam-column nodes).

Flexural capacity can be improved by the application of fibers in the direction of a member, while it is possible to increase also shear strength by applying fibers in the transverse direction.

An important contribute about seismic retrofitting strategies of existing structures by means of FRP is reported in a recent paper by Pantazopoulou et al. (2016). The paper deals with a background of the European seismic design provisions for retrofitting RC[4] elements using FRP materials.

In any of the above cases it is no possible to find a guidance that suggests how to take into account the possible presence of stress in the structural elements at the time of application of reinforcement/confinement systems, and how this can subsequently change the local and global behavior. The analytical formulations for the design of reinforcement systems do not include a possible state of stress and strain previously existing. More specifically, design formulations used for the confinement capacity project are based on experimental and/or numerical observations that involve elements not interested by a state of stress and strain before reinforcement. The consequence is that, when these formulations are used for the assessment of buildings, it is not possible to consider whether the elements are already in a stress/strain state able to change the effectiveness of the reinforcement.

Fig. 1.2 shows a typical scenario with three columns of a structural system, which need to be reinforced. In the example, due to service conditions, the columns are affected by a critical stress state (close to

[4] The term RC refers to “Reinforced Concrete”.

achieving the compressive strength of the concrete). In the central column, the reinforcement is applied after the column discharge by means of hydraulic jacks. In the right column, instead, the application of the reinforcement is carried out without unloading it, and therefore, at the moment of reinforcement, the concrete is affected by a certain state of compressive stress and strain. It seems to be easy to understand that the capacity of the reinforced members in the two different configurations may not be the same.

Although it is quite simple to state that the structural response may not be the same, it is not so easy to predict how this might change. The issue is very much discussed but at the moment a common point of view is not reached. The point is that many variables play a fundamental rule. The response may depend on the state of preservation of the concrete and on the mechanical capacity that it possesses at the time of the reinforcement, or it may depend on the type of reinforcement, also it may depend on the existing load level and therefore on a more or less accentuated level of existing damage.

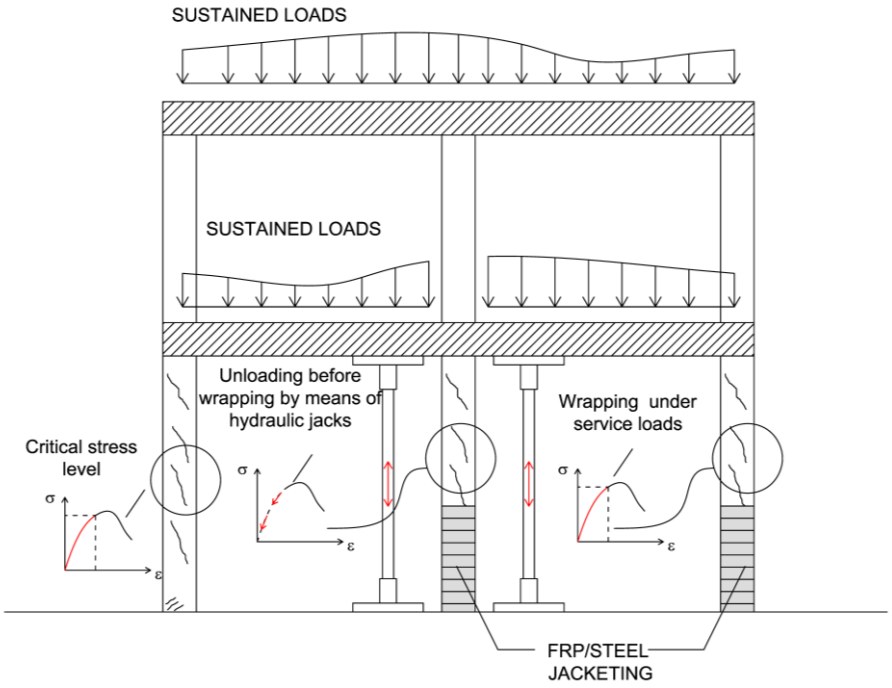

Figure 1.2. Typical scenarios for unreinforced and reinforced columns.

A preliminary physical approach can be schematized starting from the constitutive behavior of the plain concrete subjected to compressive loads. In a general load condition, a concrete column can be interested by a certain stress/strain level, varying from 0 and the compressive strength of the concrete f_{c0}. In this way, a preloading level index, equal to the ratio between the compressive stress acting on the material and its compressive strength, can be defined as follow:

$$n_P = \frac{P}{P_{\max}} = \frac{\sigma(\varepsilon)}{f_{c0}} \qquad \text{for } 0 \le n_P \le 1 \tag{1.1}$$

A given value of axial stress generates a certain level of axial and consequently lateral strain (due to the Poisson effects) and therefore, at the moment in which the confinement is applied and the column is subjected to an increasing in axial load, the behavior of the plain concrete changes in "confined concrete". Compared with the case without preload (with

confinement action starting from stress/strain zero conditions), in this case a "delayed" response of the confinement device will be obviously observed.

As the lateral confinement pressure is activated when the reinforcement is applied, there are potentially lower values compared to the cases of members not characterized by a pre-existing load. The unknown aspect lies in assessing how this "delay" influences the compression curve of the confined concrete in terms of strength and strain.

Different scenarios can be identified depending on the type of confinement device, or whether the confinement is elasto-plastic (case of steel caging) or elastic (case of FRP jackets).

Fig. 1.3 shows a qualitative scheme describing the initial hypothesis, which the numerical formulations will be subsequently developed on. The curves represented, both for the axial behavior and for the lateral confinement pressure, are designed in such a way that, given a pre-established load level (σ_{0p}, ε_{0p}), a possible behavior of the compression response is represented.

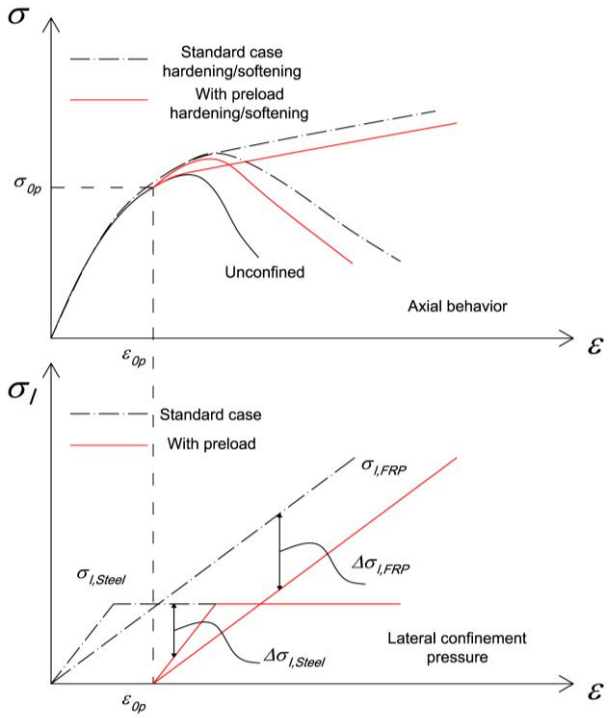

Figure 1.3. Initial assumption of the mechanical behavior of the confined concrete in presence of pre-existing load compared to the "standard" cases.

The issues above introduced will be accurately treated hereafter. In details, Chapter 2 contains an overview of the most relevant studies focusing - in accordance with the objectives of the thesis - steel jacketing and FRP wrapping. Firstly, the technological aspects of the two reinforcement strategies are described. Secondly, a comprehensive comparative study of the available analytical models is presented to evaluate the reliability in reproducing experimental results. Finally, an in-depth analysis of the state of the art regarding the capacity evaluation of the compressive behavior of confined concrete in presence of preload is discussed, highlighting the poorness in scientific sources, making also a critical analysis of the findings obtained until now. Further, an experimental investigation on RC columns strengthened with steel cages subjected to axial load and combined axial load and axial bending, for which the behavior concerning the effect on the increase of the load-bearing and deformation capacity was analyzed

according to some aspects that often radically characterize the structural behavior and that are not currently well managed by the current regulatory guidance.

In Chapter 3, the thesis analyzes in detail the main objective, that is the analysis of the effects of the confinement of columns subjected to an assigned stress-strain state. It is provided an analysis of the state of the art of numerical modeling techniques of concrete columns confined with FRP or steel jacketing carried out using the Simulia Abaqus software (in this regard, a generic overview of the theoretical aspects concerning the finite element modeling of concrete and its non-linearity is briefly discussed), highlighting the difficulties in implementing an accurate model when the aspects related to confinement are introduced within the plasticity theory. A numerical approach is then proposed for the reproduction of the compression response of circular columns confined with FRP in a monotonic compression regime. Once the proposed model has been validated on the basis of experimental data available in the literature, the new concepts of advanced modeling technique that can reproduce numerically the compression response of columns reinforced when subjected a pre-existing stress-strain state have been introduced.

The theoretical numerical approach is subsequently validated in Chapter 4 on the basis of an experimental campaign carried out with the cooperation of the Technical University of Munich (DE) on circular plain concrete columns confined with FRP sheets when subjected to different levels of short-term preloading. The experimentation consisted in a first phase of evaluating the behavior in compression under standardized conditions, without applying any load to the columns before wrapping. Subsequently a stress state was induced as a rate of the unconfined compressive strength of the concrete before wrapping. The designed preload levels were low, medium and high. The implementation of these tests required particular effort in the definition of the test setup, involving innovative procedures for the experimental reproduction of the desired phenomenon. The experimental results were then numerically reproduced with the Abaqus software through the numerical procedure described in Chapter 3, obtaining a coherent response with what was observed experimentally. Furthermore, an analytical model is also proposed for the reproduction of the compression response of columns, previously loaded, confined by FRP, exploiting the general

purposes of analysis-oriented modeling technique and introducing the hybrid mechanical behavior of the concrete.

Finally, in Chapter 5, an experimental campaign carried out on preloaded square concrete columns confined with steel jacketing is presented. The latter differs from the former described in Chapter 4 for the methods of applying the preload and application of the reinforcement system. A strengthening intervention in pre-existing stress state was simulated. Also in this case, different stress levels and in particular low, medium and high were provided. At the end of the chapter a simplified analytical model was proposed based on the same basics proposed in Chapter 4.

2. RC COLUMNS EXTERNALLY REINFORCED BY CONFINING DEVICES: ASSESSMENT OF STRUCTURAL BEHAVIOR

2.1 Confinement with FRP: overview

Mechanical properties of the concrete subjected to elastic confining pressure such as that provided by FRP sheets depend on the failure conditions of the composite jackets that result not always easy to predict accurately. Theoretical and empirical approaches yield substantially to determine the stress-strain behavior up to the failure so that the strength and deformational capacity of the confined concrete can be evaluated depending on of the mechanical properties of the concrete and the type of reinforcement.

A key aspect is the evaluation of the lateral confinement pressure f_l provided by FRP sheets, generally expressed by the forces equilibrium of the concrete core subjected to axial (and consequently lateral) expansion and the reaction of the composite confining device (Fig. 2.1), namely:

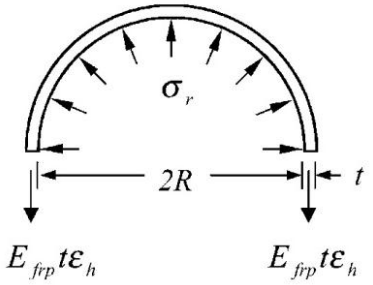

Figure 2.1. Confinement action on circular concrete section. (Lam and Teng, 2003).

$$f_l = \frac{E_{frp} \cdot \varepsilon_h \cdot t}{R} \tag{2.1}$$

In Eq. 2.1 E_{frp} and t are the elastic modulus and the thickness of the confining device respectively, ε_h is the radial strain and R is the radius of the circumference. Failure of the column is due to the to rupture of the fibers subjected to tensile stresses in the circumferential direction.

The compressive strength and the corresponding strain of the confined concrete are affected by the lateral confinement pressure evaluated by Eq. 2.1 as below explained.

The generic form of the expressions that characterize the failure criterion is:

$$\frac{f_{cc}}{f_{c0}} = c_1 + k_1 \frac{f_l}{f_{c0}} \tag{2.2}$$

$$\frac{\varepsilon_{cc}}{\varepsilon_{c0}} = c_2 + k_2 \frac{f_l}{f_{c0}} \tag{2.3}$$

in which c_1, c_2, k_1 and k_2 are calibration parameters, f_{cc} and ε_{cc} are the compressive strength and the corresponding strain of the confined concrete respectively. The term f_l/f_{c0} appearing in both Eqs. 2.2 and 2.3 represents the mechanical confinement ratio that identifies the confinement level provided by the confining devices as a function of the ratio lateral pressure/ unconfined concrete strength.

2.1.1 Compressive behavior of FRP-confined concrete

It should be noted that the first studies on this subject, carried out between 1996 and 2002, mainly concern experimental campaigns. Among the most important scientific contributions there are those of Karbhari and Gao (1997), Mirmiran et al. (1998), Mirmiran et al. (2000), Rochette and Labossiere (2000), Xiao and Wu (2000), Kshirsagar et al. (2000), Zhang et al. (2000), Shahawy et al. (2000), Pessiki et al. (2001), Campione et al. (2001), Toutanji and Deng (2001), Rousakis and Tepfers (2001), Santarosa et al. (2001), Aire et al. (2001), Shehata et al. (2002), Ilki et al. (2002), Harries and Kharel (2002), Karabinis and Rousakis (2002).

On the basis of the first experimental studies, analytical formulations that analyze the compressive behavior of specimens with circular cross-section, wrapped with Carbon Fiber Reinforced Polymer (CFRP) or Glass Fiber Reinforced Polymer (GFRP) subjected to monotonic loads were proposed by Karbhari and Gao (1997), Harmon et al. (1998), Spoelstra and Monti (1999), Thériault and Neale (2000), Xiao and Wu (2000), Fam and Rizkalla (2001),

Campione et al. (2001), Toutanji and Deng (2001), Shehata et al. (2002), Chun and Park (2002), Ilki et al. (2002), Harries and Kharel (2002), Lam and Teng (2002), Moran and Pantelides (2002), De Lorenzis and Tepfers (2003).

Between 2001 and 2002, the first relevant experimental investigations concerned square and rectangular section columns; among the most important studies there are those of Yang et al. (2001), Cole and Belarbi (2001), Wang and Restrepo (2001), Parvin and Wang (2001), Pessiki et al. (2001), Campione et al. (2001), Tan (2002), Tsai and Lin (2002), Feng et al. (2002), Shehata et al. (2002). Analytical formulations were developed including the effects of concrete strength, internal reinforcement, fiber thickness, cross-section dimensions and corner radius on the axial compression behavior (Wang and Retrepo, 2001, Tan 2002, Shehata et al., 2002).

In 2002, ACI 440.2R-02 issued by ACI 440 Committee, provided guidelines for the design, implementation and inspection of FRP reinforcement systems for reinforced structures based on knowledge gained from field research and applications.

Between 2003 and 2004, an intensification of experimental and analytical studies on this subject was noted, although the investigations under cyclic axial loads were still limited (Rousakis and Tepfers, 2001, Rousakis et al., 2003). The guidelines proposed by the CNR in 2004 within the Italian legislative framework, resulted in an information document on the design and implementation of FRP reinforcement systems for existing structures.

Finite element numerical modeling - the peculiarities and application advantages of these methods will be shown in detail later on - for structural components externally wrapped with composite materials had a limited development until 2007 (Mirmiran et al., 2000, Shahawy et al., 2000, Parvin and Wang, 2001, Feng et al., 2002, Shrive et al., 2003, Montoya et al., 2004, Malvar et al., 2004, Rousakis et al., 2007).

Important reviews of the main results of experimental tests carried out between 1994 and 2007 on prismatic RC columns externally confined with FRP under axial compression were provided by Hassan and Chaalal (2007) and Rocca et al. (2008).

Starting from 2008, important contributions to the development of advanced modeling strategies are due to Chakrabarti et al. (2008), Monti and Nisticò (2008), Koksal et al. (2009), Issa et al. (2009), Wu et al. (2009), Yu et al. (2010a,b), Xiao et al. (2010), Csuka e Kollár (2012), Al-Salloum et al.

(2012), Jiang and Wu (2012), Song et al. (2013), Nisticò (2014), Gambarelli et al. (2014), Hany et al. (2016), Pan et al. (2017). In addition, the first major researches on the influence of high strength concrete (HSC) on the confinement mechanism were published (e.g. Ozbakkaloglu and Lim, 2016).

The chronological research development shows clearly the approach to the problem, first more devoted to experimental research, especially to circular cross-sections rather than square or rectangular (Fig. 2.2), then oriented to analytical and numerical developments (Fig. 2.3).

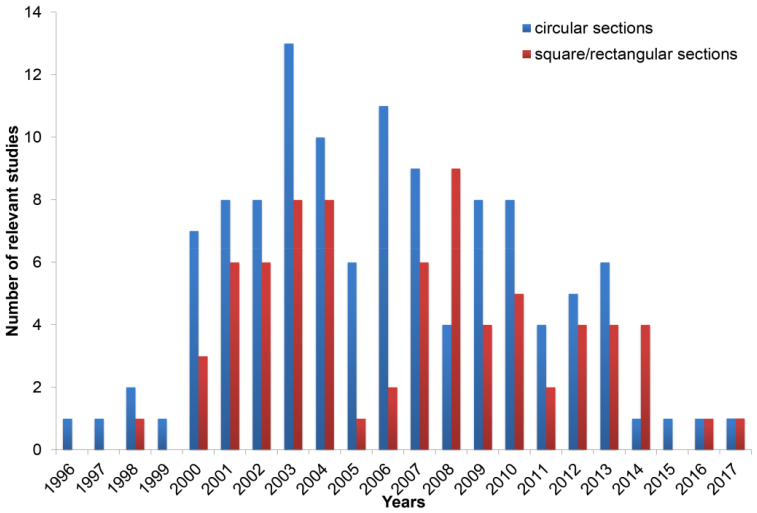

Figure 2.2. Number of relevant studies on circular, square and rectangular FRP-confined concrete.

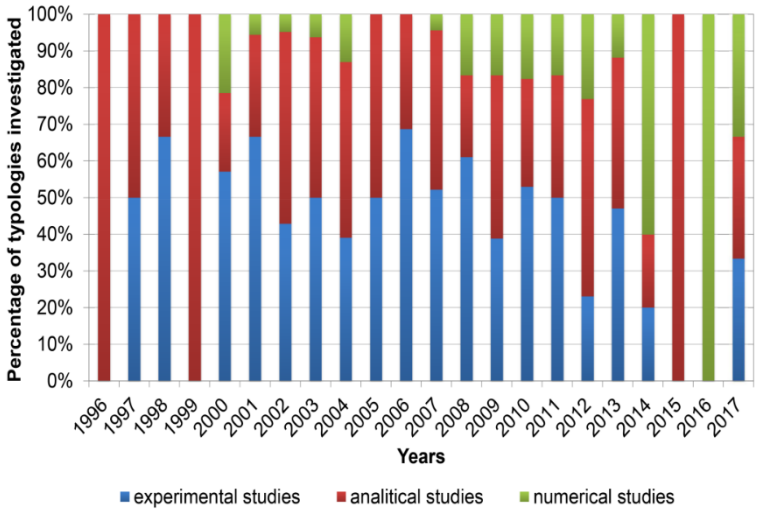

Figure 2.3. Type of studies carried out for FRP-confined concrete.

Based on the above references, in the following the most relevant studies are considered to perform a comparative analysis of the reliability in reproducing experimental results. A brief description of each model is presented according to the different assumption of the authors.

In general, these models are classified into two categories, that are design-oriented models in closed-form expressions and analysis-oriented models in which the stress–strain curve is generated via an incremental process.

Analysis-oriented models

From an in-depth analysis of the state of the art developed by Ozbakkaloglu et al. (2013) the most commonly equation used for the peak strength f_{cc} is provided by Mander et al. (1988). It is an expression based on the general formulation of William and Warnke (1975) and calibrated on the results of the experimental tests carried out by Elwi and Murray (1979) on specimens subjected to constant lateral pressure.

The equation defines the failure surface for concrete under tri-axial compression state and constitutes the failure criterion adopted in the analysis-oriented model developed by Spoelstra and Monti (1999).

In addition, an expression frequently adopted to evaluate the strain at peak stress of the confined concrete (Eq. 2.3) is given by Richart et al. (1928) and is used also by Spoelstra and Monti (1999) and by Binici (2005).

Binici (2005) proposed the recalibration of the Leon-Pramono (LPC) failure criterion, which combines the Mohr-Coulomb friction law and the Rankine criterion with a tension cut-off condition, whereby the strength of the confined concrete was expressed as a nonlinear function of the unconfined concrete compressive strength and the mechanical confinement ratio.

Albanesi et al. (2007) proposed two simplified equations to express the failure criterion for both strength and ultimate strain of the confined concrete. Both expressions linearly depend on the lateral pressure developed under compression according to Eqs. 2.2 -2.3.

Teng et al. (2007) used the results of the experimental tests carried out by Lam and Teng (2006) on cylindrical specimens confined with CFRP tested under axial compression to recalibrate the formula originally proposed by Richart et al. (1929). The value of the effectiveness confinement factor, originally obtained on the basis of experimental tests carried out on specimens subjected to active confinement pressure, was modified by the authors in order to obtain a better agreement with passive confinement mechanisms.

Xiao et al. (2010) carried out an experimental study on high strength concretes (HSC) externally wrapped with FRP in order to analyze their mechanical behavior and to reproduce it through an analysis-oriented model applicable also in the case of normal strength concrete (NSC). The authors proposed two unified equations for the calculation of the peak stress and the ultimate strain by means of nonlinear regression analysis of the experimental results by their own and by Jiang and Teng (2007) for NSC confined specimens.

Design-oriented models

Ciupala et al. (2007) developed a design-oriented model to characterize the compression behavior of columns passively confined with CFRP and GFRP, within which they defined a nonlinear failure criterion for the evaluation of ultimate stress and strain.

On the basis of an extensive experimental campaign carried out on specimens having cross sections with a curvature radius ranging from 0 to 1

(from perfect square cross-sections to equivalent circular sections) Wu and Wang (2009) defined a unified model for arbitrary shaped cross-sections validating the proposed model also with others experimental data available in the literature.

Another FRP-confined concrete model was developed by Wu et al. (2009) from an experimental investigation on HSC circular specimens confined with AFRP sheets[5]. The authors provide a linear failure criterion varying as a function of the mechanical confinement ratio according to previous authors.

Benzaid et al. (2010) carried out an experimental campaign on concrete cylinders with and without internal reinforcement and externally wrapped with FRP subjected to compression loads focusing on the real lateral strain of concrete at failure conditions and the corresponding effective maximum lateral confinement pressure. Finally, they proposed a failure criterion linearly depending on the mechanical confinement ratio.

Realfonzo and Napoli (2011), based on a large database of experimental results available in the literature, performed a statistical evaluation of the efficiency factor for the evaluation of the lateral strain of the confined concrete and proposed a new equation for the estimation of the strength and deformational capacity for cylindrical and prismatic columns.

Finally, Song et al. (2013) provided an experimental, numerical and analytical study for confined specimens subjected to centered and eccentric loads. They provided a linear relationship for the evaluation of the strength of the confined concrete, while logarithmic function was used to obtain the peak strain of the confined concrete as a function of the mechanical confinement ratio.

The expressions used by the above discussed analysis-oriented and design-oriented models for the determination of the confined concrete strength and the corresponding strain for a given lateral confinement pressure ratio are reported in Table 2.1.

A large set of experimental data of circular columns confined with FRP sheets was collected varying the mechanical confinement ratio f_l/f_{co} experimentally obtained from the most relevant studies available in the literature. Tables 2.2 and 2.3 show the results of the experimental-analytical

[5] AFRP refers to *Aramid Fiber Reinforced Polymer*.

comparisons, expressed in terms of compressive strength and corresponding strain for assigned values of f_l/f_{co}.

Comparisons show a large scatter in predicting the failure conditions of FRP-confined concrete, especially respect to the strain capacity. More reliable prediction is provided by design-oriented models.

Figure 2.4 shows that the design-oriented models seem to give a better reproduction of the strength capacity of the confined concrete compared to the results obtained from the analysis-oriented models. It can be noted that in the case of analysis-oriented models, an overestimation of the capacity is often obtained (the experimental data are often below the values obtained by the development of the failure criteria). A similar conclusion can be reached by the comparisons of the strains. Although, referring to the strains, the results show significant scatter, the design oriented models seem to be more reliable in predicting the strain capacity. Nevertheless, it is very important to underline that in terms of constitutive stress-strain relationships the design-oriented models are often too simplified as they are characterized by parabolic-linear hardening or softening curves with the second branch characterized by a certain secant stiffness, and this linearity in the second branch does not exactly reflect the behavior observed experimentally. On the other hand, the analysis-oriented models that allow the evaluation of the "step-by-step" response are more accurate in the representation of the stress-strain behavior of the confined concrete and its nonlinearity.

Table 2.1. Failure criteria of analysis-oriented and design-oriented models.

Models	Ultimate condition expressions	
	Strength	Strain
ANALYSIS ORIENTED		
(1) Spoelstra and Monti (1998)	$\frac{f_{cc}}{f_{c0}} = 2.254\sqrt{1+7.94\frac{f_l}{f_{c0}}} - 2\frac{f_l}{f_{c0}} - 1.254$	$\frac{\varepsilon_{cc}}{\varepsilon_{c0}} = 1+5\left(\frac{f_{cc}}{f_{c0}}-1\right)$
(2) Binici (2005)	$\frac{f_{cc}}{f_{c0}} = \sqrt{1+9.9\frac{f_l}{f_{c0}}} + \frac{f_l}{f_{c0}}$	$\frac{\varepsilon_{cc}}{\varepsilon_{c0}} = 1+5\left(\frac{f_{cc}}{f_{c0}}-1\right)$
(3) Albanesi et al. (2007)	$\frac{f_{cc}}{f_{c0}} = 1+3.609\frac{f_l}{f_{c0}}$	$\frac{\varepsilon_{cc}}{\varepsilon_{c0}} = 1+18.045\frac{f_l}{f_{c0}}$
(4) Teng et al. (2007)	$\frac{f_{cc}}{f_{c0}} = 1+3.5\frac{f_l}{f_{c0}}$	$\frac{\varepsilon_{cc}}{\varepsilon_{c0}} = 1+17.5\frac{f_l}{f_{c0}}$
(5) Xiao et al. (2010)	$\frac{f_{cc}}{f_{c0}} = 1+3.24\left(\frac{f_l}{f_{c0}}\right)^{0.8}$	$\frac{\varepsilon_{cc}}{\varepsilon_{c0}} = 1+17.4\left(\frac{f_l}{f_{c0}}\right)^{1.06}$
DESIGN ORIENTED		
(6) Ciupala et al. (2007)	$\frac{f_{cc}}{f_{c0}} = 1+1.7\cdot 2\left(\frac{f_l}{f_{c0}}\right)^{0.8}$	$\frac{\varepsilon_{cc}}{\varepsilon_{c0}} = 1+6.67\left(\frac{f_{cc}}{f_{c0}}-1\right)^{2/3}$
(7) Wu e Wang (2009)	$\frac{f_{cc}}{f_{c0}} = 1+2.23\left(\frac{f_l}{f_{c0}}\right)^{0.96}$	-
(8) Wu et al. (2009)	$\frac{f_{cc}}{f_{c0}} = 1+3.2\frac{f_l}{f_{c0}}$	$\frac{\varepsilon_{cc}}{\varepsilon_{c0}} = 1+9.5\frac{f_l}{f_{c0}}$
(9) Benzaid et al. (2010)	$\frac{f_{cc}}{f_{c0}} = 1+2.2\frac{f_l}{f_{c0}}$	$\frac{\varepsilon_{cc}}{\varepsilon_{c0}} = 2+7.6\frac{f_l}{f_{c0}}$
(10) Realfonzo and Napoli (2011)	$\frac{f_{cc}}{f_{c0}} = 1+3.57\frac{f_l}{f_{c0}}$	-
(11) Song et al. (2013)	$\frac{f_{cc}}{f_{c0}} = 1+4\frac{f_l}{f_{c0}}$	$\frac{\varepsilon_{cc}}{\varepsilon_{c0}} = 1.65+22.47\cdot\ln\left(\frac{f_l}{f_{c0}}+1\right)$

Table 2.2. Experimental-analytical comparisons. Analysis-oriented models.

MODELS	Experimental		Analytical				
	f_l / f_{c0}	f_{cc} / f_{c0} $\varepsilon_{cc} / \varepsilon_{c0}$	f_{cc} / f_{c0} $\varepsilon_{cc} / \varepsilon_{c0}$				
			(1)	(2)	(3)	(4)	(5)
Valdmanis (2007)	0.0584	0.9326 1.2000	1.3560 2.7801	1.3145 2.7801	1.2107 2.0533	1.2043 2.0215	1.3338 1.8565
Valdmanis (2007)	0.1225	1.3145 3.7059	1.6669 4.3347	1.6102 4.3347	1.4422 3.2112	1.4289 3.1444	1.6042 2.8798
Lam e Teng (2004)	0.1228	1.3972 5.0000	1.6682 4.3412	1.6115 4.3412	1.4433 3.2166	1.4299 3.1496	1.6053 2.8847
Micelli e Modarelli (2013)	0.1257	1.6572 2.6198	1.6807 4.4036	1.6239 4.4036	1.4537 3.2684	1.4399 3.1999	1.6166 2.9314
Berthet et al. (2005)	0.1391	1.5000 3.75	1.7378 4.6891	1.6811 4.6891	1.5022 3.5110	1.4870 3.4351	1.6688 3.1510
Lam e Teng (2006)	0.1426	1.3869 5.0781	1.7522 4.7612	1.6957 4.7612	1.5147 3.5736	1.4992 3.4959	1.6822 3.2080
Jang e Teng (2007)	0.1543	1.42 7.4074	1.7995 4.9977	1.7440 4.9977	1.5567 3.7837	1.5399 3.6997	1.7264 3.3995
Hany et al. (2011)	0.1661	1.3611 9.0000	1.8462 5.2308	1.7923 5.2308	1.5995 3.9975	1.5814 3.9069	1.7707 3.5952
Berthet et al. (2005)	0.1674	1.6078 6.25	1.8513 5.2563	1.7976 5.2563	1.6042 4.0212	1.5860 3.9299	1.7755 3.6170
Micelli e Modarelli (2013)	0.1749	1.7972 4.3976	1.8799 5.3995	1.8277 5.3995	1.6313 4.1563	1.6122 4.0610	1.8032 3.7412
Valdmanis (2007)	0.1775	1.4799 3.6923	1.8898 5.4493	1.8382 5.4493	1.6408 4.2038	1.6214 4.1071	1.8128 3.7850
Benzaid e Mesbah (2013)	0.2145	1.5177 4.6154	2.0227 6.1136	1.9817 6.1136	1.774 4.8699	1.7506 4.7531	1.9454 4.4024
Pan et al. (2017)	0.2172	1.7477 9.5524	2.0322 6.1609	1.9922 6.1609	1.7839 4.9197	1.7603 4.8014	1.9551 4.4488
He e Jin (2011)	0.2276	1.9096 4.4800	2.0673 6.3364	2.0313 6.3364	1.8214 5.1070	1.7966 4.9830	1.9915 4.6237
Lam e Teng (2004)	0.2457	1.9499 7.2000	2.1264 6.6322	2.0983 6.6322	1.8866 5.4331	1.8598 5.2992	2.054 4.9294
Benzaid e Mesbah (2013)	0.2468	1.4935 3.9394	2.1299 6.6499	2.1023 6.6499	1.8906 5.4530	1.8637 5.3185	2.0577 4.9481
Berthet et al. (2005)	0.2783	2.2500 7.5000	2.2276 7.1379	2.2161 7.1379	2.0044 6.0219	1.9741 5.8702	2.1645 5.4847
Pan et al.	0.2965	2.1131	2.2811	2.2802	2.0700	2.0377	2.2250

(2017)		12.7301	7.4053	7.4053	6.3502	6.1886	5.7960
Berthet et al. (2005)	0.3065	2.0961 5.5000	2.3097 7.5486	2.3151 7.5486	2.1062 6.5311	2.0728 6.3641	2.2581 5.9681
Lam e Teng (2006)	0.3115	2.0565 8.4000	2.3239 7.6194	2.3325 7.6194	2.1244 6.6219	2.0904 6.4521	2.2746 6.0546
Berthet et al. (2005)	0.3172	1.6863 8.5000	2.3397 7.6984	2.3520 7.6984	2.1448 6.7242	2.1103 6.5514	2.2931 6.1522
Berthet et al. (2005)	0.3348	2.1765 8.0000	2.3877 7.9385	2.4121 7.9385	2.2085 7.0424	2.1720 6.8599	2.3503 6.4562
Lam e Teng (2004)	0.3857	2.6268 9.2000	2.5176 8.5882	2.5808 8.5882	2.3920 7.9599	2.3499 7.7497	2.5120 7.3382
Valdmanis (2007)	0.3906	2.0437 5.7308	2.5296 8.6479	2.5967 8.6479	2.4097 8.0485	2.3671 7.8356	2.5273 7.4238
Pan et al. (2017)	0.4344	2.5456 12.9854	2.6316 9.1582	2.7368 9.1582	2.5679 8.8395	2.5205 8.6027	2.6630 8.1904
Pan et al. (2017)	0.5930	3.1371 16.7417	2.9453 10.7265	3.2141 10.7265	3.1401 11.7004	3.0754 11.3772	3.1329 10.9994
Benzaid e Mesbah (2013)	0.6081	2.5277 5.4925	2.9713 10.8567	3.2576 10.8567	3.1945 11.9727	3.1283 11.6413	3.1763 11.2694

Table 2.3. Experimental-analytical comparisons. Design-oriented models.

MODELS	Experimental		Analytical					
	f_l / f_{c0}	f_{cc} / f_{c0} $\varepsilon_{cc} / \varepsilon_{c0}$	f_{cc} / f_{c0} $\varepsilon_{cc} / \varepsilon_{c0}$					
			(6)	(7)	(8)	(9)	(10)	(11)
Valdmanis (2007)	0.0584	0.9326 1.2000	1.3503 4.3295	1.1458 -	1.1868 1.5545	1.1284 2.4436	1.2084 -	1.2335 2.9248
Valdmanis (2007)	0.1225	1.3145 3.7059	1.6340 5.9447	1.2972 -	1.3921 2.1641	1.3696 2.9313	1.4375 -	1.4901 4.2474
Lam e Teng (2004)	0.1228	1.3972 5.0000	1.6352 5.9511	1.2979 -	1.3931 2.1669	1.2702 2.9335	1.4385 -	1.4913 4.2533
Micelli e Modarelli (2013)	0.1257	1.6572 2.6198	1.6471 6.0125	1.3046 -	1.4023 2.1942	1.2765 2.9554	1.4488 -	1.5028 4.3107
Berthet et al. (2005)	0.1391	1.5000 3.75	1.7019 6.2916	1.3358 -	1.4453 2.3219	1.3061 3.0575	1.4968 -	1.5566 4.5774
Lam e Teng (2006)	0.1426	1.3869 5.0781	1.7159 6.3616	1.3438 -	1.4564 2.3549	1.3138 3.0839	1.5092 -	1.5705 4.6459
Jang e Teng (2007)	0.1543	1.42 7.4074	1.7622 6.5908	1.3707 -	1.4936 2.4655	1.3394 3.1724	1.5507 -	1.6171 4.8737
Hany et al.	0.1661	1.3611	1.8087	1.3980	1.5315	1.3654	1.5930	1.6644

(2011)		9.0000	6.8158	-	2.5780	3.2624	-	5.1031
Berthet et al. (2005)	0.1674	1.6078 6.25	1.8138 6.8403	1.4010 -	1.5358 2.5905	1.3683 3.2724	1.5977 -	1.6697 5.1284
Micelli e Modarelli (2013)	0.1749	1.7972 4.3976	1.8428 6.9781	1.4182 -	1.5597 2.6617	1.3848 3.3293	1.6244 -	1.6996 5.2720
Valdmanis (2007)	0.1775	1.4799 3.6923	1.8530 7.0260	1.4243 -	1.5681 2.6867	1.3906 3.3494	1.6338 -	1.7102 5.3224
Benzaid e Mesbah (2013)	0.2145	1.5177 4.6154	1.9921 7.6647	1.5086 -	1.6863 3.0374	1.4718 3.6299	1.7656 -	1.8578 6.0159
Pan et al. (2017)	0.2172	1.7477 9.5524	2.0023 7.7103	1.5149 -	1.6951 3.0636	1.4779 3.6509	1.7755 -	1.8689 6.0669
He e Jin (2011)	0.2276	1.9096 4.4800	2.0404 7.8794	1.5385 -	1.7283 3.1622	1.5007 3.7298	1.8125 -	1.9104 6.2577
Lam e Teng (2004)	0.2457	1.9499 7.2000	2.1060 8.1655	1.5795 -	1.7861 3.3339	1.5405 3.8671	1.8770 -	1.9827 6.5861
Benzaid e Mesbah (2013)	0.2468	1.4935 3.9394	2.1100 8.1827	1.5820 -	1.7897 3.3443	1.5429 3.8755	1.8810 -	1.9871 6.6060
Berthet et al. (2005)	0.2783	2.2500 7.5000	2.2220 8.6583	1.6532 -	1.8906 3.6438	1.6123 4.1151	1.9935 -	2.1132 7.1671
Pan et al. (2017)	0.2965	2.1131 12.7301	2.2855 8.9214	1.6941 -	1.9488 3.8167	1.6523 4.2533	2.0585 -	2.1860 7.4846
Berthet et al. (2005)	0.3065	2.0961 5.5000	2.3202 9.0631	1.7166 -	1.9809 3.9119	1.6743 4.3295	2.0943 -	2.2261 7.6577
Lam e Teng (2006)	0.3115	2.0565 8.4000	2.3375 9.1334	1.7279 -	1.9970 3.9597	1.6854 4.3678	2.1122 -	2.2462 7.7441
Berthet et al. (2005)	0.3172	1.6863 8.5000	2.3570 9.2121	1.7406 -	2.0151 4.0136	1.6979 4.4109	2.1325 -	2.2689 7.8410
Berthet et al. (2005)	0.3348	2.1765 8.0000	2.4170 9.4525	1.7801 -	2.0715 4.1811	1.7367 4.5449	2.1954 -	2.3394 8.1398
Lam e Teng (2004)	0.3857	2.6268 9.2000	2.5866 10.1143	1.8935 -	2.2342 4.6641	1.8485 4.9313	2.3769 -	2.5428 8.9798
Valdmanis (2007)	0.3906	2.0437 5.7308	2.6028 10.1760	1.9044 -	2.2499 4.7107	1.8593 4.9686	2.3944 -	2.5624 9.0592
Pan et al. (2017)	0.4344	2.5456 12.9854	2.7451 10.7116	2.0017 -	2.3902 5.1272	1.9558 5.3017	2.5509 -	2.7378 9.7566
Pan et al. (2017)	0.5930	3.1371 16.7417	3.2383 12.4644	2.3503 -	2.8975 6.6333	2.3046 6.5067	3.1169 -	3.3719 12.1122
Benzaid e Mesbah (2013)	0.6081	2.5277 5.4925	3.2837 12.6191	2.3833 -	2.9458 6.7767	2.3378 6.6214	3.1708 -	3.4323 12.3241

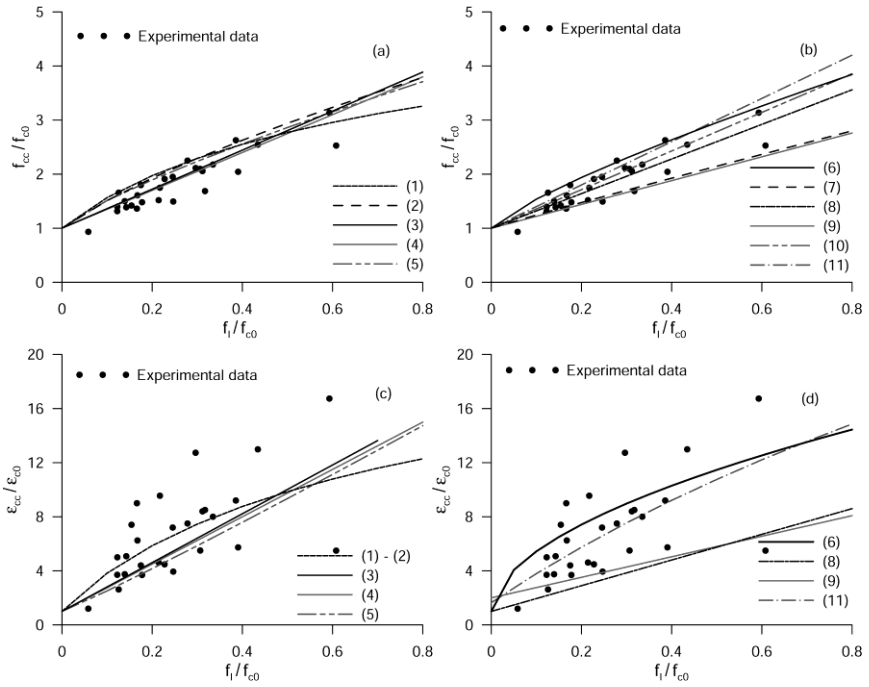

Figure 2.4. Experimental-analytical comparisons between confined compressive strength ratio and confined peak strain ratio obtained from analysis-oriented models (a)-(c), design-oriented models (b)-(d).

2.1.2 FRP-confined concrete under pre-existing loads

Hereinafter, an extensive review of all the available studies treating the behavior of concrete reinforced by confining devices while subjected to pre-existing loads is presented. The first study dates back to 2009 from Pan et al. (2009). The authors analyzed the compressive behavior of square columns without internal reinforcement subjected to different load levels before the reinforcement/confinement. The column cross sections were 110 mm in length and 200 mm in height. The concrete strength was 21.1 MPa while a loading between 20% and 80% of the strength of the unconfined concrete f_{c0} was applied before reinforcing. The test sequence consisted of a constant loading of 24 hours, after which an FRP wrapping was applied. The constant loading was maintained for further 48 hours, time necessary to make the reinforcement effective. Finally, tests up to the collapse were carried out.

After the tests, the specimens showed meanly a reduction (with respect to the case of non-preloaded specimens) of the axial stress and strain capacity much more evident when the preloading level increased.

Pan et al. (2011) provided an experimental investigation on cylindrical concrete specimens (concrete strength of 21.8-28.8 MPa, having a cross-section diameter of 110 mm and height of 200 mm. The authors observed the difference between the strength and the strain of the specimens tested with and without preload.

Shi and He (2009) investigated the before reinforcement loading effects on FRP confined circular concrete columns with and without internal reinforcement by means of the finite elements modeling software Abaqus. The study was aimed to the evaluation of the compressive behavior in terms of load-carrying and strain capacity of the confined specimens respect to the classical monotonic compressive behavior characterized by the application of the reinforcement on a non-preloaded element. The proposed numerical modeling neglected load-time dependent effects. The authors stated that the load capacity reduction due to preload was very limited and could be compensated by increasing the thickness of the FRP wraps used for confinement.

He and Shi (2009) by the same finite element modeling strategy presented a study in which they analyzed the capacity of preloaded systems subjected to lateral loads, performing push-over analysis on RC columns first preloaded at different stress levels and then laterally pushed until collapse. In this case the results were in accordance with their previous studies.

He et al. (2009) presented an experimental study on preloaded circular concrete columns with an aspect ratio of 1:3 (150 mm diameter and 450 mm height), reinforced with FRP, with and without internal reinforcement. Specimens were characterized by concrete with compressive strength of 29.55 MPa. The test procedure was similar to that used by Pan et al. (2009) and Pan et al. (2011), also for the temporal test sequence (FRP bandage were leaved to dry for a time between 48 and 72 hours, depending on the temperature conditions). Preload levels varied from 20% to 85% of f_{c0}. The authors investigated the expansion ratio of the confined concrete under preload. Later, He and Jin (2011) presented further analyses about the axial compressive behavior of the specimens tested in He et al. (2009).

However, in this case, results provided by the authors were not in accordance with Pan et al. (2009) and Pan et al. (2011). The collapse loads of the preloaded specimens were similar to that obtained without preloading. In addition, the authors found that preload levels influenced the secant stiffness of the stress-strain response respect to the non-preloaded case, resulted higher with low preload levels and lower with high preload levels. The authors stated that this slightly positive effect on the response of low preloaded specimens could be attributed to a better compaction of concrete, in a compression range that did not cause damage.

Morsy and El-Tony (2012) presented results of compression tests on circular reinforced concrete columns with dimensions of 160 mm in diameter and 1000 mm in height. The specimens were preloaded up to 85% and 100% of f_{c0} and wrapped with FRP to simulate retrofitting conditions of heavily damaged structural elements. The results showed that the specimens preloaded up to 85% of f_{c0} had a collapse load equal or slightly higher than that obtained in the case of specimens non preloaded before wrapping. Nevertheless, an increase of the ultimate strain was observed. In the case of preloaded columns up to 100% of f_{c0}, however, reduction in strength and strain capacity with respect to the case of non-preloaded specimens occurred because of the high damage undergone by the concrete.

Ivorra et al. (2013) discussed an experimental campaign carried out on concrete cylindrical specimens with a diameter of 150 mm and height 300 mm (aspect ratio 1:2). Concrete had a compressive strength of 40 MPa. Specimens were kept under compression for 24 hours and then wrapped with carbon fibers. After the wrapping, the load was held for further 96 hours. Axial and lateral strains during all the intermediate steps were monitored, indicating that creep induced load redistribution. Results obtained from the tests on the specimens subjected to preload showed higher compression strength compared to that obtained for non-preloaded specimens.

Pan et al. (2015) and Pan et al. (2017a), according to the experimental results obtained in Pan et al. (2009) and Pan et al. (2011), proposed analytical formulations for the the stress-strain response of FRP-confined concrete and preloaded FRP-confined concrete in which the ultimate strength and strain conditions were obtained by reduction coefficients evaluated by regression analysis of the experimental data. Moreover, Pan et al. (2017a) proposed finite element modeling with ANSYS software, performing numerical simulations to reproduce the experimental data.

The last available reference is due to Pan et al. (2017b) in which a design-oriented model was proposed to reproduce the experimental results previously obtained from the same authors.

The above described studies prove that different conclusions were reached by several authors on this subject. Summarizing:

- Strength and strain capacity in comparison with specimens without preload: a) reduction of strength and strain capacity; b) no significant reductions; c) no reduction of strength; d) equal failure loads and increasing of ultimate strain; e) higher failure loads respect to the case without preload;
- Stress-strain behavior in comparison with specimens without preload: I) reduction of the secant stiffness; II) Increasing of secant stiffness with low preload and decreasing with high preload; III) axial/lateral strain increase due to creep effects;

For an overall view, the key aspects of the above-discussed works are summarized in Table 2.4. Information related to the type of specimens (circular, square), the type of study (experimental, analytical, numerical) and the temporal sequence of test procedure is also provided for each study. Moreover, regarding the time related to the reinforcement phase and the load failure tests, the time of preloading before wrapping T1 and the time of preloading before failure test T2 are reported for more clarity on the time-dependent effects.

Table 2.4. Current findings on the compressive behavior of preloaded FRP-confined concrete columns.

Authors	Type of study	Type of section	T1 T2 (hours)	Findings on strength and strain	Findings on stress-strain behavior
Pan et al. (2009)	Experimental	Square	24 48	a	I
Pan et al. (2011)	Experimental	Circular	24 48	a	I
He and Shi (2009a)	Numerical	Circular	Not included	b	I
He and Shi (2009b)	Numerical	Square	Not included	b	I
He et al. (2009)	Experimental	Circular	24 72+	c	II
He. and Jin (2011)	Experimental	Circular	24 72+	c	II
Morsy, El-Tony (2012)	Experimental	Circular	Not specified	d	I
Ivorra et al. (2013)	Experimental	Circular	24 96	e	III
Pan et al. (2015)	Analytical	Circular	Not included	a	I
Pan et al. (2017a)	Analytical	Circular and square	Not included	a	I
Pan et al. (2017)	Numerical	Circular and square	Not included	a	I

It is evident that the effects of confinement observed by the various authors in the presence of preload are not always the same. The only common observation is the reduction of the secant stiffness (with respect to the case of confined non-preloaded specimens) for high preload levels, indicating that at the same axial strain, a lower lateral pressure is provided by the FRP-jackets. The other aspects, about the strain ad strength, remain in disagreement suggesting the need of more accurate studies.

2.2 Confinement with Steel Jacketing

Steel jacketing is an external reinforcement technique comprising two principal elements used to build a steel cage around an existing column. The steel cage is composed by angles and battens.

The steel angles are placed at the corners of the column concrete by using mortar or epoxy resin (sometimes the connections are made without mortar), while steel battens are usually welded to the steel angles in function of an established spacing. Increasing of strength is due to the confinement action of the steel battens that provide lateral confinement pressure to the concrete core during the expansion phenomena of the columns subjected to compressive loads. (In Fig. 2.5 the technological components of the above described technique are illustrated).

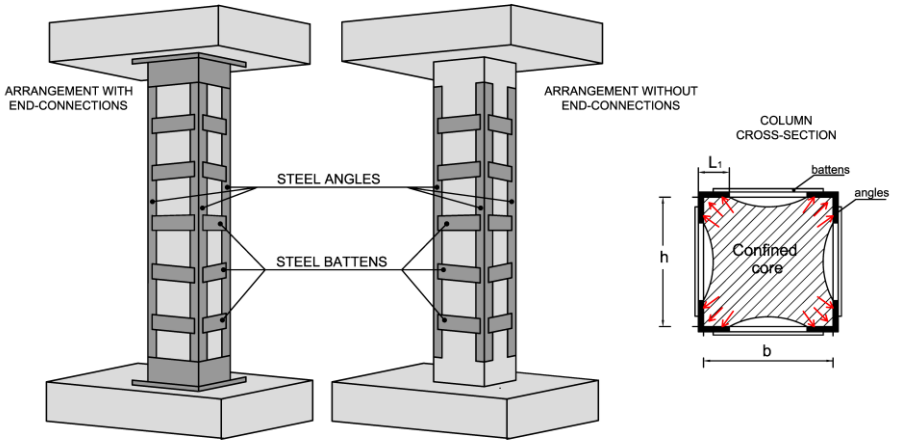

Figure 2.5. Steel Jacketing on RC columns.

Depending on the type of end-connection, strengthened columns are also able to bring load for the direct contribute of the angles. On the other hand, some previous researches demonstrated that in absence of end-connections the angles can give contribute of axial load due to the sliding-induced tangential stresses at the interface between angles and concrete (Adam et al., 2007, 2009, Badalamenti et al., 2010). Despite this, the current Italian Code (NTC 2008) and Eurocode 8 provide in the case of steel wrapping (with angles well connected or not) to consider the assessment of the performance increase only for the confinement action, neglecting the direct contribution of the angles to the flexural and axial-load capacity. Eurocode 4 considers

instead the contribution of the angles only for the case of full connections, providing design procedure of hybrid cross-sections (Fig. 2.6).

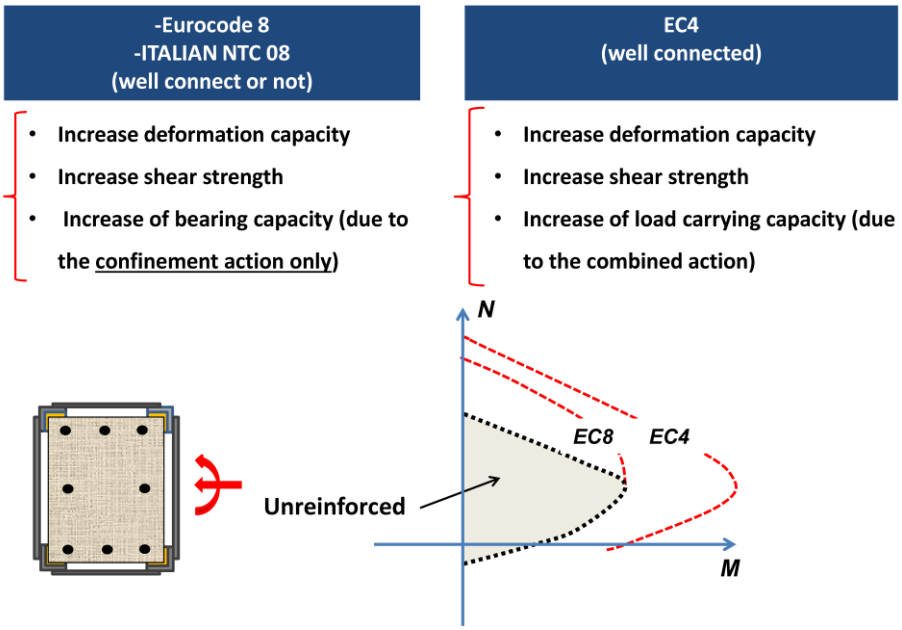

Figure 2.6. Effect on the axial and flexural behavior of RC Steel Jacketed columns in function of the type of end-connection according to the Standard Codes.

2.2.1 Review and analysis of the main parameters

Reliable predictions of the capacity of reinforced elements are basic for the design of this kind of interventions. For this reason, the use of suitable confined concrete laws is fundamental for the accuracy of the results.

In the last decade, many authors pay attention to the load-bearing capacity including confinement effects. Among the most important studies, Montuori and Piluso (2009) provided an experimental investigation on columns strengthened by steel jacketing subjected to centered and eccentric compression loads. To reproduce the experimental results, they defined a relationship for the determination of the lateral confinement pressure of columns strengthened by the internal and external reinforcement starting from the expressions provided Mander et al. (1988) for internal steel reinforcement. They proposed four different concrete laws for the analysis of the cross-section: unconfined concrete, concrete confined only by internal

hoops, concrete confined only by steel angles and battens and concrete confined by internal hoops, steel angles and battens respectively. In this conditions a univocal definition of the strength increment factor k results really difficult. To solve the problem, the authors proposed to calculate the volumetric reinforcement ratio along x and y directions by homogenizing the area of the battens as function of the internal reinforcement using the ratio (f_{yb}/f_{yk}) of the yielding stresses of battens (f_{yb}) and hoops (f_{yk}). In this way, the entire cross-section could be considered as strengthened by an equivalent reinforcement.

Moreover, the confinement effectiveness factor k_e (that considers arching action of the confined concrete) was assumed to be almost equal to the one adopted for the case of internal reinforcement. The strain limits for the confined concrete (strain at peak of strength ε_{cc} and ultimate strain ε_{ccu}) were determined according to Mander et al. (1988) rules.

Later, Nagaprasad et al. (2009) presented an experimental investigation on the same kind of columns subjected to monotonic and cyclic lateral loads to observe the deformation capacity under seismic actions. The analytical model once again was an extension of Mander et al. (1988) model referred to rectangular cross-sections. Differently from Montuori and Piluso (2009) the authors taken into account only the confinement effect exerted by the steel angles and battens, neglecting the confinement contribution of the internal reinforcement and proposing a methodology to determine the lateral confinement pressure along the principal axes. The latter was evaluated considering the effectively confined area in plan and elevation, assuming the arching lines of confining stresses between the steel angles. Strength and strain limits were determined also in this case according to Mander et al. (1988).

Another important contribute is due to Badalamenti et al. (2010) that proposed an analytical model for square columns reinforced with steel angles and battens, taking into account both cases of angles fully loaded and indirectly laded. The analytical formulation considers the confinement action provided by the reinforcement as a function of the friction coefficient between angles and concrete members. The determination of the lateral confinement pressure was carried out simplifying the actual system into a one-dimensional model considering two elastic beams (battens) on elastic springs. The authors assumed that cohesion between mortar cementitious and steel angles (c_0) was negligible and suggested a friction coefficient value

μ of 0.5. Stress-strain law adopted to reproduce the compressive behavior of confined concrete was assumed according to Mander et al. (1988), while strength of the confined concrete was computed according to Eurocode 8.

A summary of the expressions proposed for the determination of the confinement parameters of the above discussed models is provided in Table 2.5. The symbols appearing in this table have the following significance:

- $\rho_{st,x}$ and $\rho_{st,y}$ geometrical ratio of transverse reinforcement in x and y direction respectively;
- ρ_{long} geometrical ratio of longitudinal reinforcement;
- n_{bx} and n_{by} number of stirrups along x and y direction respectively;
- s spacing of internal stirrups;
- s_b spacing of steel battens;
- s_2 clear spacing of two consecutive steel battens;
- A_{sb} cross-section area of steel battens;
- b and h dimensions of the concrete cross-section;
- c concrete cover of internal stirrups;
- ϕ_{st} diameter of internal stirrups;
- ε_{su} ultimate strain of steel stirrups;
- L_1, t_1 the length and the thickness of the steel angles;
- L_2, t_2 the length in contact with the column and the thickness of the steel battens respectively;

For a more detailed description of the parameters please refer to Fig. 2.7 and/or the original source.

Table 2.5. Analytical expression of the confinement parameters according to the different models.

Models	Confinement pressure $f_{l,max}$	Effective confinement factor k_e	Strength f_{cc} and strain limits of confined concrete (ε_{cc}, ε_{ccu})
Montuori and Piluso (2009)	$f_{lx}=\rho_{st,x}f_{yb}$, $f_{ly}=\rho_{st,y}f_{yb}$ $\rho_{st,x}=\frac{n_{bx}A_{stx}}{s_i(h-2c)}+\frac{2A_{sb}}{s_b h}\frac{f_{yb}}{f_{yk}}$ $\rho_{st,y}=\frac{n_{by}A_{sty}}{s_i(b-2c)}+\frac{2A_{sb}}{s_b b}\frac{f_{yb}}{f_{yk}}$	$\left(1-\frac{s_b-\phi_{st}}{2(b-2c)}\right)$ $\left(1-\frac{s_b-\phi_{st}}{2(h-2c)}\right)$	$f_{cc}=f_c\cdot k$ $\varepsilon_{cc}=\varepsilon_c\left[1+5\left(\frac{f_{cc}}{f_c}-1\right)\right]$ $\varepsilon_{ccu}=\varepsilon_{cu}+\frac{1.4\rho_{st}f_{yk}}{f_{cc}}\varepsilon_{su}$
Nagaprasad et al. (2009)	$f_{lx}=\frac{2t_2(h-L_1)}{s_b\cdot b}f_{yb}$ $f_{ly}=\frac{b}{h}f_{lx}$	$\frac{\left(1-\frac{(b-L_1)(h-L_1)}{3bh}\right)}{1-\rho_{long}}\cdot\frac{\left(1-\frac{s_b-s_2}{2b}\right)\left(1-\frac{s_b-s_2}{2h}\right)}{1-\rho_{long}}$	
Badalamenti et al. (2010)	$f_{lx}=\frac{1.33\cdot f_{yb}}{b\cdot s_b\cdot\left(\frac{L_1}{s_b\cdot t_2}+\frac{L_2}{s_b\cdot s_2}\right)}$	$e^{-1,5\left(\frac{s_b}{b}\right)}$	$f_{cc}=f_c+3.7(f_{le,\max})^{0.86}$ $\varepsilon_{ccu}=\varepsilon_{cu}+\frac{1.4\rho_{st}f_{yk}}{f_{cc}}\varepsilon_{su}$
NTC 2008	$f_{l\max}=\rho_{st}f_{yb}$ $\rho_{st}=\frac{2(b+h)A_{sb}}{s_b bh}$	$\left(1-\frac{(b-2R)^2+(h-2R)^2}{3bh}\right)\cdot\left(1-\frac{s_b-t_2}{2b}\right)\left(1-\frac{s_b-t_2}{2h}\right)$	$f_{cc}=f_c+3.7(0.5f_{le,\max})^{0.86}$ $\varepsilon_{ccu}=\varepsilon_{cu}+\frac{0.25\alpha_n\alpha_s\rho_{st}f_{yb}}{f_{cc}}$

As regards to the reinforced cross-section having the characteristics reported in Fig. 2.7 and Table 2.6 a comparative analysis of the main confinement parameters resulting by the different models is carried out. Lateral confinement pressure $f_{le,max}$, strength of confined concrete f_{cc}, strain at the peak-strength ε_{cc}, ultimate strain of confined concrete ε_{ccu} and the strength increment factor $k=f_{cc}/f_{c0}$ (f_{c0} unconfined concrete strength) are investigated in function of the dimensionless spacing ratio (s_b/b), with s_b and b being the battens spacing and the largest dimension of cross-section respectively. The comparisons are shown in Figs. 2.8-2.9.

Table 2.6. Geometrical and mechanical properties of the reference cross-sections.

(b x h) (mm)	c (mm)	f_{c0} (MPa)	s_i s_2 (mm)	Φ_{st} Φ_l (mm)	f_{yk} f_{yb} (MPa)	l_1 (mm)	t_1 t_2 (mm)
(a)200x200	25	15	200	8	450	50	5
(b)200x300			50	12	275		

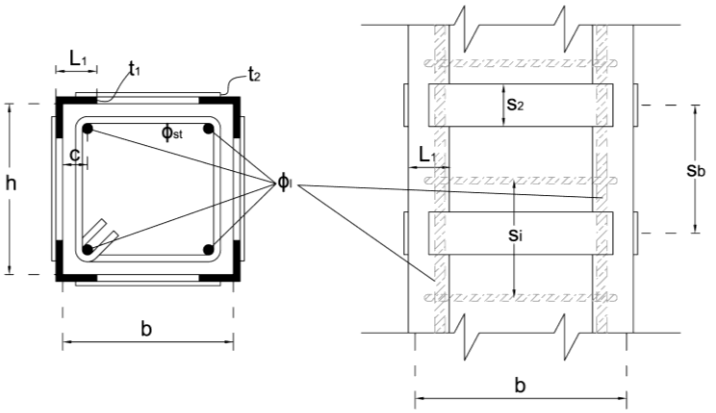

Figure 2.7. Arrangement of internal and external reinforcement on the column.

All the parameters investigated strongly decrease with the increasing of the ratio s_b/b. Moreover, the predictions coming from the different models result largely scattered. For both square and rectangular cross-sections, the strain at peak-strength ε_{cc} results enclosed between the predictions given by Nagaprasad et al. (2009) and NTC 2008.

Regarding the ultimate strain of the confined concrete ε_{ccu}, NTC 2008 returns the lowest values, while in this case, model by Badalamenti et al. (2010) returns the upper bound. Similar trend to that of ε_{cc} is observed for the strength increment factor ($k=f_{cc}/f_{c0}$). Also here the highest and lowest estimation are those provided by Nagaprasad et al. (2009) and NTC 2008 models respectively. Finally, the prediction of the effective lateral confinement pressure shows scattered only for the case of square cross sections. On the other hand, predictions for the rectangular cross-section lead to similar results using the different models. Moreover, it can be noted that according to the majority of the models the effective lateral confinement pressure of the reinforced square cross-section reaches negligible values in correspondence of a s_b/b value of approximately 1.5.

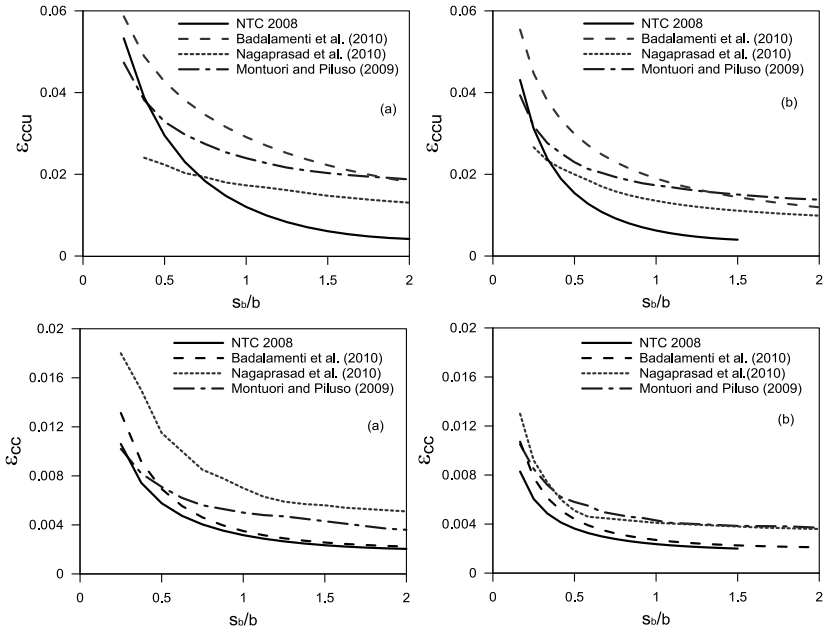

Figure 2.8. Comparisons between strain parameters.

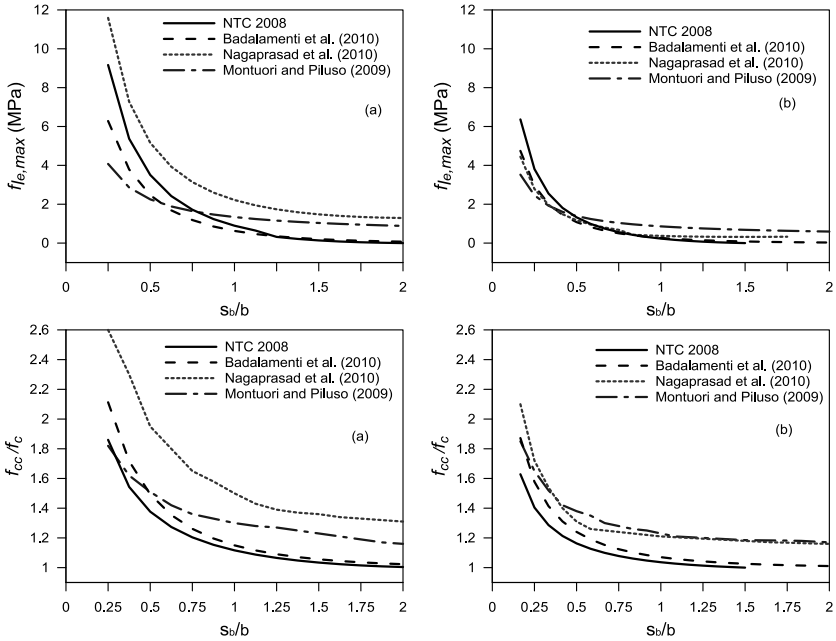

Figure 2.9. Comparisons between strength parameters.

For an accurate evaluation of the axial-load capacity of RC members strengthened with steel cages, the contribute of angles should be considered in the overall behavior. In the case of mechanical connections between angles and beams or slabs the behavior in compression of the angles including the buckling effects should be considered.

Problems related to buckling effects can significantly change the compression response of the angles, because the load-bearing capacity become reduced when the slender effects are relevant.

Specifically, buckling effects can occur before or after the achievement of the yield stress of steel and, in both cases, the compressive stress is lesser than the nominal one, so the load is also reduced. In addition, in a RC column subjected to compression loads, all the materials reach the maximum capacity for different axial strain levels, influencing the final capacity.

Badalamenti et al. (2010), based on the results of Gomes and Appleton (1997), proposed an analytical approach to evaluate the axial load-capacity of the steel angles subjected to compressive loads. Hereinafter, the proposed model is briefly discussed.

Referring to Fig. 2.10, where w_h is the lateral displacements, δ_v the axial shortening, θ is the angle defining the buckled position, the buckling load is evaluated imposing a buckled limit equilibrium condition as:

$$N_c \cdot w_h - 2 \cdot M_u^* + \frac{q \cdot l \cdot s_b^2}{8} = 0 \tag{2.4}$$

M_u^* being the ultimate bending moment of the steel angle subjected to axial force, axial bending and lateral loads q, the last assumed equivalent to the lateral confinement pressure $f_{le,max}$. The critical stress σ_c is determined for each value of axial strain of the column, dividing the resulting critical load N_c by the area of the angle. In detail, the critical stress σ_c assumes the following expression:

$$\sigma_c = \frac{1}{s_b \cdot l \cdot t_2} \cdot \frac{1}{\sqrt{2\varepsilon_s - \varepsilon_s^{\,2}}} \cdot \cdot \left\{ 2 \left[\frac{l^2 \cdot t_1 \cdot f_{yb}}{4} - \frac{\left(N_u^*\right)^2}{16 \cdot f_{yb} \cdot t_1} \right] - \sqrt{2}\, f_{l,\max} \cdot l \frac{s_b^2}{4} \right\} \tag{2.5}$$

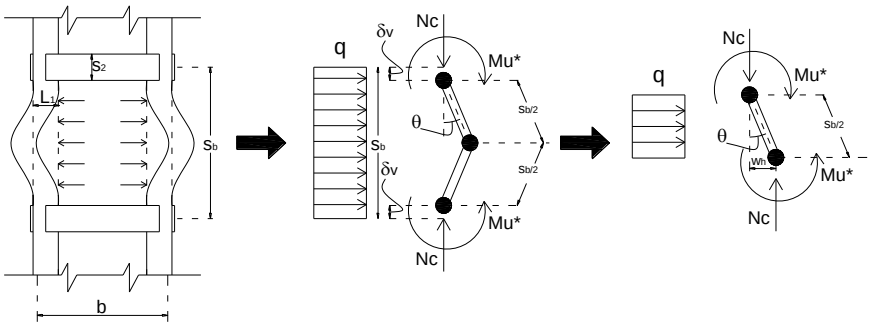

Figure 2.10. Limit equilibrium for the buckling condition of the angle.

In Eq. 2.5 N_u^* depends on the axial strain being $N_u^* = \varepsilon_s \cdot 2 \cdot l_1 \cdot t_1 \cdot E_s \le 2 \cdot l_1 \cdot t_1 \cdot f_{yb}$. Finally, axial stress-strain curve for the steel angles in compression taking into account bucking effects can be obtained by assuming the following limits for the compressive stress:

$$\sigma = \begin{cases} \min\left(E_s \varepsilon_s ; \sigma_c\right) & if \quad \varepsilon_s \le \varepsilon_{yb} \\ \min\left(f_{yb} ; \sigma_c\right) & if \quad \varepsilon_s > \varepsilon_{yb} \end{cases} \tag{2.6}$$

where ε_{yb} is the yielding strain of steel angles.

2.2.2 No-end-connected steel jacketed RC columns under axial and eccentric compressive loads.

For practical reasons, steel angles are in several cases arranged leaving a gap with the end beams or slabs. Despite this disconnection, the angles are still able to support a non-negligible portion of load because of the frictional forces developed along the column-angle contact interface. In these cases, the definition of computational numerical and analytical models for the assessment of reinforced cross sections becomes more complex and must be handled with care. The actual load-carrying capacity of the angles is a function of lateral confinement pressure, cohesive strength, and the friction coefficient between the materials.

This section focuses on the results of an experimental campaign on RC column specimens with and without steel jacketing subjected to compressive axial and eccentric tests. Also, a new approach is discussed to define a plane fiber-section model of the reinforced cross section accounting for the frictional action occurring along the column-angles interfaces. The findings

discussed in this section will be then used for the interpretation/modeling of the behavior of columns loaded before the application of steel jacketing.

Experimental tests regarded half-scale reinforced column specimens with and without steel jacketing reinforcement. Two different types of concrete strength were used to arrange specimens. Cylindrical concrete samples were previously tested after 28 days aging to determine the unconfined stress-strain properties. The Type A concrete (low strength) presented an average compressive strength f_c of 12.65 MPa and a corresponding unconfined average experimental peak-strain ε_c of 0.004. The Type B concrete (medium strength) had an average strength value f_c of 24.00 MPa with an associated average experimental peak-strain ε_c of 0.0025. The stress-strain results of the tests on concrete cylinders are shown in Fig. 2.11. The choice of specimens presenting medium and low concrete mechanical properties was made to simulate the possible actual service conditions of older RC buildings needing such interventions.

Low-strength concrete is often detected in these cases because of a bad arrangement of concrete on site, disregarding the mix design. Further, the different deformability of the two types of concrete also allowed investigation of the effectiveness of the reinforcement system with concrete types having different mechanical properties.

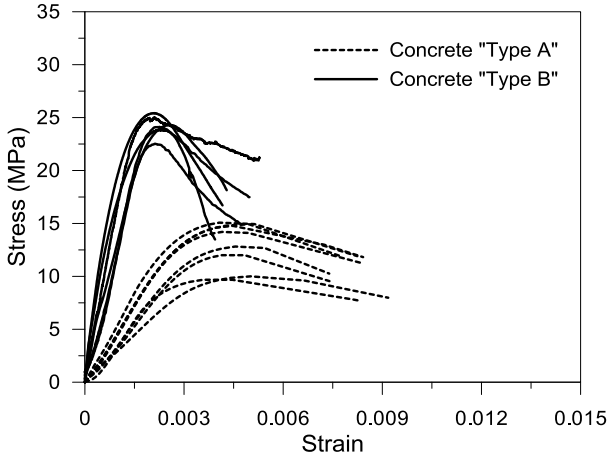

Figure 2.11. Results of compression tests on concrete cylinders.

The specimens consisted of rectangular 220 × 300 mm columns having height 820 mm. The two enlarged (top and bottom) heads were realized to avoid the influence of disturbing boundary effects.

Internal reinforcement was arranged using longitudinal rebars having nominal yielding stress f_y whereas angles and battens were of steel characterized by the yielding stress f_{ya}=f_{yb}=275 MPa. The internal lateral reinforcement was characterized by variable internal stirrups spacing along the column height. This expedient allowed the concentration of deformations within the central portion of the specimen, preventing possible local failures in proximity of the ends due to the abrupt variation of the cross section.

The steel jacketing reinforcement was arranged by placing an intermediate layer of cementitious mortar between steel and concrete surfaces. Battens were welded to the angles without preheating so as to generate a passive confinement pressure as the deformation of the column increased during the test. A spacing of 30 mm was left between the angles and the heads of the columns.

The design details of specimens are reported in Fig. 2.12, and actual pictures of reinforced and unreinforced specimens are shown in Fig 2.13, respectively.

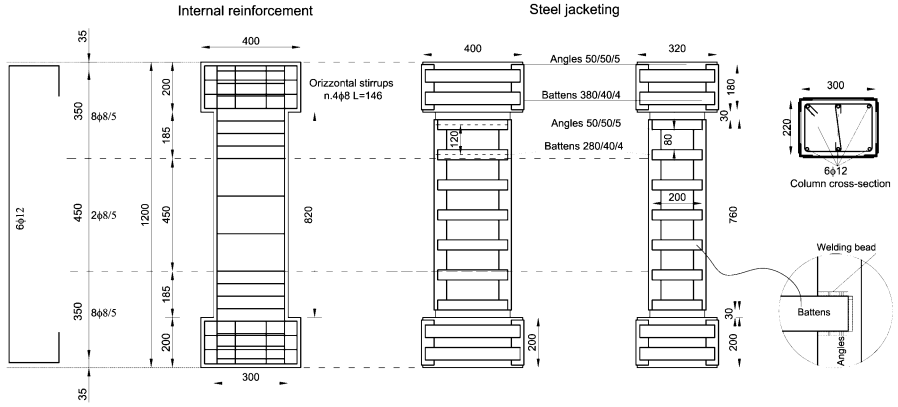

Figure 2.12. Design details of the specimens with and without steel jacketing.

Figure 2.13. Specimens with and without steel jacketing.

Test set up and instrumentation

Test set up and instrumentation

RC specimens with and without steel-jacketing were tested in compression and in combined axial load and flexure. (Fig. 2.14). In the latter, the compression was applied at a fixed eccentricity, making use of a special pin device. In this type of test, axial load and bending moment increase simultaneously. The ultimate condition of the specimen is reached because of a combination of axial load with bending moment.

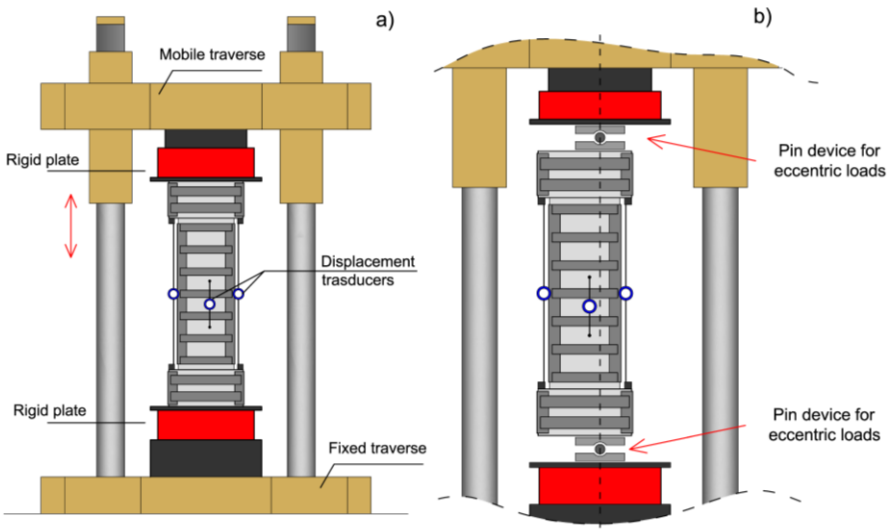

Figure 2.14. Test setups: (a) axial compressive tests; eccentric compressive tests.

Two possible cases of eccentricity along the orthogonal axes of inertia were considered. In particular, the eccentricities of 65 and 55 mm were assigned along the x and y directions, respectively. This low-eccentricity range was fixed to reach the ultimate state of the specimens under prevalence of axial load to simulate the real loading condition of non–seismically designed base columns. The matrix of the tests is reported in Table 2.7. The non-reinforced specimens are named with the symbols CA# or CB#, depending on the type of concrete (Type A or Type B). For the reinforced ones, the symbol R precedes the name. The eccentric tests along the x and y directions are indicated by inserting the suffixes EX# and EY#.

Table 2.7. Schematization of tests.

Specimens	Concrete type	Concrete strength (MPa)	Steel Jacketing	Load eccentricity (mm)
CA1	A	12.65	No	/
CA2	A	12.65	No	/
CAEX1	A	12.65	No	65
CAEY1	A	12.65	No	55
RCA1	A	12.65	Yes	/
RCA2	A	12.65	Yes	/
RCA3	A	12.65	Yes	/
RCAEX1	A	12.65	Yes	65
RCAEY1	A	12.65	Yes	55
CB1	B	24.00	No	/
CB2	B	24.00	No	/
CBEX1	B	24.00	No	65
CBEY1	B	24.00	No	55
RCB1	B	24.00	Yes	/
RCBEX1	B	24.00	Yes	65
RCBEY1	B	24.00	Yes	55

The tests were displacement-controlled in order to get the entire load-strain response.

A view of the test apparatus is shown in Fig. 2.15.

Figure 2.15. Load testing machine and computers acquisition data.

Axial strains were measured by means of two systems of digital transducers (Fig. 2.14). Four of these had a gauge length equal to the internal length of the specimen (820 mm) and were placed at the corners. The other four transducers were placed on the sides of the column in the middle height, with a gauge length of 250 mm. The double system of transducers allowed comparison of deformations over two measuring ranges and recognition of strain concentration in the middle height of the specimen where the stirrup step was lower.

All the transducers provided similar results and were averaged up to the strain corresponding to the stress peak. Beyond this point, only the internal gauge recordings were processed (gauge length 820 mm).

Test results

The results are shown in Fig. 2.16 for the reinforced and non-reinforced specimens in terms of axial load and average axial strain. During the axial compressive tests, a significant increase of bearing and deformation capacity was observed for the steel-jacketed columns. This was mainly recognized for the low strength specimens (Type A), where the load capacity increase

reached +60%. The increase of load-carrying capacity of Type B specimens was instead +25%. The increase of deformation significantly involved strains at stress peak (+620% and +258% for concrete Types A and B, respectively) and ultimate strains (+368 and +160% for concrete Types A and B, respectively). The different efficiency of the reinforcing system observed for the two types of concrete can be attributed to their different deformability: the larger deformability of the low-strength concrete results in the activation of a larger confinement action exerted by the steel jacketing. Also, for the eccentric compressive tests, the presence of the steel jacketing conferred a large load increase. Even in this case, this was mostly evident for low-strength concrete specimens. Load increments were approximately +70% and +35% for Types A and B concrete specimens, respectively. Average peak strains had increments of +240% and +280% (concrete Types A and B, respectively), whereas average ultimate strain increased by +360% and +75% (Types A and B, respectively). The relevant contribution of the reinforcement system to the overall response demonstrated that angles, although disconnected at the ends, were also still able to increase flexural capacity. Indeed, the ultimate state was reached because of the combination of the axial load and the bending moment arising from the eccentricity. Consequently, an indirect load transfers to the angles occurred in the interface layer.

Also, the deformation capacity was significantly improved for the steel-jacketed columns, for which a large sub-horizontal post-peak branch resulted instead of the rapid post-peak decay of the unreinforced specimens. The results of the tests are also reported in Table 2.8 in terms of peak load and corresponding strain (P_0, ε_0) and ultimate load and strain (P_u, ε_u).

Table 2.8. Test results.

Specimens	P_0 (kN)	ε_0	P_u (kN)	ε_u
CA1	1142.00	0.0040	971.00	0.0076
CA2	1195.00	0.0044	1015.00	0.0077
CAEX1	610.00	0.0046	399.30	0.0114
CAEY1	711.91	0.0054	604.24	0.0075
RCA1	1864.63	0.0324	1650.61	0.0355
RCA2	1882.12	0.0248	1748.83	0.0309
RCA3	1880.45	0.0336	1750.45	0.0412
RCAEX1	1047.43	0.0162	801.24	0.0436
RCAEY1	1205.34	0.0178	981.60	0.0403
CB1	2055.00	0.0028	1746.00	0.0095
CB2	1845.00	0.0029	1568.00	0.0072
CBEX1	976.00	0.0038	747.88	0.0164
CBEY1	1139.04	0.0035	966.78	0.0122
RCB1	2439.50	0.0102	2073.85	0.0217
RCBEX1	1370.32	0.0212	1300.31	0.0294
RCBEY1	1476.04	0.0314	1400.94	0.0208

From the observation of the specimens at the end of the tests (Fig 2.17), the effect of the steel reinforcement was also evident. For both axial and eccentric compressive tests on the unreinforced specimens, the damage was concentrated in the middle zones of the columns as well as the cracks, which also had a larger width. Cover spalling and buckling of rebars were also recognized. For the reinforced specimens, damage was less evident and spread out over the entire length of the column. Concrete spalling and buckling of rebars were avoided by the confinement action exerted by the reinforcement. For compressive axial tests, the collapse of the specimens occurred because of the failure of welding. However, this was recognized only in correspondence with very large deformations.

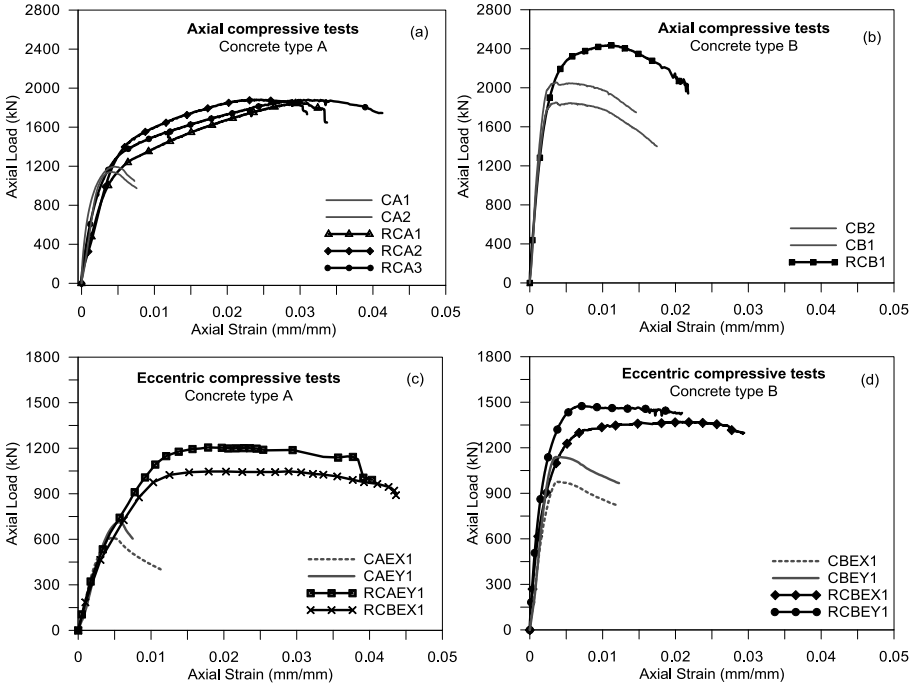

Figure 2.16. Results of compressive tests: Axial loads without eccentricity (a and b); eccentric loads (c and d).

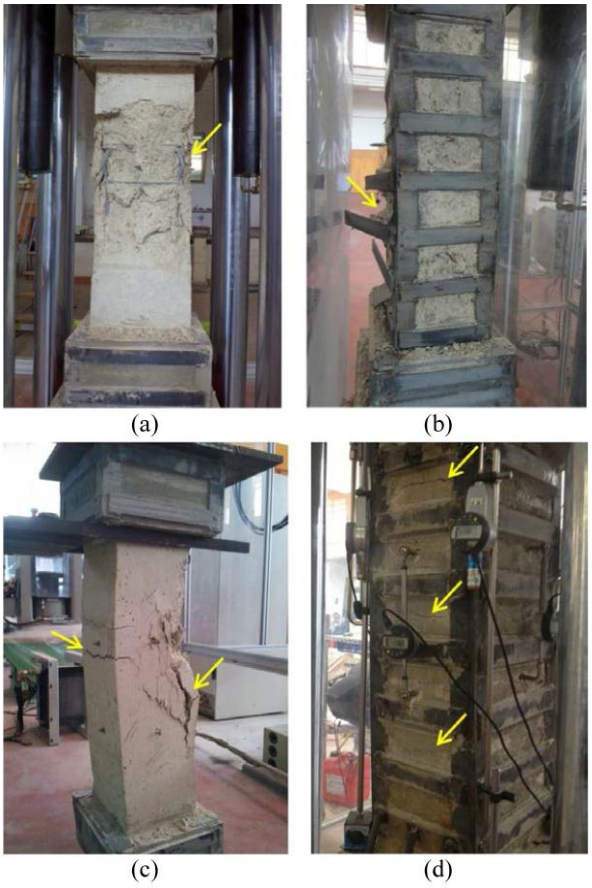

Figure 2.17. Typical failure of unreinforced and reinforced specimens: Axial load without eccentricity (a and b); eccentric load (c and d).

2.2.3 Numerical modeling

Fiber-section elements with distributed plasticity can be considered an effective strategy of modeling. For the case of RC columns reinforced by steel jacketing, the definition of reliable stress-strain relationships for the fiber cross section needs special care with respect to the unreinforced case. On the one hand, the stress-strain law for concrete has to account for a double confinement action, the first exerted from the internal reinforcement, the second from the steel jacketing. On the other hand, a relative sliding between steel and concrete fibers may occur along the interface (Fig. 2.18) inducing tangential forces due to cohesion and friction. Standard fiber

models cannot account for this interaction because they are based on the hypothesis of conservation of plan cross sections.

The method here proposed (described in detail in the following sections) uses a macroscopic approach to overcome this limitation.

An equivalent stress-strain law is attributed to the fibers of the angles to fictitiously consider the actual mechanical response of the interface that is supposed to be governed by a Mohr-Coulomb type relation. The definition of the governing parameters and the subsequent validation analyses are carried out basing on the previously described experimental campaign.

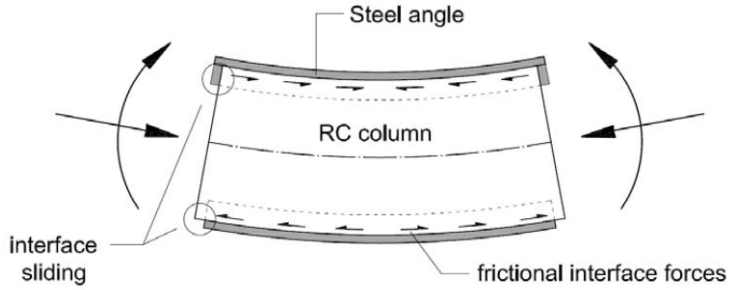

Figure 2.18. Interface interaction between angles and columns.

Definition of fiber cross-section for numerical simulation

The proposed assembly of a fiber cross section (Fig. 2.19) provides the definition of three different uniaxial stress-strain laws for concrete, rebars, and angle fibers, respectively.

A parabolic stress-strain law with linear tension softening is used for concrete fibers. The confinement model by Montuori and Piluso (2009) is adopted to calculate peak (f_{cc}, ε_{cc}) and ultimate (f_{cu}, ε_{cu}) stress and strain values. The model provides the use of a single concrete stress-strain law for the entire section. The lateral confinement pressures $f_{le,x}$ and $f_{le,y}$ are calculated according to the expressions provided in Table 2.4 regarding Montuori and Piluso (2009).

Steel rebars are modeled using an elasto-plastic law with linear hardening (η = 0.01). The nominal yielding stress (450 MPa) and Young's modulus (210000 MPa) are assigned. For the angle fibers, an elastic perfectly plastic law is used. This represents the normal stress-strain path of the angles induced by the tangential stresses developed along the interface. Therefore, the nominal stress-strain law of steel is replaced by a fictitious one

depending on the interface properties. For the case of a perfect end connection, the nominal yielding stress and Young's modulus of steel can be used. The proposed stress-strain model and its calibration are described in the following sections.

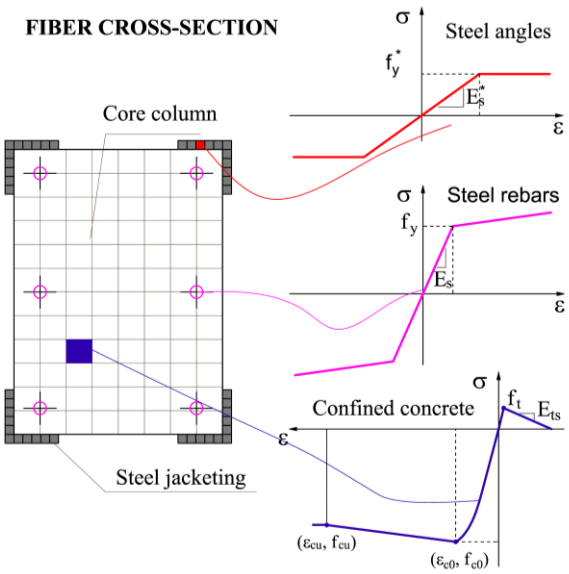

Figure 2.19. Definition of the fiber cross section.

The experimental tests described in the previous sections for the specimens reinforced with steel jacketing were simulated with the aid of the *OpenSees* platform software, making use of force-based nonlinear beam-column fiber-section elements. The internal and external restraining conditions were properly reproduced as well as the loading conditions occurring in the actual tests (Fig. 2.20). For the axial compressive tests (Fig. 2.20 b), only the internal length (between the heads) was considered. The different stirrup spacing occurring in segments 1–3, 4–2, and 3–4 was included in the models defining two different cross sections, with constitutive laws for concrete accounting for the respective confinement levels. For the eccentric compressive tests, the model was slightly modified to introduce eccentric loading conditions. In this case, the heads of the specimens were also modeled using rigid links at segments 1-7-6 and 2-8-5 (Fig. 2.20 c). The increases of the displacement were imposed on the nodes 2 and 5 for the simulations of the axial and eccentric tests, respectively.

The *Concrete 02 model*, implemented in *OpenSees*, was used for concrete fibers. The confined stress and strain values for the different segments of the specimens were calculated as described in the previous section and are reported in Table 2.9. For steel rebars and angles, the *OpenSees Steel 02* model was used.

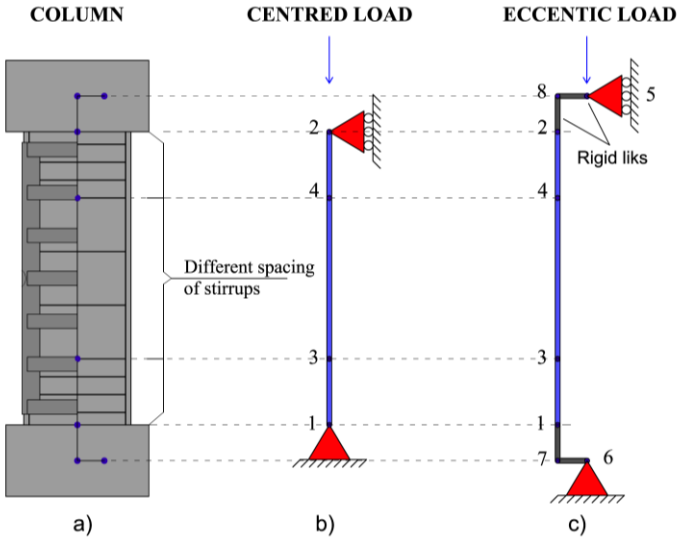

Figure 2.20. Definition of the numerical models in *OpenSees* for the numerical simulation of the tests; (a) physical scheme, (b) axial compressive tests, (c) eccentric compressive tests.

Before formulating specific stress-strain laws for the angles, preliminary numerical simulations of the compressive tests were carried out, hypothesizing two limit cases. For the first case, the perfect end connection of angles was considered. Nominal steel yielding stress and elastic moduli were attributed to the elasto-plastic stress-strain law of the angles. The overall confinement effect was also included in the concrete law. For the second case, the strength contribution provided by the angles was neglected (steel angles removed from the fiber cross section model), considering only their confinement action, as suggested by Eurocode 8 and the Italian Technical Code.

Numerical simulations were compared with the experimental results of the axial compressive tests discussed previously for specimens with steel jacketing.

Table 2.9. Confined concrete stress and strain for different segments of the specimens.

Concrete type A							
Segments	$f_{le,x}$ (MPa)	$f_{le,y}$ (MPa)	k	f_{cc} (MPa)	f_{ccu} (MPa)	ε_{cc}	ε_{ccu}
3-4	2.51	1.82	1.54	19.5	18.0	0.00200	0.0480
1-3/2-4	3.78	2.73	1.81	23.0	21.0	0.0240	0.0380
Concrete type B							
Segments	$f_{le,x}$ (MPa)	$f_{le,y}$ (MPa)	k	f_{cc} (MPa)	f_{ccu} (MPa)	ε_{cc}	ε_{ccu}
3-4	2.51	1.82	1.2	28.8	24.5	0.0065	0.0240
1-3/2-4	3.78	2.73	1.58	38.0	34.5	0.0130	0.0210

The results of the comparisons are shown in Fig. 2.21 for the two different types of concrete. As was expected, the two limit hypotheses constituted two boundary conditions with respect to the experimental results. This allowed two main considerations: (1) if steel angles are not connected at the ends, their contribution to the overall strength is lower but non-negligible (as technical codes recommend); and (2) steel angles absorb a portion of the load that depends on the tangential stresses transferred along contact surfaces. In consideration of this, the definition of a proper stress-strain law necessarily has to account for frictional phenomena occurring.

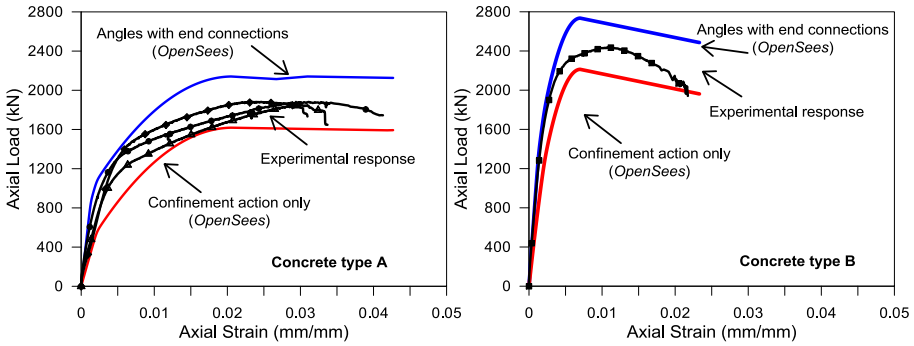

Figure 2.21. Comparisons between experimental results and numerical limit curves for concrete type A and type B.

Proposed Equivalent Stress-Strain Model for the Angles

Based on the previous considerations, the proposed stress-strain model starts from two main assumptions: (1) the interface mortar between steel angles and concrete provides a cohesive strength c_0 along the contact surface, and (2) frictional forces are also developed and depend on the lateral confinement pressure f_{le} (exerted by the steel jacketing because of the core expansion) through the friction coefficient μ.

As a consequence of this, the normal stresses acting on the columns (Fig. 2.22 a) are partially transferred to the angles as tangential stresses (Fig. 2.22 b), which follow a Mohr-Coulomb type law (Fig. 2.22 c). In this case, the stresses transferred to the angles through the interface may not exceed the stress value $\tau_{\max}$, which can be calculated as follows:

$$\tau_{\max} = c_0 + \mu \cdot f_{le} \tag{2.7}$$

where f_{le} = minimum of lateral confinement pressures determined by:

$$f_{le} = \min(f_{le,x}; f_{le,y}) \tag{2.8}$$

in which:

$$f_{le,x} = k_e \cdot \rho_{st,x} \cdot f_{yb}; \qquad f_{le,y} = k_e \cdot \rho_{st,y} \cdot f_{yb} \tag{2.9}$$

After the achievement of the maximum tangential stress τ_{max}, the lateral confinement pressure remains constant and equal to f_{le}, whereas the vertical deformation continues to increase. Beyond this limit stress value, the angles start sliding without absorbing further increases of vertical load.

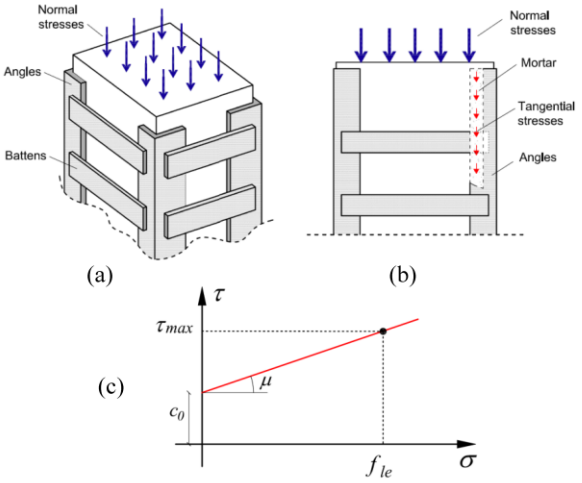

Figure 2.22. Stress transfer to steel angles: (a) normal stresses on column; (b) tangential stresses transferred along the interface; (c) Mohr-Coulomb type model for tangential stresses.

Because of this tangential stress distribution, the maximum loading capacity of the angles (P^*_a) is evaluable by imposing the equilibrium equation of the angles along the direction of the contact surface; that is:

$$P_a^* = 2 \cdot n_a \cdot l_1 \cdot l_0 \cdot \left(c_0 + \mu \cdot f_{le}\right) \qquad (2.10)$$

in which n_a is the number of the angles, l_1 is the internal side of the angles in contact with the concrete column, l_0 is the overall vertical length along the columns.

When the maximum load P^*_a is achieved, the maximum normal stress acting on the cross section of angles is:

$$f_y^* = \frac{P_a^*}{A_a} \qquad (2.11)$$

where A_a is the total cross-section area of the angles.

The nominal yielding stress of steel constituting angles is thus substituted by the stress f^*_y and the elastic perfectly plastic constitutive model proposed is used instead of the nominal one.

Because f^*_y depends on the extension of the contact lengths (l_0 and l_1) and frictional properties (c_0 and μ), large values of these parameters may result in f^*_y values exceeding the nominal yielding strength of the angles. In this case, the yielding stress of steel is used ($f^*_y \leq f_{ya}$).

The elastic modulus E^*_s, defining the slope of the linear branch, can be determined by evaluating the strain ε^*_y, in correspondence of which the angles start sliding. It was experimentally observed that the sliding of the angles occurred in correspondence with an axial strain value close to the unconfined strain at the stress peak ε_c. The suitability of this value was also confirmed by the numerical simulations shown in Fig. 3.14. Therefore, if one sets $\varepsilon^*_y=\varepsilon_c$, the elastic modulus is:

$$E_s^* = \frac{f_y^*}{\varepsilon_c} \tag{2.12}$$

Therefore, the cohesion value c_0 = 0.10 MPa was adopted as suggested by Adam et al. (2007). As also mentioned by the authors, this value is intended as an upper bound in consideration of the fact that the tests are pseudo static. Lower values of cohesion could be adopted (up to 0) to consider severe cyclic damage of the interface.

The determination of the friction coefficient was instead carried out simulating the axial compressive tests of the specimens with steel jacketing for different values of μ. Numerical responses were then compared with experimental results (Fig. 2.23). The comparisons of experimental and numerical results highlight that the overall load-carrying capacity of the reinforced columns significantly depended on the friction coefficient values used to define the capacity models of the angles. For both types of concrete, very good matching between numerical and experimental curves was found using the friction coefficient value μ=0.4. This is consistent with the experimental and numerical determinations from other studies. For example, Baltay and Gjelsvik (1990) and Adam et al. (2007) found that for this kind of reinforcement system, the friction coefficient could vary in the range 0.2–0.6. Similarly, Badalamenti et al. (2010) suggested the value 0.5 for the friction coefficient. In the latter study, however, the authors neglected the influence of cohesion and thus the lower value here obtained appears to be consistent and probably more realistic.

In Figs. 2.23 a-b the contribution of the angles to the overall response is also shown as a function of the friction coefficient. The results (loads and stresses on the angles) are also reported in Table 2.10.

Table 2.10. Load and stress values on the angles obtained by the proposed model.

Concrete type	c_0 (MPa)	μ	f_{le} (MPa)	P_a* (kN)	f_y* (MPa)	f_y*/f_{ya}*	ε_y*	Es* (MPa)
A	0.1	0.2	1.82	152.2	80.12	0.29	0.004	20030.31
		0.4		271.7	142.97	0.52	0.004	35744.84
		0.6		391.1	205.83	0.75	0.004	51459.36
B	0.1	0.2	1.82	152.2	80.12	0.29	0.0025	32048.50
		0.4		271.7	142.97	0.52	0.0025	57191.74
		0.6		391.1	205.83	0.75	0.0025	82334.98

By assuming μ=0.4, the percentages of the total load carried by the angles were 13.1% for concrete Type A and 10.4% for concrete Type B. Such a contribution is not negligible if one considers that in real cases, the load capacity of the angles increases with the length of the columns (and hence of the contact length) and that Eurocode 4 states a lower bound of 20% to consider the hybrid cross section in the case of perfect end connections.

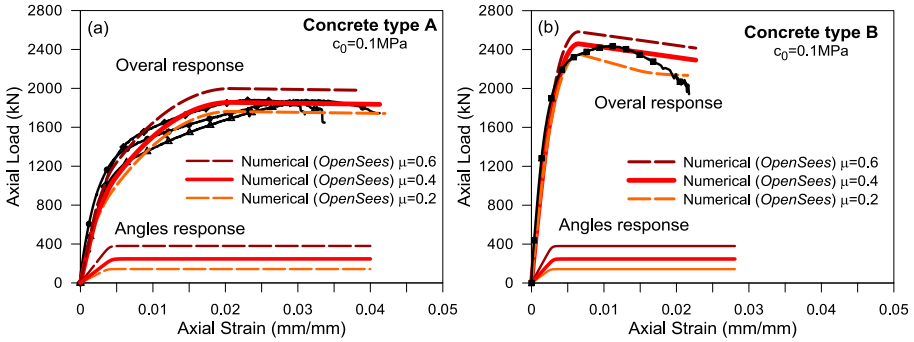

Figure 2.23. Overall column responses varying friction coefficient: (a) concrete type A; (b) concrete type B.

It can also be observed that for both cases, the choice of setting the sliding strain ε*$_y$ equal to ε_c was suitable because it properly allows individuating the change of slope occurring in correspondence with the sliding of the angles.

Effectiveness of the model in presence of bending

The effectiveness of the model when bending occurs was observed simulating the eccentric compressive tests previously presented for the

reinforced specimens. The parameters previously calibrated in pure compression for the friction coefficient (μ=0.4) and cohesion (c_0 = 0.1 MPa) were still used here. The comparisons, regarding both the eccentric loading conditions along the x (e_x=65 mm) and y (e_y=55 mm) directions revealed (Fig. 2.24) quite good accuracy in predicting initial stiffness, peak load, and post-peak branch for all the cases considered. A low discrepancy between experimental and numerical response was observed only in correspondence with the strain at peak load. This is attributed to the moderate dispersion affecting the experimental values of the peak strain.

This, besides proving the adequacy of the model to be used in combined axial load and flexure, also confirmed the suitability of the calibration made for the values of friction coefficient and cohesion, at least for the cases considered here.

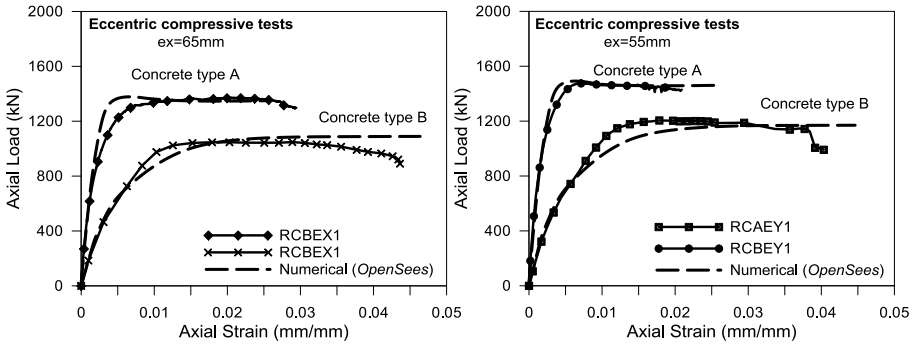

Figure 2.24. Comparisons between experimental and numerical results for eccentric compressive tests.

2.2.4 Analytical approach for the definition of Moment-axial force ultimate domains

The stress-strain model proposed for the angles can also be used to write simplified equilibrium equations of a reinforced cross section that can be specialized to provide axial force-bending moment domains, which are very useful in practice. The stress-block model can be used for concrete in compression after a proper calibration of the stress-block parameters α and β, modulating the static equivalence between the actual confined stress-strain curve and the rectangular one (Fig. 2.25). The stress-strain model for steel rebars is still assumed to be elasto-plastic with linear strain hardening.

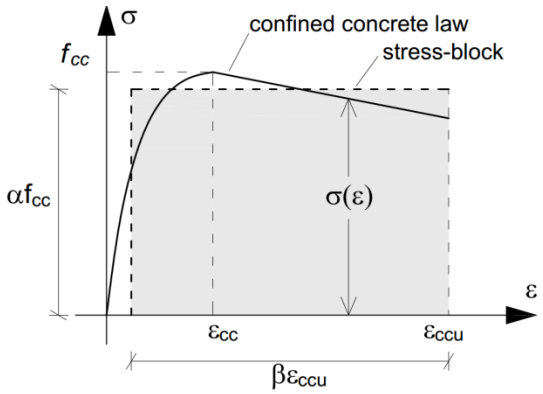

Figure 2.25. Equivalence of the stress-block with the actual confined concrete stress-strain curve.

Calibration of the stress-block parameters

Stress-block parameters can be calibrated for a specified confined concrete law as a function of the increment factor *k* resulting from the confinement. To write equilibrium equations, it is more practical to calibrate the product $\alpha\beta$ (instead of α) and β. The generic expressions for these two parameters, which result in imposing the equivalence of areas and resulting moments, are (Karthik and Mander, 2011).

$$\alpha\beta = \frac{\int_0^{\varepsilon_{ccu}} \sigma(\varepsilon)\cdot d\varepsilon}{f_{cc}\cdot\varepsilon_{ccu}}; \qquad \beta = 2 - 2\frac{\int_0^{\varepsilon_{ccu}} \sigma(\varepsilon)\cdot\varepsilon\cdot d\varepsilon}{\varepsilon_{ccu}\int_0^{\varepsilon_{ccu}} \sigma(\varepsilon)\cdot d\varepsilon} \tag{2.13}$$

As for the numerical case, a simple Kent-Park type stress-strain model for concrete (Kent and Park 1971) is adopted. This is governed by the following expressions:

$$\sigma(\varepsilon) = \begin{cases} f_{cc}\left[2\left(\frac{\varepsilon}{\varepsilon_{cc}}\right) - \left(\frac{\varepsilon}{\varepsilon_{cc}}\right)^2\right] & 0 \le \varepsilon \le \varepsilon_{cc} \\ f_{cc}\left[1 - 0.15\frac{\varepsilon - \varepsilon_{cc}}{\varepsilon_{ccu} - \varepsilon_{cc}}\right] & \varepsilon_{cc} \le \varepsilon \le \varepsilon_{ccu} \end{cases} \tag{2.14}$$

By normalizing Eq. 2.14 with respect to the confined concrete strength f_{cc} and defining the normalized variable $\tilde{\varepsilon} = \varepsilon / \varepsilon_{cc}$ Eq. 2.14 can be rewritten in dimensionless form as:

$$s(\tilde{\varepsilon}) = \begin{cases} f_{cc}\left(2\cdot\tilde{\varepsilon} - \tilde{\varepsilon}^2\right) & 0 \le \tilde{\varepsilon} \le 1 \\ \left(1 - 0.15\dfrac{\tilde{\varepsilon} - 1}{\mu_c - 1}\right) & 1 \le \varepsilon \le \mu_c \end{cases} \tag{2.15}$$

where $s(\tilde{\varepsilon})$ is the generic normalized stress, $\mu_c = \varepsilon_{ccu} / \varepsilon_{cc}$ is the ductility factor of the concrete.

Based on the previous positions, the stress-block coefficient expressions become:

$$\alpha\beta = \frac{\int_0^{\mu_c} s(\tilde{\varepsilon})\cdot d\tilde{\varepsilon}}{\mu_c}; \qquad \beta = 2 - 2\frac{\int_0^{\mu_c} s(\tilde{\varepsilon})\cdot\tilde{\varepsilon}\cdot d\varepsilon}{\mu_c \cdot \int_0^{\mu_c} s(\tilde{\varepsilon})\cdot d\tilde{\varepsilon}} \tag{2.16}$$

The latter depend on the ductility factor μ_c and implicitly on the increment factor *k*; that is (Mander et al., 1988):

$$\varepsilon_{cc} = \varepsilon_c\left[1 + 5(k-1)\right] \tag{2.17}$$

To provide a tool for the direct estimation of the stress-block coefficients $\alpha\beta$ and β, a parametric study of Eq. (2.16) was carried out by varying parameters *k* and μ_c. Results are shown in the diagrams reported in Fig. 2.26.

The product $\alpha\beta$ (Fig. 2.26 a) does not depend on the increment factor *k* but is influenced only by the ductility factor. In detail, $\alpha\beta$ increases with μ_c but with a lower rate of change as the values of ductility grow. With regard to β, it is noteworthy that its trend is instead influenced by the parameter *k*, but only for the lower ductility values. The diagrams in Fig. 2.26 can also be used for rapid calculation of the stress-block parameters.

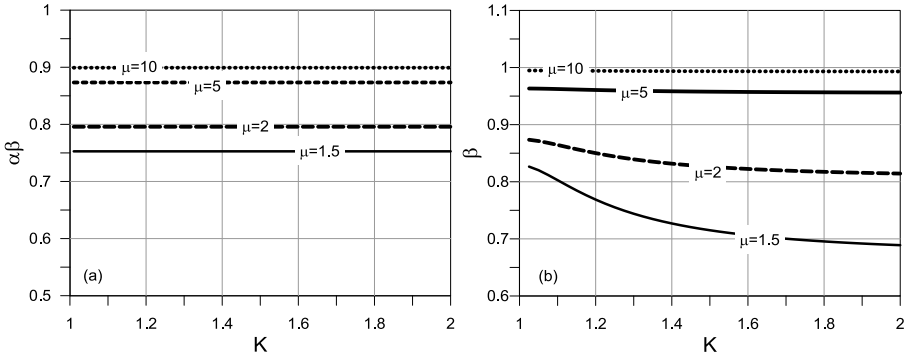

Figure 2.26. Diagrams for calculation of stress-block parameters for different values of *k* and μ.

Ultimate domains

With reference to the geometry described in Fig. 2.27 and the stress-strain laws assumed for the materials, the equilibrium equations of the reinforced cross-section (translational and rotational with respect to the lower rebars centroid) can be written in the following form:

$$N_u = \alpha \cdot \beta \cdot b \cdot x_c \cdot f_{cc} + A'_s \cdot \sigma'_s + A'_a \cdot \sigma'_a - A_s \cdot \sigma_s - A_a \cdot \sigma_a \qquad (2.18)$$

$$M_u = \alpha \cdot \beta \cdot b \cdot x_c \cdot f_{cc} \cdot \left(d - \frac{\beta \cdot x_c}{2} \right) + A'_a \cdot \sigma'_a \cdot \left(d + t - l/4 \right) + \\ + A'_s \cdot \sigma'_s \cdot \left(d - \delta \right) + A_a \cdot \sigma_a \cdot \left(\delta + t - l/4 \right) - N_u \left(\frac{d - \delta}{2} \right) \qquad (2.19)$$

where x_c is the neutral axis distance with respect to reference most compressed concrete fiber, σ'_s and σ_s are the stresses on the upper and lower rebars, A'_s and A_s are the respective areas, σ'_a and σ_a are the stresses on the upper and lower angles and A'_a e A_a the respective areas.

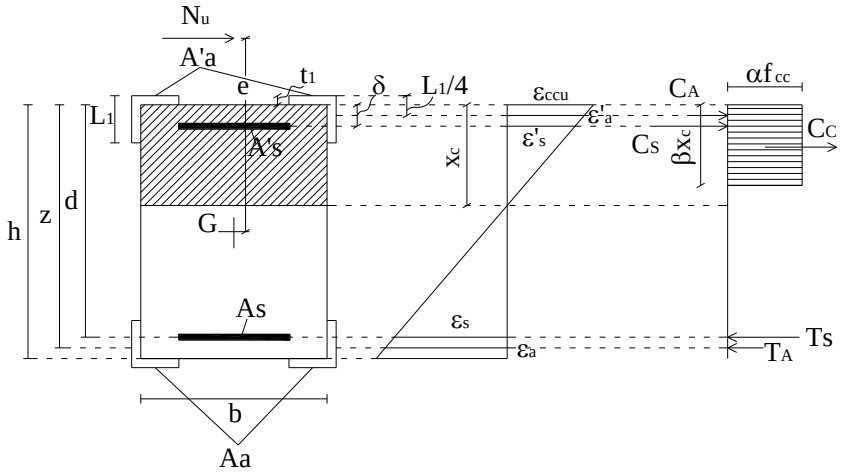

Figure 2.27. Ultimate state equilibrium of the reinforced cross-section.

In the previous equations it is assumed that the mechanical response of the angles is supposed to be concentrated in correspondence of the centroid, which is located at the distance *l/4* from the edge. The other symbols can be easily deduced from the geometry illustrated in Fig. 2.27. Eqs. 2.18 and 2.19 can be specialized considering the limit state regions conditions shown in Fig. 2.28 to define analytical continuous and/or simplified axial force – bending moment domains.

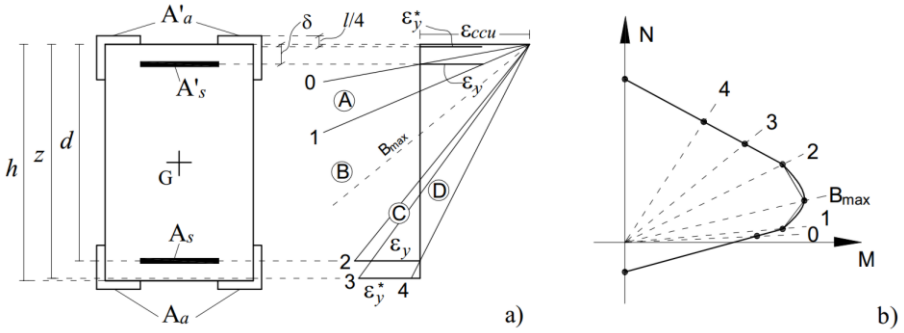

Figure 2.28. Definition of ultimate domains: a) Limit state regions for the reinforced cross-section; b) Typical continuous and simplified domains.

With reference to Fig. 2.28, continuous values of M_u and N_u are evaluable referring to the stress and strain limits reported for regions A to E, varying

each time the neutral axis position between the limit values given by the limit conditions. The definition of further limit conditions, although possible, results not significant to increase the accuracy of the domains. In Fig. 2.27 ε'_a and ε_a are the generic strains of upper and lower angles, ε'_s and ε_s are the generic strains of upper and lower rebars and $z = h + t - l/4$ is the distance between the most compressed concrete fiber and the centroid of the angles in tension.

For both continuous and simplified domains the limit conditions of pure compression and pure tension have to be added. For these conditions the equilibrium equations assume the form:

$$N_u = b \cdot h \cdot f_{cc} + 2 \cdot A_a \cdot f_y^* + 2 \cdot A_s \cdot f_y; \qquad M_u = 0; \left(x_c = +\infty\right) \tag{2.20}$$

$$N_u = -2 \cdot A_a \cdot f_y^* - 2 \cdot A_s \cdot f_y; \qquad M_u = 0; \ \left(x_c = -\infty\right) \tag{2.21}$$

At the same time a simple linearized form of the domain can be obtained by evaluating the limit values M_u and N_u only in correspondence of the boundary conditions (0 to 2) reported in Fig. 2.28. Condition B_{max} has to be also considered in this case, being this the one associated to the maximum bending moment capacity occurring in correspondence of the ultimate axial load $N_u = 0.5 \cdot \alpha \cdot f_{cc} \cdot b \cdot h$.

It can be simply proved that the bending moment in question is:

$$M_{u,B_{\max}} = \frac{\alpha \cdot b \cdot h^2 \cdot f_{cc}}{8} + A'_a \cdot f_y^* \cdot \left(d + t - l/4\right) + \\ + A'_s \cdot f_y \cdot \left(d - \delta\right) + A_a \cdot f_y^* \cdot \left(\delta + t - l/4\right) \tag{2.22}$$

The validation of the analytical formulation was carried out for the steel jacketed four specimens subjected to eccentric axial loading of the experimental investigation described in section 2.2.2. Fig. 2.29 shows the experimental values of the peak axial loads and the associated moments (obtained as maximum axial load multiplied for the fixed eccentricity) together with the ultimate domains of the cross sections obtained with the proposed analytical continuous and simplified procedures. For the definition of the equivalent stress-strain response of the angles, the frictional parameters previously calibrated (c_0=0.10 MPa and μ=0.4) were used, together with the corresponding stress limits for f^*_y presented in Table 2.11.

In Fig. 2.29, the experimental results of the centered compressive tests carried out for the retrofitted specimens are also reported. Also, the numerical domains, obtained from the fiber discretization in *OpenSees*

according to the proposed model, are shown in the same diagram. For both numerical and analytical domains, the confinement and stress-block parameters (referring to the specimens) were those reported in Table 2.12.

Table 2.11. Confinement and stress-block parameters for the specimens.

Concrete type	k	μ_c	$\alpha\beta$	β
A	1.54	2.4	0.811	0.863
B	1.20	3.7	0.842	0.960

The comparison shows very good reliability achieved by both analytical and numerical methods. Experimental, analytical, and numerical values are also compared in Table 2.12. Also, the simplified analytical approach for the fast definition of the domains is effective without losing accuracy. In conclusion, the level of approximation reached provides reliable estimations by the use of the proposed methods.

Table 2.12. Experimental centered and eccentric test values of axial force and bending moments and respective values predicted by the numerical and analytical domains.

	Experimental		Numerical		Analytical	
Specimen	P_0 (kN)	M_0 (kNm)	P_0 (kN)	M_0 (kNm)	P_0 (kN)	M_0 (kNm)
RCA1	1864.63	0				
RCA2	1882.12	0	1855.85	0	1860.52	0
RCA3	1880.45	0				
RCAEX1	1047.63	57.61	1040.35	57.46	1089.63	61.30
RCAEY1	1205.34	78.34	1169.99	79.92	1197.71	81.04
RCB1	2439.50	0	2459.18	0	2474.32	0
RCBEX1	1370.32	75.36	1310.98	72.28	1400.00	75.40
RCBEY1	1476.04	95.94	1491.76	96.11	1430.51	97.43

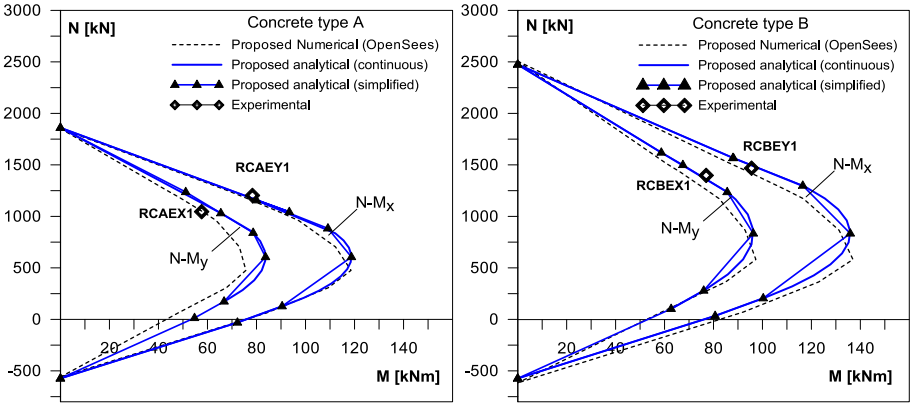

Figure 2.29. Comparison of experimental results with definition of ultimate domains.

As an ending of this chapter, comparisons between the proposed model and experimental results available in the literature are shown. Here, the compressive behavior of the confined concrete is evaluated in both cases of angles fully loaded (including buckling effects) or indirectly loaded, taking into account frictional effects (Fig. 2.30).

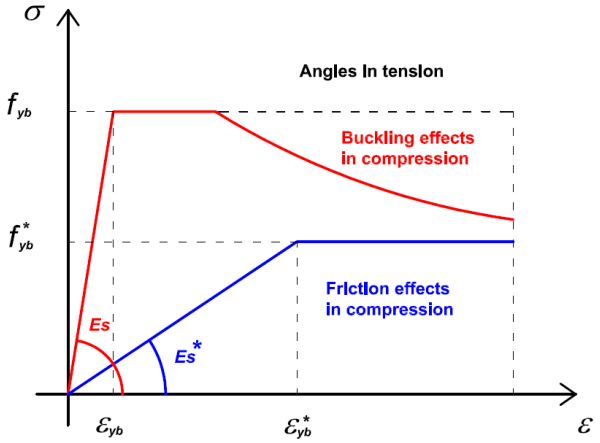

Figure 2.30. Stress-strain response of directly and indirectly loaded angles.

Geometrical and mechanical parameters of the specimens are reported in Tables 2.13-2.14. The symbols assumed for specimens are referred to the respective authors. In particular symbols C1-C15 correspond to Cirtek et al. (2001), A1-2 to Adam et al. (2007, 2009), M1-2 to Belal et al. (2015), T1-8

to Tarabia and Albakry (2014), Ca1-3 to Campione (2012, 2013) and F1-F4 the experimental results presented in the previous section.

The comparisons between analytical and experimental results are shown in Fig. 2.31 (a-b) in terms of ultimate total axial load composed by confined concrete and angles contribute. In both cases the model returns a good agreement in predicting the maximum capacity of the strengthened specimens, especially in the case of angles with no-end connections.

Table 2.13. Geometrical and mechanical characteristics of the strengthened specimens with end connections.

Spec.	Column	Battens	Angles		Internal reinforcement		Concr.	N exp
	b x h x l (mm)	s_2 t_2 s_b (mm)	l_1 l_0 (mm)	f_{yb} (MPa)	Φ_l s_i (mm)	f_{yk} (MPa)	f_c (MPa)	kN
Ca1	215x215x 600	40x3 560	30x3 600	239	12 200	461	10.00	2050
Ca2	215x215x 600	30x3 300	30x3 600	239	12 200	461	10.00	2400
Ca3	215x215x 600	30x3 200	30x3 600	239	12 200	400	10.00	1850
A2	300x300x 2500	160x8 475	80x8 2500	275	12 200	420	10.60	1750
T1	150x150x 1000	50x5 170	50x4.5 1000	415	10 100	420	57.80	2100
T3	150x150x 1000	50x5 260	50x4.5 1000	415	10 100	420	57.80	2050
T4	150x150x 1000	50x5 170	50x4.5 1000	415	10 100	420	57.80	1800
T5	150x150x 1000	50x5 170	30x3 1000	485	10 100	420	47.50	2500-2100
T7	150x150x 1000	50x5 260	30x3 1000	485	10 100	420	47.50	2550-2300
T8	150x150x 1000	50x5 170	30x3 1000	485	10 100	420	47.50	2750-2550

Table 2.14. Geometrical and mechanical characteristics of the strengthened specimens without end connections.

Spec.	Column	Battens	Angles		Internal reinforcement		Concr.	N exp
	b x h x l (mm)	s_2 t_2 s_b (mm)	l_1 l_0 (mm)	f_{yb} (MPa)	Φ_l s_i (mm)	f_{yk} (MPa)	f_c (MPa)	kN
C1	300x300x 1500	55x6 220	60x6 /	288	14 200	501	12	2050
C2	300x300x 1500	50x6 150	60x6 /	288	14 200	501	12	2400
C3	300x300x 1500	50x6 275	60x6 /	288	14 200	501	12	1850
C4	300x300x 1500	50x6 400	60x6 /	288	14 200	501	12	1750
C5	300x300x 1500	55x10 220	60x6 /	288	14 200	501	12	2100
C6	300x300x 1500	70x5 220	60x6 /	288	14 200	501	12	2050
C7	300x300x 1500	40x5 220	60x6 /	288	14 200	501	12	1800
C8	300x300x 1500	55x6 220	60x6 1450	288	14 200	501	12	2500-2100
C9	300x300x 1500	50x6 220	40x5 1450	288	14 200	501	12	2550-2300
C10	300x300x 1500	50x6 220	50x5 1450	288	14 200	501	12	2750-2550
C11	300x300x 1500	50x6 220	70x8 1450	288	14 200	501	12	3050-2650
C12	300x300x 1500	60x6 195	60x6 1450	288	14 200	501	12	2870
C13	300x300x 1500	60x6 195	60x6 1450	288	14 200	501	12	2575
C14	300x300x 1500	60x6 195	60x6 1450	288	14 200	501	12	2917
C15	300x300x 1500	60x6 195	60x6 1450	288	14 200	501	12	2533
A1	300x300x 2500	160x8 475	80x8 2500	275	12 200	400	10.6	2650
A3	300x300x 2500	160x8 570	80x8 2500	275	12 200	400	8.3	1955
A4	300x300x 2500	160x8 570	80x8 2500	275	12 200	400	12.4	2324
A5	300x300x 2500	160x8 570	80x8 2500	275	12 200	400	15.5	2599
M1	200x200x 1200	100x5 590	50x5 1200	240	12 200	360	34	1821
M2	200x200x 1200	50x5 240	50x5 1200	240	12 200	360	34	1649

T2	150x150x 1000	50x5 170	50x4.5 1000	415	10 100	420	57.8	1990
T6	150x150x 1000	50x5 170	30x3 1000	485	10 100	420	47.5	2000
F1	300x200x8 20	40x4 120	50x5 820	275	12 150	450	12.65	1864.63
F2	300x200x8 20	40x4 120	50x5 820	275	12 150	450	12.65	1882.45
F3	300x200x8 20	40x4 120	50x5 820	275	12 150	450	12.65	1880.45
F4	300x200x8 20	40x4 120	50x5 820	275	12 150	450	24	2439.5

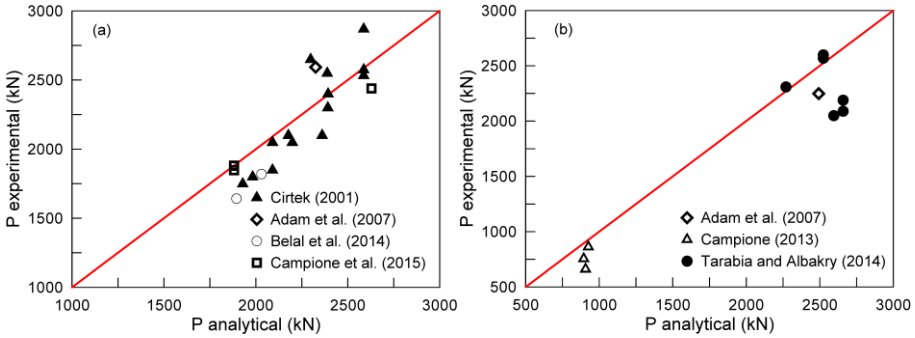

Figure 2.31. Experimental-analytical results of specimens strengthened with no-end connected angles (a) and with end-connected angles (b).

3. FINITE ELEMENT MODELLING OF FRP/STEEL-CONFINED CONCRETE

3.1 Introduction

Previous chapters have shown how the definition of the load-bearing capacity of structural elements subjected to compression loads may be complicate when the effects of confinement cannot be neglected. Especially in the case of FRP confinement rather than steel confinement, where high lateral confinement pressures are generated, sometimes the solution of the problem cannot be determined in an exact form and an iterative process is required to obtain the step-by-step response (Spoelstra and Monti, 2000).

In these situations, classical formulations could be not reliable and higher computational efforts are required to define theoretical basis able to reproduce the experimental behavior. On the other hand, software based on the finite element modeling technique provides high computational capabilities to reproduce complex phenomena. However, the aspect related to the definition of the material properties is of the utmost importance to obtain good results.

This chapter focuses on the aspects concerning the finite element modeling of reinforced concrete columns in cases of external confinement with steel or FRP jacketing through the use of *Simulia* Abaqus software, with detailed attention to the modeling of the materials. In the first part, a brief discussion of the main aspects of the concrete nonlinearity modeling is presented, then an overall analysis of the available studies in the case of FRP/Steel-confined concrete is done before the introduction of a finite element modeling proposal of confined concrete under monotonic compressive loads. Finally, in accordance with the aim of the present thesis, a numerical procedure to reproduce the preloading effects on the load-bearing capacity of confined concrete is proposed and discussed in both cases of elastic confinement (FRP-confined concrete) and elasto-plastic confinement (externally steel-confined concrete).

3.2 Concrete Damaged Plasticity Model

There are different models allowing to define the non-linear mechanical behavior of concrete with the Abaqus software; Drucker-Prager (D-P) type plasticity model and Concrete Damaged Plasticity Model (CDP) are the most reliable models among all the available options of the software. According to the *plasticity theory* the nonlinear behavior of the concrete is identified by three key components: the *yield criterion*, the *hardening/softening rule* and the *flow rule*. More advantages however are achievable by using CDP model thanks to the possibility to take into account the damage effects (according to the *plasticity theory*) including the reduction of the elastic stiffness during the loading process for monotonic and cyclic loads. In the present work, CDP model was used to perform simulation in the case of confinement under monotonic loads.

This model uses the concept of isotropic damaged elasticity in combination with isotropic tensile and compressive plasticity to represent the inelastic behavior of the concrete. CDP is able to properly account for the concrete confinement effect and assumes that the two main failure mechanisms are the tensile cracking and the compressive crushing.

The identification of CDP model parameters for an actual concrete should be carried out starting from uniaxial compression tests, uniaxial tension tests, the knowledge of the failure surface in biaxial plane stress and several triaxial tests of concrete. Many authors investigated the parameters of CDP on the compressive and tensile behavior of the concrete, providing several strategies to define input data in the implementing stages (Sümer and Aktaş, 2015, Szczecina and Winniki, 2015).

As regards to the compressive behavior, the CDP model assumes that the uniaxial tensile and compressive response of concrete is characterized by damaged plasticity, as shown in Fig. 3.1. Under uniaxial tension the stress-strain response follows a linear elastic relationship until the onset of micro-cracking which corresponds to the achievement of the failure stress σ_{t0}. Beyond the failure stress, the formation of micro-cracks is represented by means of a softening stress-strain response. Under uniaxial compression the response is linear until the value of the initial yield σ_{c0} is reached. Then, the post-elastic behavior is typically characterized by stress hardening followed by strain softening.

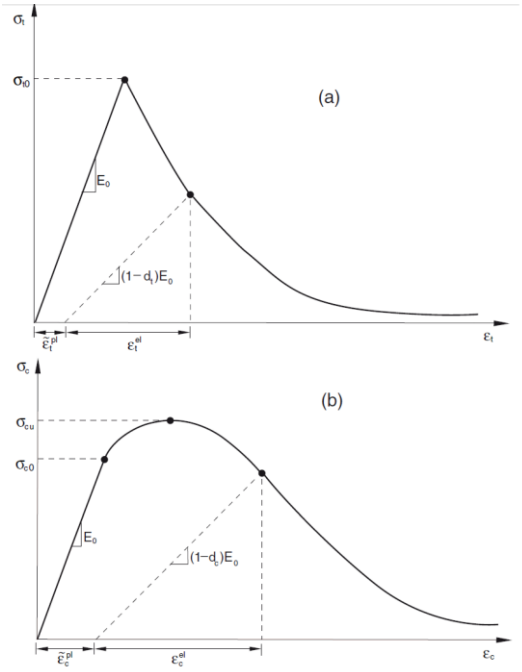

Figure 3.1. Response of concrete under uniaxial tension (a) and compression (b). (Abaqus Theory Guide, 2013)

When the concrete specimen is unloaded from any point on the strain softening branch, the unloading response is characterized by a certain loss of the initial stiffness. Such a degradation of the elastic stiffness is described by means of two *damage variables*, d_c and d_t, which are assumed to be functions of the plastic strains ($\tilde{\varepsilon}_c^{pl}$, $\tilde{\varepsilon}_t^{pl}$).

In detail, in the case of uniaxial tensile stress:

$$\sigma_t = (1-d_t)E_0\left(\varepsilon_t - \tilde{\varepsilon}_t^{pl}\right) \tag{3.1}$$

In the case of uniaxial compression stress:

$$\sigma_c = (1-d_c)E_0\left(\varepsilon_c - \tilde{\varepsilon}_c^{pl}\right) \tag{3.2}$$

The "effective" tensile $\bar{\sigma}_t$ and compressive $\bar{\sigma}_c$ stresses which determine the size of the yield surface can be defined as:

$$\bar{\sigma}_t = \frac{\sigma_t}{(1-d_t)}E_0\left(\varepsilon_t - \tilde{\varepsilon}_t^{pl}\right) \tag{3.3}$$

$$\bar{\sigma}_c = \frac{\sigma_c}{(1-d_c)}E_0\left(\varepsilon_c - \tilde{\varepsilon}_c^{pl}\right) \tag{3.4}$$

As a consequence, the stress-strain relations for the general three-dimensional multiaxial condition are given by the scalar damage elasticity equation:

$$\sigma = (1-d) D_0^{el} : (\varepsilon - \varepsilon^{pl}) \tag{3.5}$$

that, excluding the damage parameters, from the *linear elasticity theory* in which the total stress σ is classically defined from the total elastic strain tensor ε^{el} , becomes:

$$\sigma = D_0^{el} \varepsilon^{el} \tag{3.6}$$

where D_0^{el} is the initial undamaged elasticity matrix. In Eq. 3.5, ε^{pl} represents the plastic strain tensor.

The *yield* criterion defines the yield condition under multiaxial stress state. It makes use of the *yield function* of Lubliner et al. (1989), with the modifications proposed by Lee and Fenves (1998) to take into account the different evolution of strength under tension and compression. In terms of effective stresses, the yield function takes the form

$$F = \frac{1}{1-\alpha}\left(\bar{q} - 3\alpha\bar{p} + \beta\left(\tilde{\varepsilon}^{pl}\right)\left\langle -\hat{\bar{\sigma}}_{\min}\right\rangle - \gamma\left\langle -\hat{\bar{\sigma}}_{\min}\right\rangle\right) - \bar{\sigma}_c\left(\tilde{\varepsilon}_c^{pl}\right) = 0 \tag{3.7}$$

where:

$$\alpha = \frac{f_{b0}/f_{c0} - 1}{2\, f_{b0}/f_{c0} - 1} \tag{3.8}$$

$$\beta = \frac{\bar{\sigma}_c\left(\tilde{\varepsilon}_c^{pl}\right)}{\bar{\sigma}_t\left(\tilde{\varepsilon}_t^{pl}\right)}(1-\alpha)(1+\alpha) \tag{3.9}$$

$$\gamma = \frac{3(1-K_c)}{2K_c - 1} \tag{3.10}$$

In these equations, $\bar{p}$ and $\bar{q}$ are respectively the hydrostatic pressure expressed in terms of effective stresses and the Mises equivalent effective stresses, defined as follow:

$$\bar{p} = -\frac{I_1}{3} = -\frac{(\sigma_{11} + \sigma_{22} + \sigma_{33})}{3} \tag{3.11}$$

$$\bar{q} = \sqrt{3J_2} = \sqrt{3\left(\sigma_{11}^2 + \sigma_{22}^2 - \sigma_{11}\sigma_{22}\right)} \tag{3.12}$$

Furthermore, $\hat{\bar{\sigma}}_{\min}$ is the minimum principal effective stresses; K_c is the ratio between the second stress invariant on the tensile meridian to that on the compressive meridian at initial yield for any given value of the pressure

invariant such that the minimum effective principal stress is positive; $\langle \bullet \rangle$ is the Mecauley bracket defined as $\langle x \rangle = 1/2(|x| + x)$; f_{b0}/f_{c0} is the ratio between the compressive strength under biaxial loading and the uniaxial compressive strength; $\bar{\sigma}_t(\tilde{\varepsilon}_t^{pl})$ and $\bar{\sigma}_c(\tilde{\varepsilon}_c^{pl})$ are the effective tensile and compressive cohesion stresses respectively; $\bar{\sigma}_c(\tilde{\varepsilon}_c^{pl})$ is the compressive strain-hardening/softening function, coming from the *hardening/softening rule*, that determines the evolution of the yield surface with the plastic deformation. $\tilde{\varepsilon}_t^{pl}$ and $\tilde{\varepsilon}_c^{pl}$ are respectively the tensile and compressive equivalent plastic strains. The compressive stresses and strain are considered positive and the tensile stresses and strains are considered negative.

This yield function represents a modification of the Drucker-Prager criterion in the meaning that the failure surface in the deviatoric cross-section needs not to be a circle and it is governed by the parameter K_c. This parameter is always higher than 0.5 and when it assumes the value of 1, the deviatoric cross-section of the failure surface becomes a circle, as in the classic Drucker-Prager strength criterion. The CDP model recommends to assume K_c = 2/3. So doing, the shape of the yield surface (a combination of three mutually tangent ellipses) is similar to the one obtained according to the strength criterion formulated by William and Warnke (1975) that is a theoretical-experimental criterion based on triaxial stress test results.

In Figs 3.2 and 3.3 typical yield surfaces for plane stress conditions and in the deviatoric plane are shown.

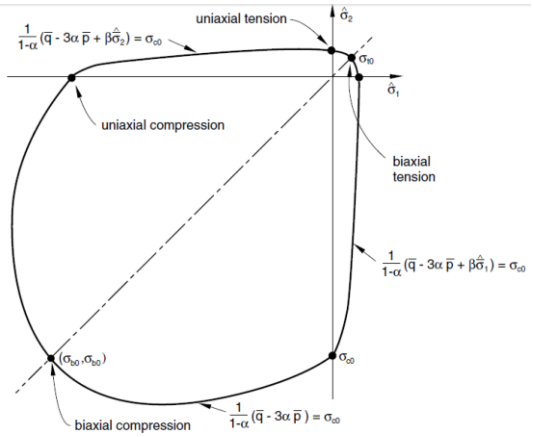

Figure 3.2. Yield surface in plane stress (Abaqus Theory Guide, 2013)

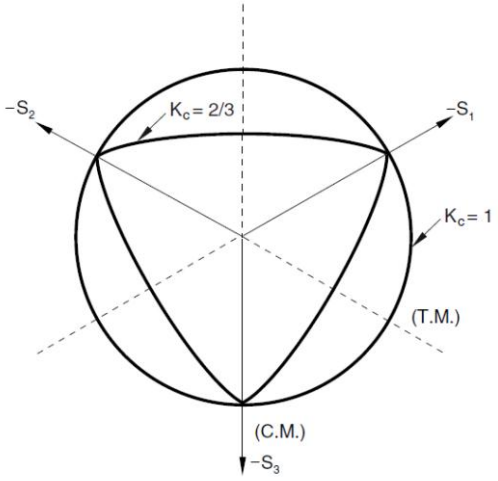

Figure 3.3. Yield surface in deviatoric plane corresponding to different values of K_c (Abaqus Theory Guide, 2013)

The *flow rule* determines the direction of plastic deformation and dictates the evolution of the plastic lateral to plastic axial strain increment. The CDP model assumes *non-associated potential plastic flow*:

$$d\varepsilon_{ij}^{p} = \lambda \frac{\partial G}{\partial \sigma_{ij}}; i, j = 1,2,3 \tag{3.13}$$

The flow potential G used for this model is the Drucker-Prager hyperbolic function:

$$G = \sqrt{\left(e\, f_{t0} \tan\psi\right)^2 + \bar{q}^2} - \bar{p}\tan\psi \tag{3.14}$$

in which ψ is the dilation angle measured in the plane $\bar{p}$ - $\bar{q}$ plane at high confining pressure (Fig. 3.4); f_{t0} is the uniaxial tensile stress at failure; e is a parameter, referred to the *eccentricity*, that defines the rate at which the function approaches the asymptote (the flow potential tends to a straight line as the eccentricity tends to zero). This flow potential, which is continuous and smooth, ensures that the flow direction is always uniquely defined.

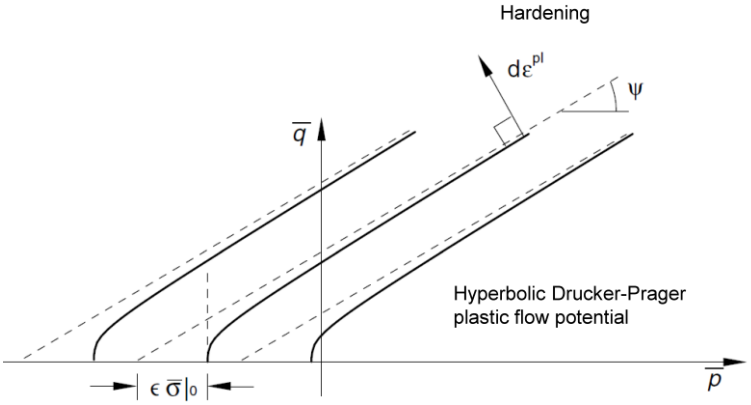

Figure 3.4. Family of hyperbolic flow potential in the meridian plane

3.3 FEM of externally-confined concrete. Available studies

In the last decade several authors focused the computational aspects concerning the implementation of a Steel and/or FRP-confined concrete model in Abaqus. Most of the available studies have been carried out using *Drager-Prager Plasticity Model* (e.g. Karabins et al., 2008, Yu et al., 2010a, Wu and Jang, 2012, Youssf et al., 2014, Jang and Wu, 2014). The available studies highlighted that in presence of high confining pressures the plasticity model need to be recalibrated to adequately take into account triaxial compressive state of concrete.

The same considerations were found for *Concrete Damaged Plasticity Model* for which some resources are available in literature (Papanikolau and Kappos, 2007, Yu et al., 2010b, Tao et al., 2013, Hany et al., 2016, Ozbakkaloglu et al., 2016, Kabir and Shafei, 2012, Michal and Andrzej, 2015).

Yu et al. (2010a,b)

Yu et al. provided two companion paper (2010a,b) in which the FE modeling of concrete including Dracker-Prager (D-P) type plasticity model and Concrete Damaged Plasticity model (CDP) is in depth discussed and analyzed.

The interesting aspects provided by the authors are the lack in reproducing actual behavior of concrete subjected to tri-axial stress state by assuming default parameters of the program. In fact, plasticity modeling of concrete, as discussed in the previous section, was defined for concrete at low confining pressure (Lubiner et al., 1989), therefore, when the concrete is subjected to high confining pressure, the plasticity parameters provided for the unconfined concrete are not suitable and need to be accurately modified.

The authors analyzed in depth the aspect related to the definition of the plasticity formulation for concrete and provided a procedure to obtain confining pressure-dependent parameters in function of the mechanical properties of the confining jackets.

This procedure is possible with Abaqus by using "Solution-dependent field variables" (SDFV) that allow using the "user-defined subroutine USDFLD". A solution-dependent field variable is a field variable that varies throughout the solution process (such as the displacement and the stresses). This facility provides the flexibility for the material models in Abaqus to account for additional material characteristics.

The SDFV was adopted by the authors to define the dependence of strain hardening/softening on the confining pressure and the dependence of the flow rule on the confining pressure, plastic deformation and the rate of the confinement increment. The procedure is briefly described hereinafter:

- first step - a series of axial stress-strain relationships of actively-confined concrete are obtained for various active confining pressures for a given values of unconfined concrete strength and the corresponding strain of concrete (using Teng et al., 2007 model);
- second step - the corresponding axial stress-plastic strain relationships of concrete for different confining pressures based on initial elastic modulus and the initial Poisson ratio are obtained;
- third step - these relationships are used as input into Abaqus in the required format (the confining pressure dependent conditions are defined using SDFV option);

The unconfined stress-strain law for concrete assumed by the authors is elastic-perfectly plastic type.

At the end of the paper the authors demonstrated that by assuming a non-associated flow rule is adequate to reproduce compressive behavior of actively-confined concrete, but causes not representative results in the case of FRP-confined concrete.

Tao et al. (2013)

The authors investigated the compressive behavior of concrete-filled steel stub columns and highlighted the challenge in the finite element modeling because of the problems related to the passive confinement effects on the concrete stress-strain behavior. The authors stated that it is impossible to obtain an accurate evaluation of the lateral strain and axial strain of the confined concrete during compression tests and they tried to perform a simplified finite element modeling by means of Abaqus software in which Damaged Plasticity Model for Concrete was used.

The authors discussed the main aspect of the CDP model when implemented to reproduce compressive behavior of CFST[6] columns. In detail, the shape of the yield surface of the concrete plasticity model, the dilation angle and the strain hardening/softening function were analyzed and assessed.

Regarding the shape of yield surface, the parameter *Kc* was assumed according to Yu et al. (2010a) depending on uniaxial compressive strength of concrete.

The dilation angle, that defines the plastic flow potential, and in particular its influence on the compressive response of the confined concrete was investigated firstly by a parametric sensitive analysis and then by means of a regression analysis. An empirical equation was proposed to obtain the dilation angle in function of the mechanical confinement ratio.

Regarding the strain hardening/softening function, the authors observed that, by implementing the actual unconfined concrete stress-strain law in compression, almost identical slopes of strain softening were obtained for concrete under different constant active confinement pressures. This aspect is obviously not consistent with the experimental observations that evidence that in descending branches the slopes are lesser when the confining pressure

[6] CFST Columns refers to Concrete Filled Steel Tubular Columns

increases. On the basis of what above described, they proposed a new strain hardening/softening function for the concrete depending on the mechanical confinement ratio to obtain a better agreement with experimental results. In particular, the stress-strain law proposed by Samani and Attard (2012) was used to obtain the first branch up to the peak strength, while, modification of the second branch of the stress-strain law was performed using stress-strain law proposed by Binici (2005), in which the slope of the softening branch was modified in function of the mechanical confinement ratio.

Teng et al. (2015)

The authors provided an interesting scientific contribute to the finite element modeling techniques used to reproduce the compressive behavior of FRP and/or Steel confined circular concrete columns considering the presence of internal discrete steel reinforcement.

The model adopted for the concrete was a plastic damage concrete model according to Yu et al. (2010b) in which the relationship for the determination of the lateral confinement pressure was replaced by Jang and Teng (2007) model, that was more suitable in the case of weakly confined concrete.

Moreover, the authors focus the main aspect of the stress distribution on 3D elements depending on the type of end-restrains. Different from Yu et al. (2010b) that modeled only a slice instead of the entire column, the authors stated that the theoretical approach used by Yu et al. (2010b) could be suitable to reproduce the average behavior of the mid-height region of a column, but cannot represent the non-uniform deformation over height.

They demonstrated that without the inclusion of end-restrain in the 3D FE model, the distribution of both axial displacement and stresses are uniform, while with end-restraints the distribution become highly non-uniform in axial and radial directions. This fact produces lower values of axial stresses for a given value of hoop strains compared to that obtained from Jang and Teng (2007) model. Therefore, end-restrains have negative effects on the response of FRP-confined plain concrete cylinders in terms of strength and strain capacity. In order to have an accurate reproduction of the compressive behavior of the confined concrete regarding axial stress-strain curves and lateral strain-to-axial strain prediction, equation proposed by Jang and Teng (2007) was recalibrated so that to include the end restrains in the FE model. Moreover, after the assessment of the compressive capacity of FRP-confined concrete, particular attention was made to the confined

mechanism provided by the internal reinforcement. Differently from Yu et al. (2010b), this new approach was capable to obtain also compressive curves with strain-softening behavior. It has to be remembered that in the previous work, the unconfined concrete stress-strain law used as input parameter was parabolic up to the peak unconfined strength and then a perfectly plastic behavior was considered for FRP-confined concrete, therefore, the FE model was not able to predict softening behavior.

Hany et al. (2016)

The authors provided a numerical proposal to reproduce the compressive behavior of FRP-confined concrete using modified concrete damaged plasticity model with Abaqus software. Their approach was to highlight the limitation of the CDP model when used for confined concrete and proposed simplified strategies to overcome the problems in reproducing the compressive behavior in the case of active and passive confinement. The proposed model was suitable for application to different type of cross-sections and for concrete characterized by low or high strength.

The authors investigated all the aspect concerning the implementation of FRP-confined concrete model in Abaqus, focusing on the nonlinear mechanical properties of the concrete.

Considering the behavior of the concrete, according to previous researches, it was demonstrated that the compression hardening/softening rule is one of the most important parameters controlling the behavior of confined concrete when modeled using the Finite Elements. The authors adopted the stress-strain model under uniaxial compression for the unconfined concrete provided by Popovics (1973) to highlight the problem in reproducing the compressive confined response. In fact, by using the actual stress-strain law for unconfined concrete, the resulting curve of FRP-confined concrete led to the results shown in Fig. 3.5.

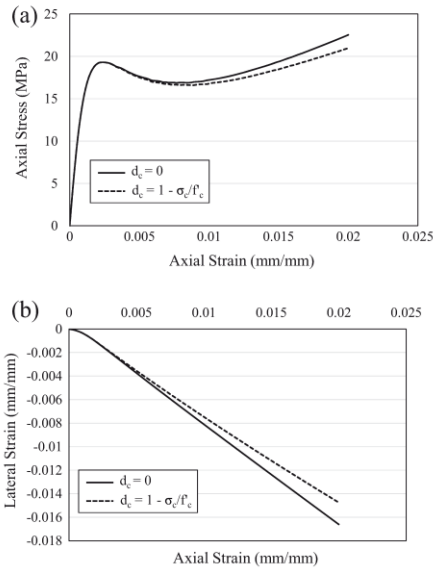

Figure 3.5. Results provided by Abaqus with standard input value for CDPM. (Hany et al., 2016).

It seems to be clear that the numerical results are not representative of the actual behavior in compression experimentally observed. In Fig. 3.5 also the influence of damage parameter is shown through the two limit cases: no damage (*dc=0*) for the entire stress-strain response of the unconfined concrete and damage $dc=1-\sigma_c/f_c$ for a point on the post-peak stress-strain curve at a stress σ_c. As it is shown in Fig. 3.5 the damage parameter has a little effect on the stress-strain curve of the FRP-confined concrete and more important effect on the lateral dilation. Hence, since the effect was recognized to be limited and authors considered only the monotonic behavior, the damage was neglected and *dc=0* was assumed.

The authors analyzed each of the plasticity parameters to build up the concrete behavior. Regarding the flow potential eccentricity *e* and the viscosity parameter, according to Tao et al. (2013), default values were assumed because no important influence on the prediction was observed by changing the values.

The ratio between compressive strength under biaxial stresses to the uniaxial strength was adopted according to Papanikolau and Kappos (2007) while, the parameter *Kc*, that controls the shape of the yield surface was

assumed according to Yu et al. (2010b) if Teng et al. (2007) model is used to compute the peak stress of concrete confined by constant confining pressure.

Regarding the dilation angle, differently from Yu et al. (2010b) that defined confining pressure-dependent dilation properties, the authors provided a procedure to calibrate a constant ψ parameter in function of the stiffness of the composite jackets. They stated that by defining a constant dilation angle in CDPM almost the same lateral strain-axial strain curves are obtained for different values of the FRP-jacket stiffness. It is possible to recognize that by increasing the stiffness of the jackets, dilation properties of the concrete and consequently dilation angle reduce progressively. Since in general, beyond an axial strain close to 0.002 the lateral strain-to axial strain curve becomes almost linear, in FE modeling a constant dilation angle can be suitable to reproduce the entire compressive behavior of FRP-confined concrete.

The procedure is also extended in the case of square and rectangular cross-section including discontinue confinement devices. This was possible by introducing a confinement effectiveness coefficient representing the effectively confined area to the cross section area. Moreover, also vertical effectiveness coefficient was adopted in the case of partially wrapped columns. In this way, equivalent circular section could be considered to obtain dilation angle value.

As proposed by Yu et al. (2010b), the compression hardening/softening rule for FRP confined concrete can be constructed as a set of points on a series of curves of actively-confined concrete. Nevertheless, the authors assume the concept of stress-path independency on the basis of experimental observations of Lim and Ozbakkaloglu (2014) that demonstrated that at a given axial and lateral strain and confining pressure, a slightly lower stress is exhibited by FRP-confined concrete. The differences between the two curves become higher in the case of High Strength Concrete. Therefore, the confining pressure was modulated by using expression calibrated by regression analysis obtained on the basis of experimental data. Moreover, the authors provide a modification of the hardening/softening rule for actively confined concrete as an input parameter by using Teng et al. (2007) model.

He et al. (2017)

The authors investigated the axial compressive behavior of steel-jacketed RC columns with recycled aggregate concrete. The study concerned experimental investigation and numerical simulations by means of Abaqus Software by which the authors implemented constitutive law for the concrete in compression according to Yang et al (2015). The recommended relationship for the concrete was provided in the past by Han et al. (2007) which proposed to modify the hardening/softening behavior of the concrete in function of the mechanical confinement factor. The stress-strain law was suitable for both cases of recycled concrete aggregates or normal concrete aggregates. Moreover, the authors investigated the effects of preload to the original columns before reinforcing with steel tube infill concrete. Unfortunately, the numerical technique adopted to consider the presence of preload during the numerical simulations are not specified.

Shafei and Rahmdel (2017)

The authors provide an experimental and numerical study on concrete square columns partially confined with steel jacketing subjected to compressive loads. Numerical modeling of the experimental results was carried out by means of Abaqus software, using "cap plasticity model" for concrete. The authors focused the dilation properties of the confined concrete depending on the mechanical confinement ratio. On the basis of the experimental observations, they noticed that specimens with low external confinement are not affected by volumetric restrain and show volumetric expansion. While specimens with high confinement level exhibit volumetric contraction. The numerical model accounted for the concrete was therefore modified regarding the plastic flow of the confined concrete combined with shear-cap plasticity formulations. The authors compare also results provided by CDP model highlighting differences in terms of volumetric response. The results indicate that using default values for CDPM led to not representative behavior in compression when the concrete is subjected to volumetric contraction.

3.4 Axial compressive behavior of FRP-confined concrete: A numerical proposal

3.4.1 Modeling of FRP Jackets

Elastic properties of the FRP sheets are specified in Abaqus by "LAMINA" material type, which allows correlating the longitudinal and transverse elastic modulus E_1, E_2, the rigidity modulus G_{12},G_{13},G_{23}, and the Poisson coefficient N_{u12}. In the case of unidirectional fibers, it is possible to specify only E_1 and to assign very small values for the other elastic properties. In this way the system in not affected by an interaction with the other directions.

3.4.2 Modeling of concrete

As before mentioned, Concrete Damaged Plasticity Model allows reproducing the behavior of concrete by defining the plasticity and/or the damage parameters. By using the plasticity model available in ABAQUS, it is possible to take into account concrete cracking in tension as well as crushing in compression. Formulations defining the behavior of concrete under multi-axial stress state include the *damage variable*, the *yield criterion*, the *flow rule* and the *hardening/softening* rule that defines the non-linear behavior of concrete. The *yield criterion* described in Lubliner et al. (1989) and modified in Lee and Fenves (1998) sets out the yielding conditions when concrete is under multi-axial compression. The *flow rule* determines the direction of the plastic deformations and describes the relationship of plastic lateral strain and plastic axial strain increments, assuming a *non-associated potential plastic flow*.

The above formulations can be managed in Abaqus (Theory and User manuals, 2013) by the users defining the *plasticity parameters.* These are the dilation angle ψ (description of the lateral strain vs. axial strain curve), the ratio of the compressive strength under biaxial loading and uni-axial compressive strength f_{b0}/f_{c0}, the flow potential eccentricity e, the viscosity parameter μ and the ratio K_c of the second stress invariant on the tensile meridian and that on the compressive meridian for the yield function.

While it was demonstrated that no particular changes are observed by varying the default value for the flow potential eccentricity e (e = 0.1), the others parameters can significantly affect the results of the analysis. As reported by Michael and Andrzej (2015), the viscosity parameter μ can

characterize the damage propagation and affects the tensile strength. In terms of compression tests, no significant differences are observed on the accuracy of the results, and therefore, according to Hany et al. (2016), a very small value of μ is considered in the present study (10^{-6} is assumed, while zero is the recommended value). Regarding the f_{b0}/f_{c0} factor, based on a power regression analysis, Papanikolaou and Kappos (2007) give an empirical equation that provides the best fitting with a large number of cases, comprising confined specimens with low-to-high strength concrete and confinement ratios. This equation was adopted later by Hany et al. (2016) and Tao et al. (2013) to characterize the behavior of concrete with FRP-confinement, actively confined concrete, and steel-confined concrete. Considering the reliability of the proposed equation, the model below has been assumed for the ratio f_{b0}/f_{c0}:

$$\frac{f_{b0}}{f_{c0}} = 1.5 \cdot \left(f_{c0}\right)^{-0.075} \tag{3.15}$$

A recent study published by Ozbakkaloglu et al. (2016) presents a comprehensive analysis of the damaged plasticity model for FRP-confined concrete, taking into account a wide range of compressive strength values (from normal-strength to high-strength concrete). Based on the results of a regression analysis performed for a large number of tested specimens, they define an empirical relationship to obtain f_{b0}/f_{c0} and K_c factors. An interesting aspect of this study is the fact that the authors obtain the coefficients as a function of the strength of unconfined concrete, only. Since the differences of the results between the equation proposed by Ozbakkaloglu et al. (2016) for f_{b0}/f_{c0} are negligible with respect to Eq. (3.15) adopted in the present study, the relationship to obtain the value of K_c proposed in Ozbakkaloglu et al. (2016) is assumed for the following development, that is:

$$K_c = 0.71 \cdot \left(f_{c0}\right)^{-0.025} \tag{3.16}$$

Dilation angle

The definition of the *dilation angle* ψ is a critical step because the stress-strain response of concrete with elastic confinement is affected by the lateral to axial strain behavior. Therefore, also lateral confinement pressure and strength properties are significantly influenced by its definition. Several formulations and analytical proposals are available in literature to

approximate the dilation angle (Hany et al., 2016, Youssf et al., 2014). The present model adopts the equation proposed by Hany et al. (2016), that allows obtaining the dilation angle value in function of the unconfined concrete strength f_{c0} and the radial stiffness K_l of the FRP sheets. The advantage offered by this approach is the possibility to obtain a constant value of ψ to define in the input phase without dependence on the evolution of the plastic strains. The expression of ψ is given by:

$$\psi = -1.4587 \cdot \frac{K_l}{f_{c0}} + 57.296 \tag{3.17}$$

with:

$$K_l = \frac{2 \cdot E_{frp} \cdot t_{frp}}{D} \tag{3.18}$$

in which E_{frp} is the longitudinal elastic modulus of the fibers, t_{frp} is the thickness of the sheets and D is the diameter of the circular columns. Based on the findings of Hany et al. (2016), a linear relationship exists between dilation angle ψ and the ratio between the radial stiffness of the composite jackets and the unconfined compressive strength of concrete K_l / f_{c0} expressed by Eq. 3.17. Since the dilation angle assumes possible values from 0° to 56°, for values of K_l / f_{c0} higher than 40 the theoretical dilation of concrete cannot be reproduced accurately by using CDPM.

Modified hardening/softening rule

As shown in several recent studies (Yu et al., 2010b, Hany et al., 2016), the actual law of unconfined concrete to evaluate the effect of confinement in case of elastic confinement inevitably leads to reproduce a not realistic trend of the confined concrete in the second hardening phase (after the chance in slope of the axial stress-strain response).

Based on the considerations provided by Tao et al. (2013), a simplified procedure to obtain stress-strain laws of unconfined concrete to be also used for FRP-confined concrete, is here proposed. By this procedure, the computational effort is reduced and potential convergence problems are avoided.

The derivation of a fictitious law starts with the modification of the stress-strain relationship proposed by Popovics (1973) and considers three sections of the stress-strain curve. The first section, ascending up to the unconfined concrete strength/strain (f_{c0}, ε_{c0}), remains unchanged. Then, strain

values increase ($\varepsilon_{c0} \rightarrow \varepsilon_c^*$) at constant stress f_{c0}, while the softening (third) section of the curve is defined according to Popovics (1973) with ε_{c0} being substituted by ε_c^*. In doing so, also the curve's shape factor r and consequently the slope of the softening branch is modified.

Numerical tests were conducted to obtain an accurate hardening response of the confined concrete with different values of $k\varepsilon$ and varying concrete strength, types of FRP sheets and numbers of layers. It was found that $k\varepsilon$ increases when the mechanical confinement ratio is increased. Based on a regression analysis of the results, an equation is proposed to determine $k\varepsilon$ and consequently ε_c^* as a function of the nominal mechanical confinement ratio ω as defined in Eq. 3.22. In summary, the three sections of the proposed stress-strain curve are described by the following equation:

$$\frac{\sigma}{f_{c0}} = \begin{cases} \dfrac{x_1 \cdot r_1}{r_1 - 1 + x_1^{r_1}} & 0 \le \varepsilon \le \varepsilon_{c0} \\ 1 & \varepsilon \le \varepsilon \le \varepsilon_c^* \\ \dfrac{x_2 \cdot r_2}{r_2 - 1 + x_2^{r_2}} & \varepsilon \ge \varepsilon_c^* \end{cases} \tag{3.19}$$

The parameters r_1 and r_2 appearing in the Eq. (3.19) affect the shape of the uniaxial compressive curve and result defined as:

$$x_1 = \frac{\varepsilon}{\varepsilon_{c0}},\ x_2 = \frac{\varepsilon}{\varepsilon_c^*},\ r_1 = \frac{E_c}{E_c - E_{\text{sec},1}},\ r_2 = \frac{E_c}{E_c - E_{\text{sec},2}} \tag{3.20}$$

$$\varepsilon_c^* = \varepsilon_{c0} + k\varepsilon,\ k\varepsilon = 0.00065 + 0.0007 \cdot \omega,\ \frac{k\varepsilon}{\omega} = 0.0014 \cdot \omega^{-0.56} \tag{3.21}$$

$$\omega = \frac{4 \cdot t_{frp} \cdot E_{frp} \cdot \varepsilon_{ju}}{D \cdot f_{c0}} \tag{3.22}$$

Hereby, $E_{\text{sec},1}$ and $E_{\text{sec},2}$ are the secant elastic modulus at ε_{c0} and ε_c^*, respectively. The others terms are given in Popovics (1973). The concrete law is exemplarily shown graphically in Fig. 3.6 for selected input parameters. The modified shape of the fictitious unconfined concrete stress-strain law results also in according to that obtained by Hany et al. (2016) during the process of generating input curves of actively-confined concrete coming from the modification of the strain hardening/softening rule (please refer to Hany et al. 2016). Moreover, differing from Yu et al. (2010a,b) that used elasto-perfectly plastic law for unconfined concrete, this assumption

allows obtaining FRP-confined concrete with softening behavior. It is important to specify that the input parameters are defined in this phase without considering plastic strain, therefore before introducing as input in Abaqus.

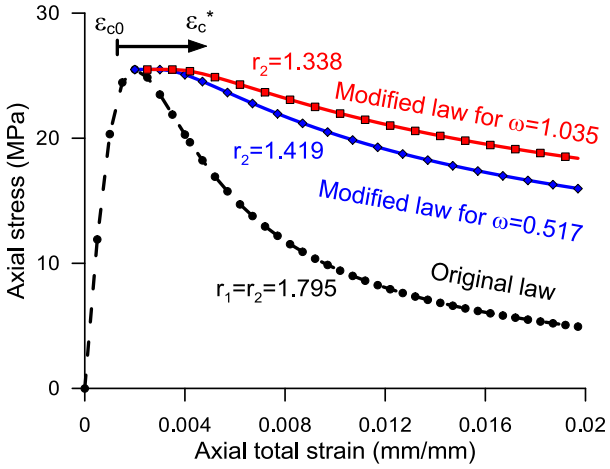

Figure 3.6. Original and modified input for unconfined concrete data.

As an example, numerical analysis on an exemplary concrete cylinder was carried out to observe differences between compressive response obtained with modified hardening/softening parameters and by taking into account actual unconfined concrete stress-strain law as input parameter.

The specimen characteristics are diameter d=110 mm, height h=220 mm, unconfined concrete strength f_{c0} and strain at unconfined peak stress ε_{c0} equal to 17.50 MPa and 0.0013 respectively. The composite jackets consist in carbon fibers having thickness t_f of 0.222 mm and tensile strength f_j of 4410 MPa. Interaction properties between concrete and FRP-jackets are defined by "tie-constrains" so that no sliding is considered. This assumption can be considered reliable for circular specimens according to Yu et al. (2010a,b), Teng et al. (2015), Hany et al. (2016). Rigid body at the top and the bottom of the specimen are defined in which reference points allow to define boundary conditions.

The theoretical specimen is made of a material (CDPM) whose parameters are reported in Table 3.1.

Table 3.1. Mechanical parameters of the theoretical specimen material (CDPM).

Dilation angle ψ	*fb0/fc0*	*Kc*	*e*	Viscosity
22.06	1.2101	0.66096	0.1	10^{-6}

The assembled FE model and the meshing are shown in Figs. 3.7 a-b, while, as a results of the compression test displacement controlled, compressive stresses on the cylinder and tensile stresses on the jackets corresponding to an intermediate step of the analysis are reported in Figs. 3.7 c-d.

The numerical results obtained using the actual stress-strain law for the unconfined concrete compared with that obtained by using modified stress-strain law are shown in Fig. 3.8. As it is possible to observe in the figure, FE results with modified model for concrete reproduce compressive response according to the actual compressive behavior of FRP-confined concrete. In the following sections, comparisons with existing data were performed to validate the proposed simplified numerical model.

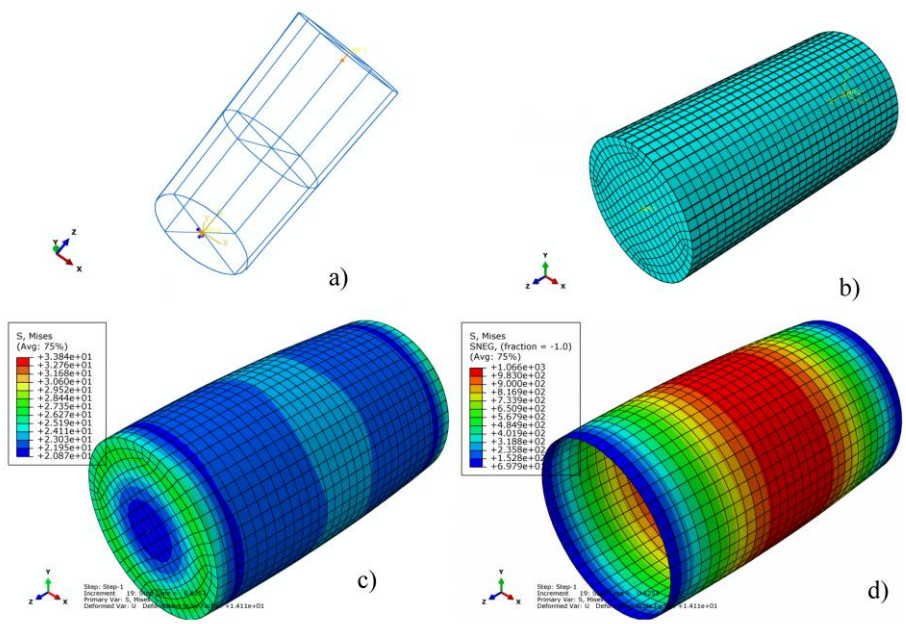

Figure 3.7. Assembled FE model with boundary conditions (a); meshing (b); stress distribution on concrete cylinder (c); stress distribution on FRP jacketing (d).

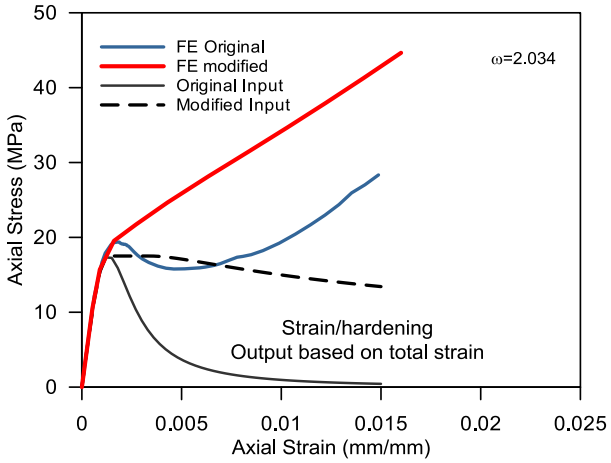

Figure 3.8. Axial stress-strain results for confined concrete using actual and modified stress-strain law for unconfined concrete.

3.4.3 Calibration and validation of the proposed model

This section presents firstly the calibration of the finite element modeling proposal for monotonic compression tests, then a comparison with more experimental results is reported to validate the simplified numerical proposal.

Experimental data of some of the most relevant studies available in literature (Lam and Teng, 2004, Berthet et al., 2005, Lam et al., 2006, Jang and Teng, 2007, Valdmanis et al., 2007, Hany et al., 2015) are summarized in function of the mechanical characteristics of the specimens in order to define the parameters of the model (see Table. 3.2). If not available, ε_{c0} = 0.002 was assumed for the strain valued reached at the unconfined peak stress; further, the axial elastic modulus of concrete was calculated according to Mander et al. (1988):

$$E_c = 5000\sqrt{f_{c0}} \tag{3.23}$$

For each specimen, geometrical characteristics and mechanical parameters evaluated by Eq. 3.21 are reported in Table 3.2.

A comparison in terms of compressive axial stress to axial strain and lateral to axial strain of experimental and numerical results is presented in Fig. 3.9. Moreover, Figs. 3.10 a-b show the factor $k\varepsilon$ as a function of the mechanical confinement ratio ω and its coefficient evaluated by non-linear regression.

A good agreement between experimental and numerical curves is reached for both strength and deformational behavior by using modified stress-strain law for unconfined concrete. With regard to the lateral to axial strain curves, the adoption of constant dilation angle by Eq. (3.17) according to Hany et al. (2016) resulted as a good strategy to simplify numerical analysis, obtaining reliable results. Small differences are observed only in case of a high mechanical confinement ratio ($\omega > 1$) because negative values of the dilation angle would be obtained by Eq. (3.17), but, since the lower limit of the dilation angle is represented by zero value, a very small value (near to zero) was assumed to avoid convergences problems.

Table 3.2. Mechanical parameters from experimental data found in the literature.

Specimen	d x h (mm)	ε_{c0}	ω	$k\varepsilon$	$k\varepsilon$ Eq. (4.21)	$k\varepsilon/\omega$	$k\varepsilon/\omega$ Eq. (4.21)
Valdmanis et al. (2007)	150x 300	0.0018	0.233	0.0008	0.0008	0.0034	0.0031
Lam et al. (2006)	152x 305	0.0025	0.369	0.00094	0.0009	0.0025	0.0024
Valdmanis et al. (2007)	150x 300	0.0017	0.401	0.00120	0.0009	0.0029	0.0023
Jang-Teng (2007)	152x 305	0.0024	0.412	0.00077	0.0009	0.0018	0.0023
Lam-Teng (2004)	152x 305	0.0020	0.422	0.00097	0.0009	0.0022	0.0022
Berthet et al. (2005)	160x 320	0.0020	0.440	0.0010	0.0009	0.0022	0.0022
Hany et al. (2015)	200x 500	0.0020	0.498	0.0008	0.0009	0.0016	0.00206
Berthet et al. (2005)	160x 320	0.0020	0.517	0.0010	0.0010	0.0019	0.0020
Valdmanis et al. (2007)	150x 300	0.0026	0.710	0.0012	0.0011	0.0016	0.0016
Lam et al. (2006)	152x 305	0.0025	0.780	0.0011	0.0011	0.0014	0.0016
Berthet et al. (2005)	160x 320	0.0020	0.809	0.00125	0.0012	0.00154	0.0015
Lam-Teng (2004)	152x 305	0.0020	0.845	0.00117	0.0012	0.0013	0.0015
Berthet et al. (2005)	160x 320	0.0020	0.880	0.0014	0.0012	0.0015	0.0015
Berthet et al.(2005)	160x 320	0.0020	1.015	0.0014	0.0013	0.0013	0.0014
Berthet et al. (2005)	160x 320	0.0020	1.035	0.0015	0.0014	0.0014	0.0013
Lam-Teng (2004)	152x 305	0.0018	1.327	0.00162	0.00158	0.0012	0.0011
Valdmanis et al. (2007)	150x 300	0.0026	1.420	0.0016	0.0016	0.0011	0.0011

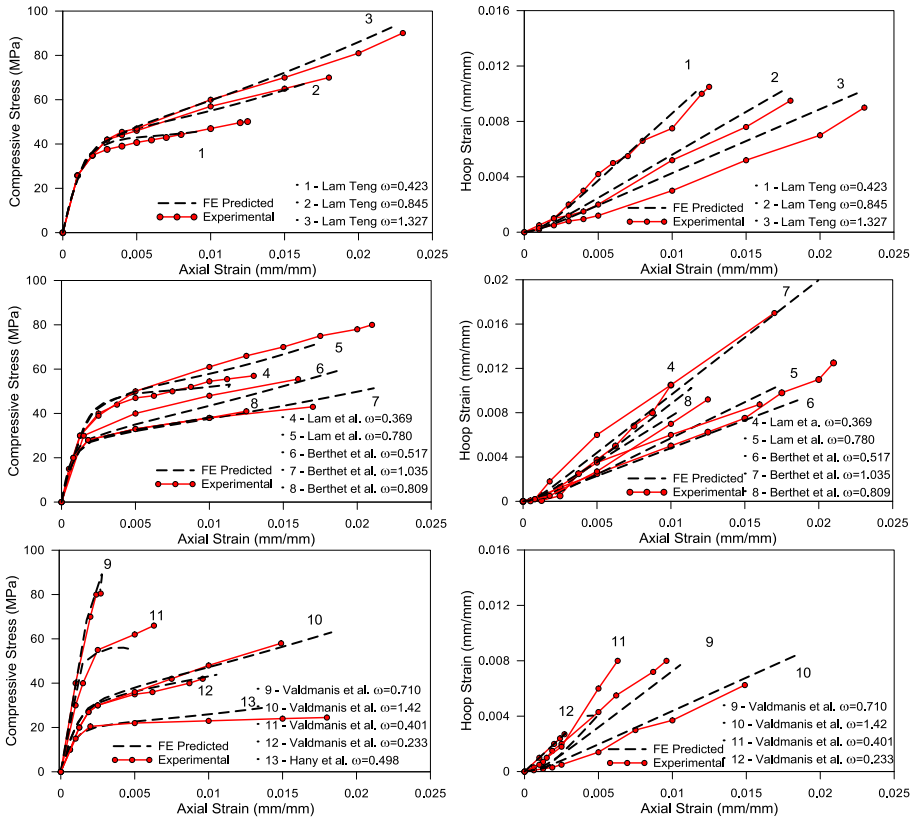

Figure 3.9. Comparisons between FE model response and experimental response obtained after the calibration of the model.

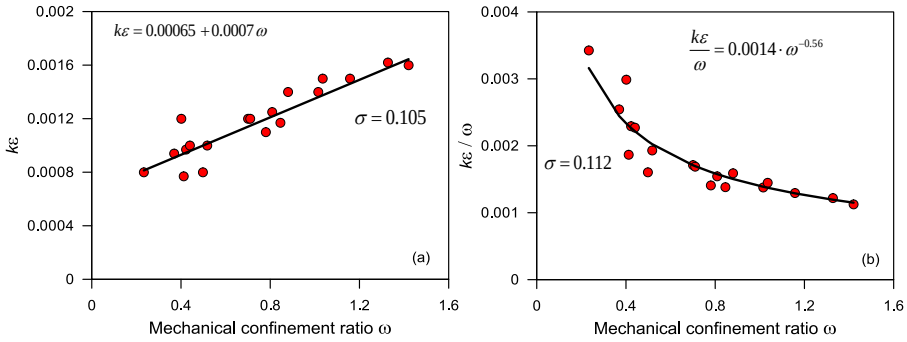

Figure 3.10. $k\varepsilon$ (a) and $k\varepsilon/\omega$ vs mechanical confinement ratio ω.

More experimental-numerical comparisons were carried out to validate the numerical proposal with experimental studies on FRP-confined concrete cylinders subjected to monotonic compressive loads provided in recent years. Geometrical and mechanical characteristics of the specimens of the experimental investigations carried out by He and Jin (2011), Benzaid and Mesbah (2013), Micelli and Modarelli (2013), Pan et al. (2017) are shown in Table 3.3, while experimental-numerical comparisons in terms of axial stress-to-axial strain are shown in Fig. 3.11. In this figure, the reliability of the proposed model is confirmed for a wide range of mechanical confinement ratios of specimens.

Table 3.3. Mechanical parameters from experimental data used for the validation of the numerical model.

Specimen	d x h (mm)	ε_{c0}	ω	$k\varepsilon$ Eq.(4.21)	ε_c*
Micelli and Modarelli (2013)	150x300	0.00626	0.3947	0.00093	0.00719
Benzaid and Mesbah (2013)	160x320	0.00273	0.4327	0.00095	0.00368
Micelli and Modarelli (2013)	150x300	0.0049	0.5323	0.00102	0.00592
Benzaid and Mesbah (2013)	160x320	0.00264	0.5443	0.00103	0.00367
Pan et al. (2017)	110x200	0.00150	0.7451	0.00234	0.00384
He and Jin (2011)	160x320	0.0025	0.8063	0.0012	0.0037
Pan et al. (2017)	200x500	0.0013	1.017	0.00272	0.00402
Benzaid and Mesbah (2013)	160x320	0.00273	1.2981	0.00156	0.00429
Pan et al. (2017)	110x200	0.00157	1.4902	0.00169	0.00326
Pan et al. (2017)	110x200	0.00132	2.0341	0.00207	0.00339

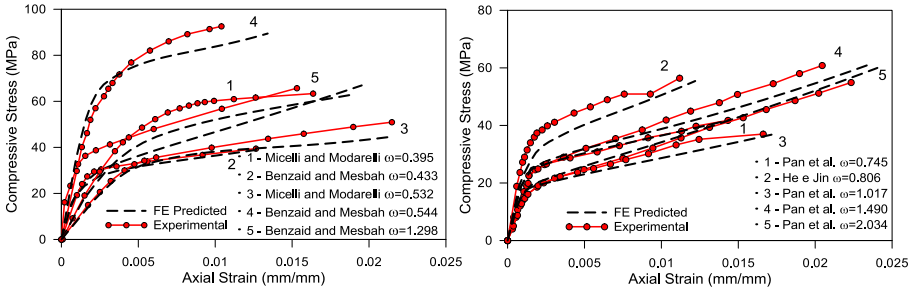

Figure 3.11. Comparisons between numerical and experimental data obtained from the validation of the model.

3.5 Confinement after preloading: A proposal of FE procedure

Respect to the case of strengthening of columns without preload, in the presence of applied sustained load before strengthening (a situation that reflect several cases of reinforcement of existing buildings), the confining element gives its contribute starting from a certain stress/strain level. On the other hand, if the reinforcement is applied without pre-stressing (steel or FRP wrapping according to the object of the present work), its stress state is zero and does not provide any contribute under static conditions. Specifically, the confinement can start to give its contribute only in the case of further load increments (static or dynamic). However, the contribute of the reinforcement on the improving in bearing capacity, in this case, is still unclear.

The main problem of reproducing this phenomenon through a finite element calculation code lies in the determination of the effect of secondary loads on deformed geometries, as reported also by Shi and He (2009). In fact, if the problem above described has to be analyzed, when a certain level of preload is applied on an unconfined column, a level of axial and transverse deformation that would require the definition of the geometry of the reinforcement system on a deformed configuration of the non-confined system has to be taken into account when the jacket has to be modeled to the preloaded columns. The problem is solved in this work through the use of the de-activation/reactivation elements technique for a certain step of analysis. It is thus possible to define the assembled system before the analysis assigning the properties to the materials used for the confinement in such a way to activate its contribution on the global response only when desired.

The simulation of the preload conditions is therefore obtained by articulating the analysis into two steps:

- the displacement applied under displacement-controlled increments to the top section of the specimen is modulated according to the fixed preload level, which is equivalent to loading the unconfined column until the predefined stress level is reached;
- the bandage is activated and the load test continues until the failure of element, signaled by the interruption of the convergence of the analysis.

The same results can be obtained by performing load-controlled increments in the first step up to a certain load level corresponding to an established preloading level index and defining the second step in the same way as previously described. In this work the first procedure is considered suitable to reproduce the preload because, if the columns need to be preloaded over the post-peak region, potential numerical errors are avoided.

Long-term effects on concrete are neglected in this work. The hypothesis seems to be reasonable if one considers that, in practical applications, the columns that need reinforcement devices are at an advanced stage of their nominal life, so that the effects of creeps, subject over time to stabilization, are negligible at that point. The numerical procedure is qualitatively schematized in Fig. 3.12.

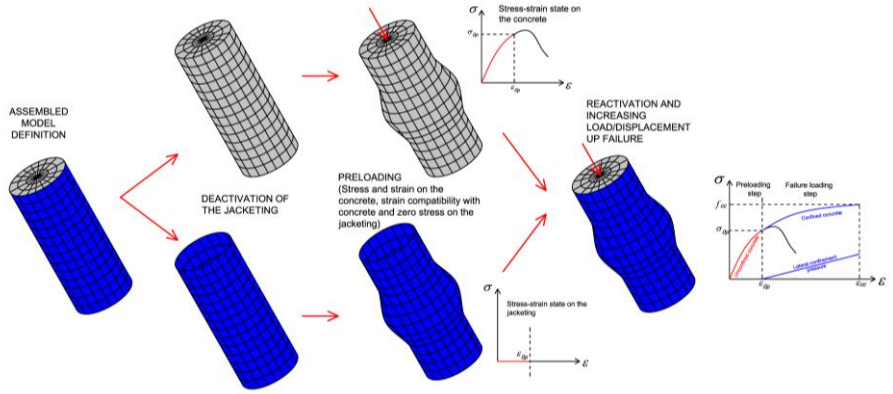

Figure 3.12. Numerical computation of the preloading process.

The model change interaction is briefly described in the following section according to the Abaqus Manual and Guidelines (Abaqus Theory and User Manuals, 2013).

Model change interaction and deactivation/reactivation elements

It is possible to remove specified elements from the model in a general step of analysis. Directly before the removal, Abaqus stores the forces so that the region to be removed is still existing on the remaining part of the model at the nodes of the boundary between them. These forces are ramped down to zero during the removal step; therefore, the effect of the removed region on the rest of the model is completely absent only at the end of the

removal step. The forces are ramped down gradually to ensure that the element removal has a smooth effect on the overall model.

No further element calculations are performed for elements being removed, starting from the beginning of the step in which they are removed. The removed elements remain inactive in all subsequent steps unless a deliberate reactivation is defined.

When stress/displacement elements are reactivated in a strain-free state, they become fully active immediately at the moment of reactivation. They are reset to an "annealed" state (zero stress, strain, plastic strain, etc.) in the configuration in which they lie at the start of the reactivation step.

Since these elements are reactivated in a "virgin state" (i.e., with zero stress), they exert zero nodal forces on the rest of the model. This result allows reactivation to be done immediately, without an adverse effect on the smoothness of the solution. After reactivation, the strains and the deformation gradients are based on the displacements after the moment of reactivation, rather than on their total displacements. Thus, the current configuration at the start of the reactivation step is the new initial configuration. This kind of reactivation usually is used to model the creation of an undeformed and unstrained region of the model that is sharing a boundary with another, possibly stressed, deformed region.

For shell and membrane elements the thickness of the reactivated elements is as specified at the start of the analysis.

Confinement under preloading conditions: sensitive analysis

Using the modeling technique described above, the results obtained from numerical simulations are reported both in the case of FRP confinement (case 1) and Steel Jacketing (case 2).

The numerical model used for case 1 consists of a concrete cylinder, without internal reinforcement, diameter d=150mm and height h=450mm, with unconfined compressive strength f_{c0}=15 MPa and strain at peak stress ε_{c0}=0.0025. The cylinder has been reinforced with carbon fiber with elastic modulus E_{frp}=230 GPa and a thickness t_{frp}=0.260 mm corresponding to two wrapping of the composite material.

The numerical model used for the case 2 instead consists of a square concrete column without internal reinforcement, sides b=150 mm and height h=1000 mm, with unconfined concrete with compressive strength f_{c0}=25 MPa and strain at peak stress ε_{c0}=0.002. The model has been reinforced with

S275 steel (f_y=275 MPa yield strength). The steel cage consists of angles type 50/50/5 plates type 60/4, arranged at pitch s_b=140 mm.

In Fig. 3.13 a-b the models after meshing are shown for both cases (1 and 2).

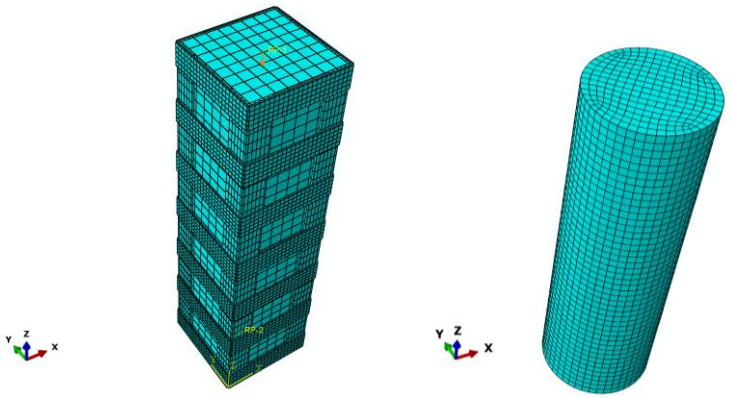

(a) (b)

Figure 3.13. Concrete model with steel jacketing (a); concrete model with FRP jacketing (b).

The simulations were articulated in such a way as to have two analysis steps:

- step 1, in which the behavior of non-confined concrete is analyzed (the preload process is simulated);
- step 2, in which the behavior of the confined concrete is analyzed, both under preload and monotonic conditions.

Specifically, simulations under preload conditions require that in the first step a force/displacement is applied to the non-confined element (with the reinforcement device deactivated) and the stress/strain state at the end of the analysis corresponds to the tensional state relative to the preload level. In the second step, the confinement device become active in deformed conditions, characterized by the congruence of the nodal displacements of the concrete meshes, but with zero stress/strain state.

For both numerical models, axial stresses, lateral stresses and axial total strains corresponding to the middle section were recorded during the analysis.

In Fig. 3.14 the stress and strain distributions in the concrete cylinder confined with FRP are shown for three significant steps of the numerical

process. The end of the first step (Fig. 3.14 a-b) in which the unconfined concrete cylinder reached the preload without any contribution of the FRP jacket; the beginning of the second step at increment 0 (Fig. 3.14 c-d) in which the concrete cylinder keeps the same stress/strain configuration of the previous step and the FRP jacket becomes "active" in a virgin stress/strain state but having the same shape of the cylinder; a certain increment of the second step (Fig. 3.14 e-f) in which the FRP gives its contribute to the global response. In this phase, the strain compatibility is still given by "tie constrains interaction" and the strains of the jacket are lower than the cylinders because they are computed in the analysis before the preloading step. The same considerations apply also for the case of confinement with steel jacketing (Fig. 3.15 a-e).

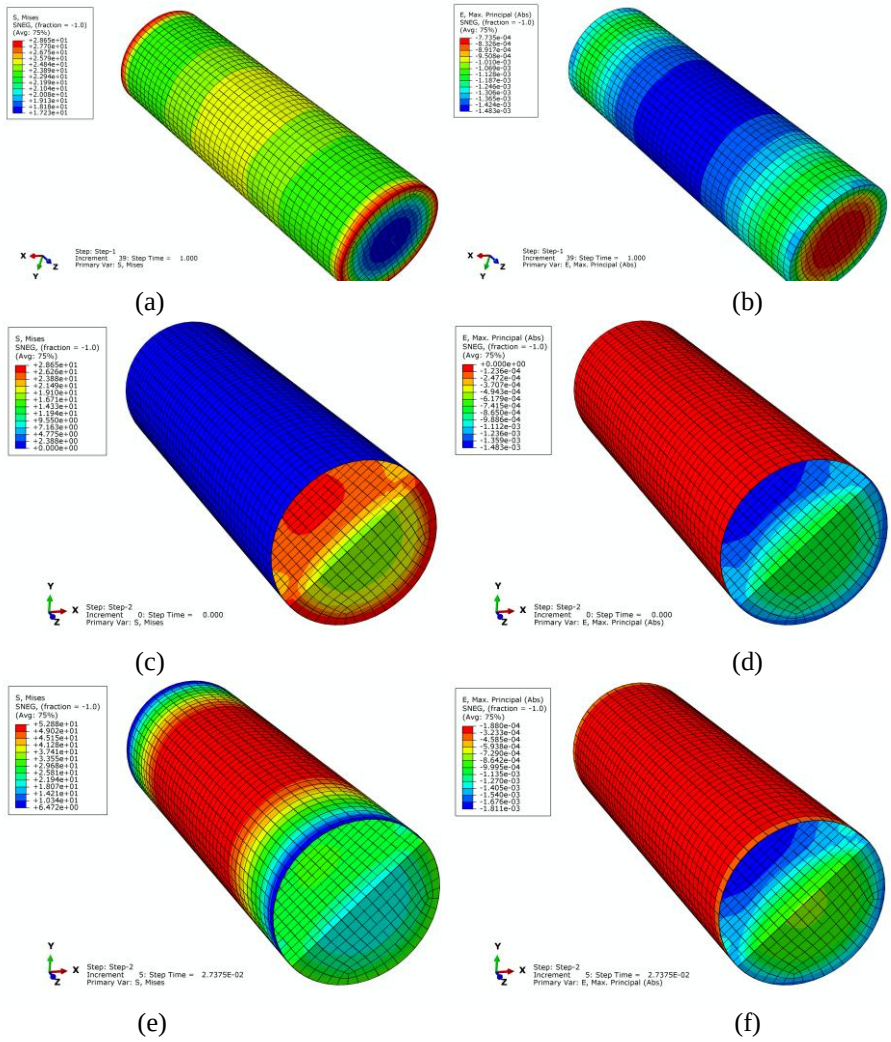

Figure 3.14. Stresses and strains distribution in the model (case 1) during: end of first step (a and b); second step at increment 0 (c and d) and increment 5 (e and f).

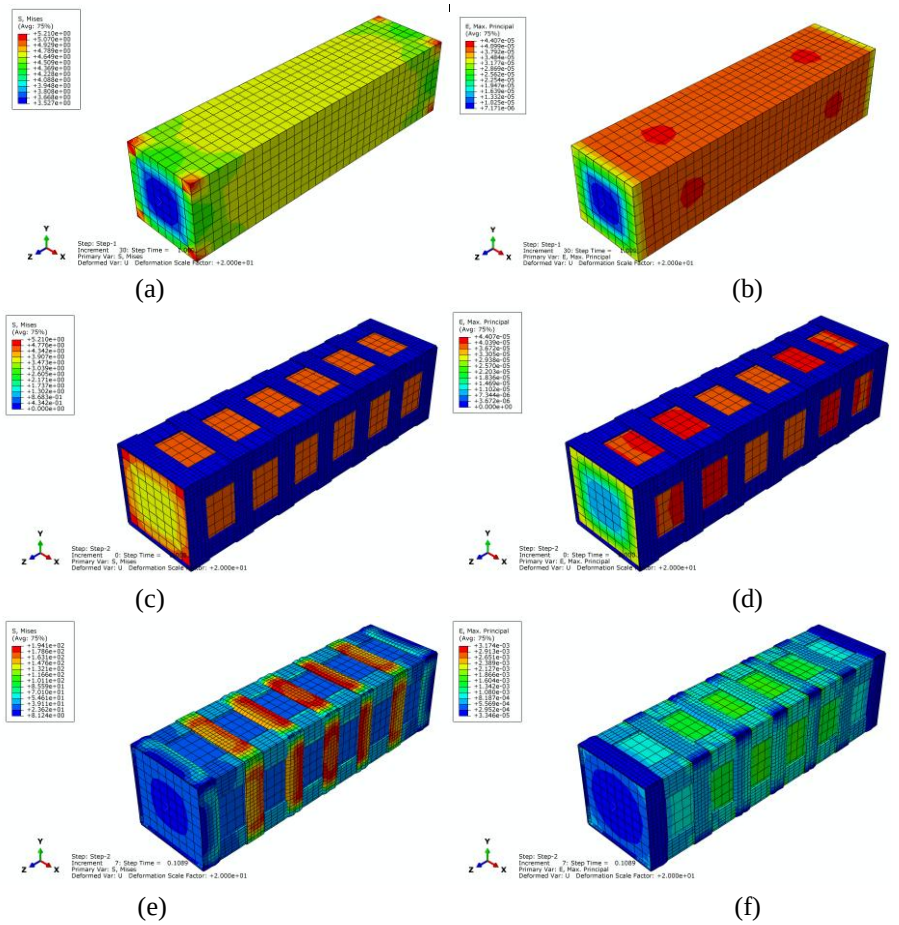

Figure 3.15. Stresses and strains distribution in the model (case 2) during: end of first step (a and b); second step at increment 0 (c and d) and increment 7 (e and f).

In the case of FRP confinement there are no differences in terms of confined compressive strength, as the failure conditions occur only when the fibers reach the ultimate strain. In these cases, i. e. for curves characterized by "strain-hardening" behavior, the confined concrete strength is correlated to the lateral confinement pressure, which always reaches the same maximum value (Fig. 3.16 a). In the case of confinement with Steel Jacketing, exhibiting a strain-softening behavior, it is noticeable that the

strength decreases as the imposed preload level increases (Fig. 3.16-b). In this phase, no evaluation of load carrying provided by the angles was considered in the output. Of course, this contribute should be evaluated in a global analysis to provide the overall response.

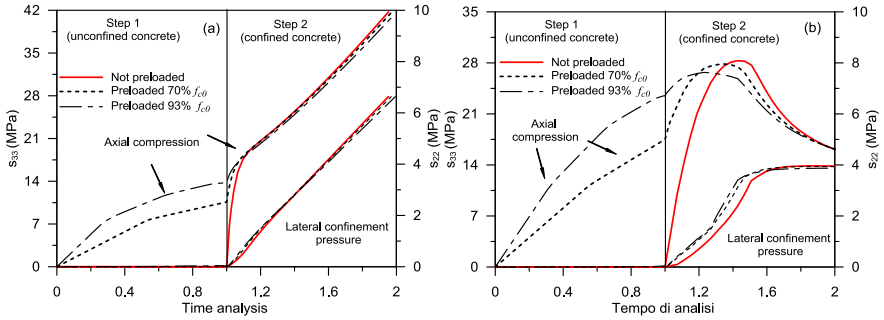

Figure 3.16. FE computational process for case 1 (a) and case 2 (b).

A more comprehensible capacity assessment emerges by the axial stress-strain response as shown in Fig. 3.17 a-b.

In the case of FRP-confinement, when the preload increases, the secant stiffness is reduced, followed by a slight increase in the ultimate axial strain of the confined concrete, while the strength of the confined concrete remains almost unchanged. This effect is justified by the delayed application of the FRP bandage, since, as stated before, the failure always occurs due to the same final ultimate strain of the fibers, which, when applied late, is achieved for higher axial strain levels of the concrete. It is interesting to note, as for the diagrams in Fig. 3.17-a, the same strength exhibited under failure conditions.

In the case of confinement with Steel Jacketing, on the other hand, as preload level increases, there are progressive reductions in the strength, followed also in this case by a reduction of the secant stiffness of the stress-strain curve.

Specifically, the preload levels shown in Fig 3.17 (a-b) are respectively 70% f_{c0} and 93% f_{c0}. For preload level lesser than 50% of f_{c0}, there are no particular variations in the response of the reinforced system, while once these percentages have been exceeded, the reduction in the secant stiffness is not negligible, becoming significant for high preload levels (n_p>0.7).

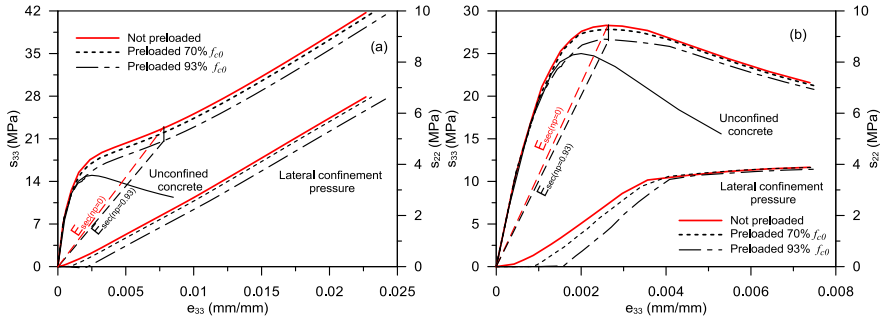

Figure 3.17. FE Model - Axial stress-strain behavior and lateral pressure evolution: case 1 (a) and case 2 (b).

4. EXPERIMENTAL INVESTIGATION ON AXIALLY PRELOADED FRP-CONFINED CONCRETE COLUMNS

4.1 Introduction

The lack in understanding the behavior of concrete FRP-confined after preload highlighted in the previous section points out the need to deepen the study in this field. In this Chapter first the experimental investigation carried out in the laboratory of structures of the Department of Civil, Geo and Environmental Engineering of the Technical University of Munich is presented and discussed. Then, comparisons between experimental data and numerical results obtained from the FE modeling technique described in Chapter 3 are performed for each experimental case. Furthermore, an analytical formulation is proposed and compared with the experimental results.

4.2 Experimental program

Compression tests were carried out on nineteen circular plain concrete specimens with two different types of concrete, "Concrete type A" and "Concrete type B", having mechanical characteristics described in the next section, and two different FRP reinforcement configurations: cylinders of type A and type B were reinforced with three and two Carbon FRP layers respectively. For each specimen an overlapping of 157 mm (1/3 of the circumference) was realized. Specimens had no internal reinforcement in order to simplify as much as possible confinement mechanism so that any eventual change or modification respect to the classical behavior was efficiently observed.

The tests were summarized into three categories, namely compression tests on unconfined cylinders, compression tests on confined cylinders and compression tests with preload. Compression tests on the unconfined concrete cylinders allowed to get the ultimate axial load of the plain concrete

in order to fix the upper limit for the determination of the preloading level index n_P, that was defined in Chapter 1 as the ratio of the preloading force applied to the specimens before wrapping (P or $\sigma(\varepsilon)$) and the ultimate unconfined axial load/strength capacity (P_{max} or f_{cm}). For simplicity during the reading of the dissertation, the equation previously defined is shown below:

$$n_P = \frac{P}{P_{\max}} = \frac{\sigma(\varepsilon)}{f_{cm}} \tag{4.1}$$

Specimens preparation

Specimens were made using PVC molds having dimension of 150x1000 mm. During the casting process soft vibration of molds ensured a minimum void content. The same procedure was adopted also for the concrete cylinders used for the mechanical characterization of the concrete.

Some days after the casting of the concrete, the specimens were cut for a height of 600 mm, considering the central part of the formwork to have as much as possible uniform and compact cementitious conglomerate for the specimens.

Leveling of the end cross-section of the specimens were performed to have perfect orthogonal contact during the compression tests avoiding potential eccentricity due to imperfection of the contact surfaces.

Wrapping was carried out on specimens under standard conditions: after 28 days of curing, the concrete cylinders were cleaned and totally dried. For each layer of FRP wrap, two plies of epoxy, one on the cylinder surface and the other on the surface of the installed wrap, were applied using paintbrushes to entirely saturate the layers with epoxy. The same procedure was performed for the preloaded specimens after the preloading test (the carbon fibers sheets were applied to the concrete cylinders under deformed configuration, as will be explained in the next chapter).
In Fig. 4.1 a-d the above described process is illustrated.

Figure 4.1. Preparation of the specimens: casting of the concrete (a); cutting the cylinders (b); leveling of the end cross-section (c); FRP wrapping (d).

Mechanical characterization of the concrete consisted in monotonic and cyclic compression tests and splitting tests on cylinders having 150x300 mm size for the determination of the compressive strength, the elastic modulus of the material (Fig. 4.2) and the tensile strength (Fig. 4.3). The tests provided an average compressive strength f_{cm} of 38.13 MPa and 41.7 MPa, a tensile strength f_{tm} of 2.87 MPa and 3.07 MPa and an elastic modulus E_{cm} of 32.586 GPa and 35.253 GPa, for concrete type A and type B respectively. The

results of the mechanical characterization are summarized in Table 4.1. Strengthening of the specimens was made by unidirectional carbon fiber textile having nominal thickness t_f equal to 0.131 mm (based on the total area of the carbon fibers) nominal tensile strength of the fibers f_{ju} equal to 4300 MPa, elastic modulus E_{jm} of 234 GPa and ultimate strain ε_{ju} of 1.8%. Epoxy resin for the CFRP consisted of two components, which are the main component and the hardener. The mixing ratio by weight was 4:1 based on the provisions of the technical sheet.

Figure 4.2. Characterization of the compressive strength and the elastic modulus of the concrete.

Figure 4.3. Characterization of the tensile strength of the concrete

Table 4.1. Mechanical characteristics of the concrete.

Test type	Concrete type	Number of tests	Average value (MPa)	Standard deviation
Compressive strength f_{cm}	A	3	38.13	1.401
	B	3	41.7	1.058
Tensile strength f_{tm}	A	3	2.87	0.068
	B	3	3.07	0.106
Elasticity modulus E_{cm}	A	3	32586	479.24
	B	3	35253	317.88

Test set up and instrumentation

The tests were carried out using calibrated compression testing machines with nominal maximum loading capacities of 5 MN and 10 MN, displacement controlled by a servo-hydraulic management system electronically controlled through a computer interface. During the preloading and the failure test, the load was applied displacement controlled with a deformation rate of 0.2 mm/(m·min).

The specimens were placed into a specially designed frame system, consisting of two triangular steel plates with drilled holes in which threaded steel bars were inserted having the function - as a result of the screwing of the nuts and loading the disc springs positioned at the ends of the bars - to keep constant and to center the compression load. By means of a load cell, placed between the bottom plate and the specimens, the load was monitored and subsequently correlated with the corresponding deformations (see Fig. 4.4).

The load was transmitted from the machine to the specimen by applying a uniform compression load on adequately designed disc springs. When the preloading target level was reached, the screwing of the nuts on the threaded bars began up to the unloading of the machine so that, at the end of the preloading test, compression load on the specimens was provided only from the bars.

After the strengthening under preload of the concrete specimens and the curing process of the epoxy resin the specimens were placed into the load testing machines to perform the failure test. The latter test was arranged in such way that the load was applied directly to the specimens by means of steel plates placed in contact between the upper steel plate of the test frame and the upper steel plate of the testing machine. This procedure was

necessary because, otherwise, disc springs had not enough load capacity to bear the ultimate compressive load of the strengthened specimens and they would be inevitably destroyed during the failure test. Arrangement of the test scheme for the preloading and the failure test is reported in Fig. 4.5a and 4.5b respectively.

Figure 4.4. Assembled test frame system.

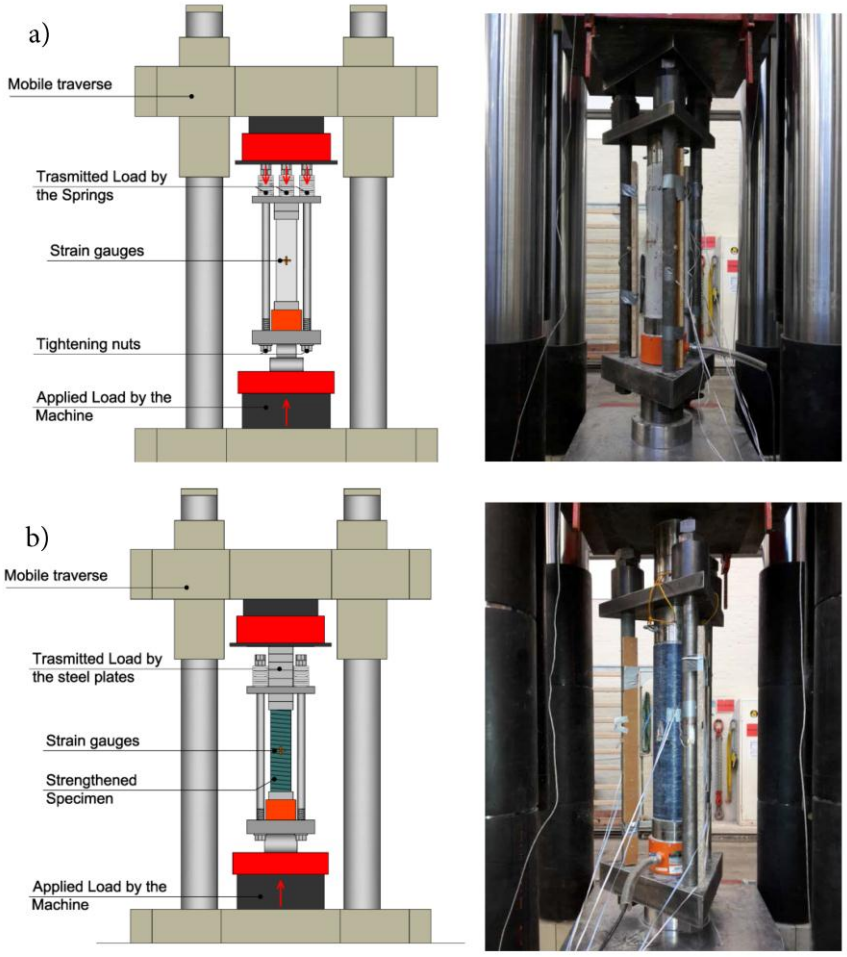

Figure 4.5. Arrangement of the tests scheme: preloading test (a); failure test (b).

Test procedure is summarized as follow:

- Bonding of strain gauges on the unconfined specimens;
- Preloading of the specimens;
- Stabilization of the load level;
- Removing of strain gauges from the plain concrete specimen and wrapping of the column with CFRP sheets and epoxy resin;
- Bonding of strain gauges on the confined concrete specimen at the same points of the previous ones;
- Moving of the specimens into the testing machine;

- Application of load until failure.

In order to obtain the entire load-strain response of the specimens, a correlation of the strains during the test process was performed. Strains of the unconfined concrete were recorded during the preloading step and, consequently, axial and hoop strains were monitored during the transition period before the bandage. Before the wrapping, strain gauges were removed from the specimens.

Preloading level index and classification of the specimens

Three different preloading levels (lower, medium and high) to observe differences respect to the reference specimens without preload were provided. For the concrete type A (f_{cm}=38.13 MPa, 3 layers of carbon fiber sheets) preloading levels of about 40%, 60% and 80% of f_{cm} were performed, while for the concrete type B (f_{cm}=41.7 MPa, 2 layers of carbon fiber sheets) preloading levels of about 55%, 70% and 90% of f_{cm} were applied.

Specimens were classified by a label in function of the concrete type and the preloading level: the first letter of this label indicates the concrete type (A or B), the second letter indicates the types of test (S to indicate strengthened specimens without preloading, P preloaded specimen), the following number indicates the preloading level and the last number identifies the number of the specimen of the same category (Table 4.2). To provide an example, specimen AP80-1 indicates specimens with concrete type A, preloaded up to 80% of the strength of the unconfined concrete, strengthened with 3 carbon fibers sheets.

Table 4.2. Classification of the specimens and preload levels.

Series	Specimen	f_{cm} (MPa)	E_{cm} (MPa)	t_f (mm)	ρ 4 t/D	n_P (%)	Force (kN)
A	A1	38.13	32586	/	/	/	/
	AS1	38.13	32586	0.393	0.0105	/	/
	AS2	38.13	32586	0.393	0.0105	/	/
	AS3	38.13	32586	0.393	0.0105	/	/
	AP40-1	38.13	32586	0.393	0.0105	39	292
	AP40-2	38.13	32586	0.393	0.0105	39	292
	AP60-1	38.13	32586	0.393	0.0105	58.4	393
	AP60-2	38.13	32586	0.393	0.0105	58.4	393
	AP80-1	38.13	32586	0.393	0.0105	78	525
	AP80-2	38.13	32586	0.393	0.0105	78	525
B	B1	41.7	35253	/	/	/	/
	BS1	41.7	35253	0.262	0.007	/	/
	BS2	41.7	35253	0.262	0.007	/	/
	BP55-1	41.7	35253	0.262	0.007	55	393
	BP55-2	41.7	35253	0.262	0.007	55	393
	BP70-1	41.7	35253	0.262	0.007	71	525
	BP70-2	41.7	35253	0.262	0.007	71	525
	BP90-1	41.7	35253	0.262	0.007	88.5	655
	BP90-2	41.7	35253	0.262	0.007	88.5	655

Disc springs

The main problem after the preloading step consisted to keep a constant load level in the specimens. To reduce the problem of the loss of load due to the creep and relaxation effects, non-linear disc springs were used. The springs had a non-linear behavior depending on the thickness/spring travel[7] ratio; by using the springs in parallel the restoring force corresponding to a certain level of displacement increases, while by using the springs in series, a lower stiffness and a lower variation of the load varying the spring travel is obtained (Fig. 4.6). After the preloading step, strains due to creep effects in the concrete specimens were compensated by the travel of the non-linear springs, reducing the loss of load on the specimen during the subsequent steps.

[7] Spring travel refers to the shortening/elongation of the spring.

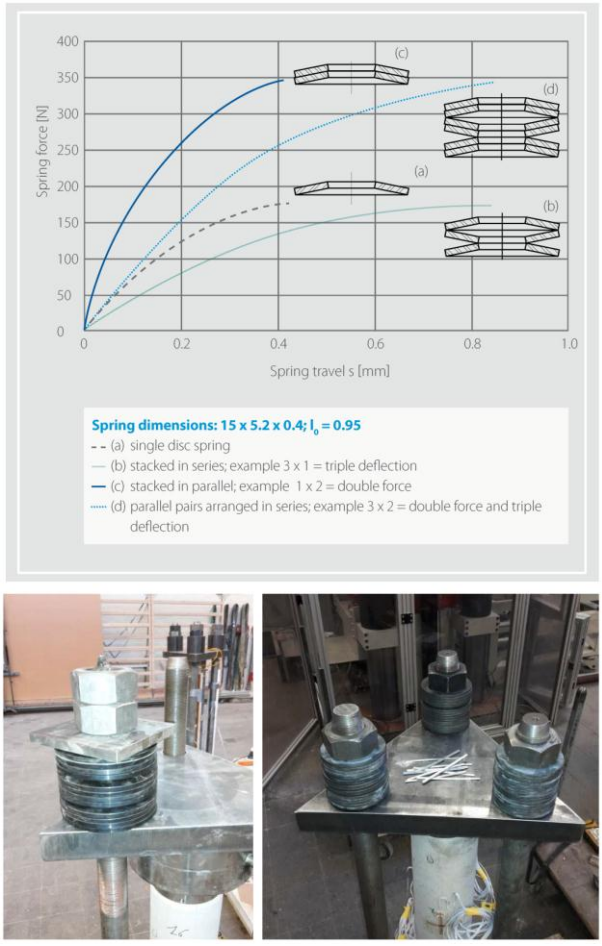

Figure 4.6. Disc springs used to keep constant the load on the specimens.

The design of the disc springs started from the evaluation of the creep of the plain concrete according to Eurocode 2 prescriptions. In details Eurocode 2 provides analytical relationships to obtain strain-induced by the creep effects on compressed members.

Once the creep strains of the preloaded specimens were obtained, calculation of the shortening of the specimens allowed to estimate the travel of the springs so that an adequate design of how to assemble them was done. This allowed a limited loss of load during the intermediate phases of the tests (that are preloading, wrapping, drying of the epoxy resin before failure loading).

Strain measurement

Two types of strain gauges were used for the acquisition of the strains during the different load stages: 90° 2-element Cross Plane type (60 mm gauge length) and single element type (linear strain record, 6 mm gauge length) for the plain concrete and the CFRP surface respectively. A single layer of strain gauges placed in the middle height of the specimens at an angular distance of 120°, so that for each specimen it was possible to get the average of three records for both hoop and axial strains (Fig. 4.7a).

During the preloading step, the load was kept centered by monitoring the tensile force at the threaded bars by means of linear strain gauges positioned at the middle height by an 180° angle (Fig. 4.7a).

Regarding the application of the strain gauges to the CFRP-confined specimens a special glue having function of smoothing the surfaces between carbon fibers and strain gauges was used to ensure electrical insulation during the acquisition process (Fig. 4.8).

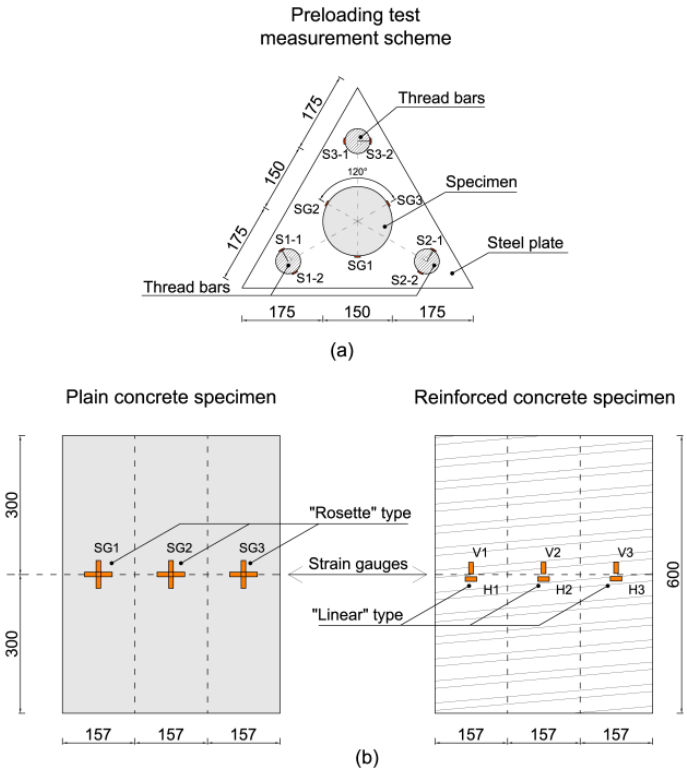

Figure 4.7. Strain gauges layout: preloading test measurement scheme (a), strain gauges arrangement on the specimens in developed view (b).

Figure 4.8. Application of strain gauges on the plain concrete and strengthened specimens.

4.3 Discussion of the results

In this section first the preloading tests are discussed, then the results of the collapse tests which allowed the determination of the maximum load capacity and the strain limits of the non-preloaded and the preloaded CFRP-confined specimens are presented.

Preloading tests

The preloading procedure was certainly the most difficult stage. During this phase, the application of the load to the plain concrete specimens was accurately carried out to avoid accidental eccentricity to the specimens, especially during the screwing of the nut done to maintain the load on the specimens after the unloading of the compression machine.

As described before, the traction force of the threaded bars was monitored by means of the strain gauges so to control the screwing process and maintain the same load for each bar. At the end of this stage, the load of the testing machine was zero but the load applied to the specimens – monitored also by a load cell properly placed – resulted equal to the target preload force. Some pictures showing this phase are reported in Fig. 4.9. The results of the preloading tests obtained for each specimens are illustrated in Fig. 4.10 and Fig. 4.11, showing in the first phase (preloading of the specimens) the increasing of the load testing machine force and the force measured through the load cell, while in the second phase it can be observed a reduction of the load transmitted by means of the load testing machine followed by the increasing of the load carried out by the threaded bars.

Figure 4.9. Plain concrete specimens: Application of the preload.

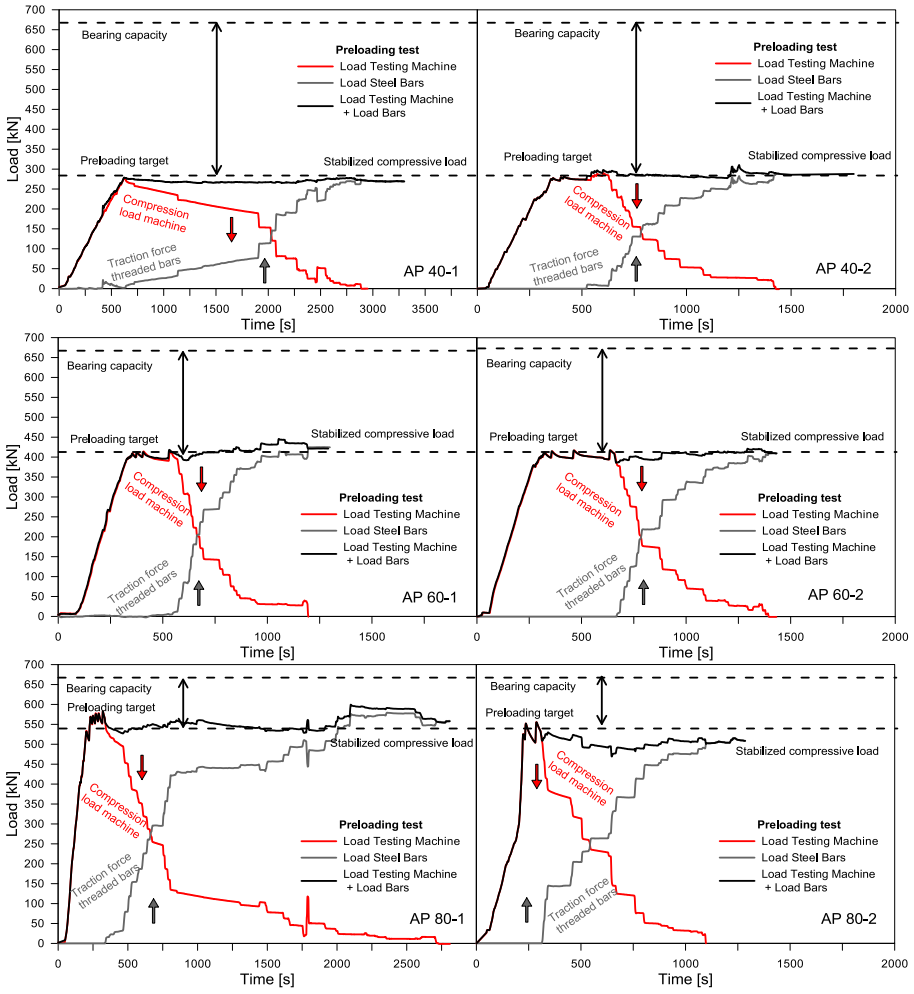

Figure 4.10. Preloading on specimens type A.

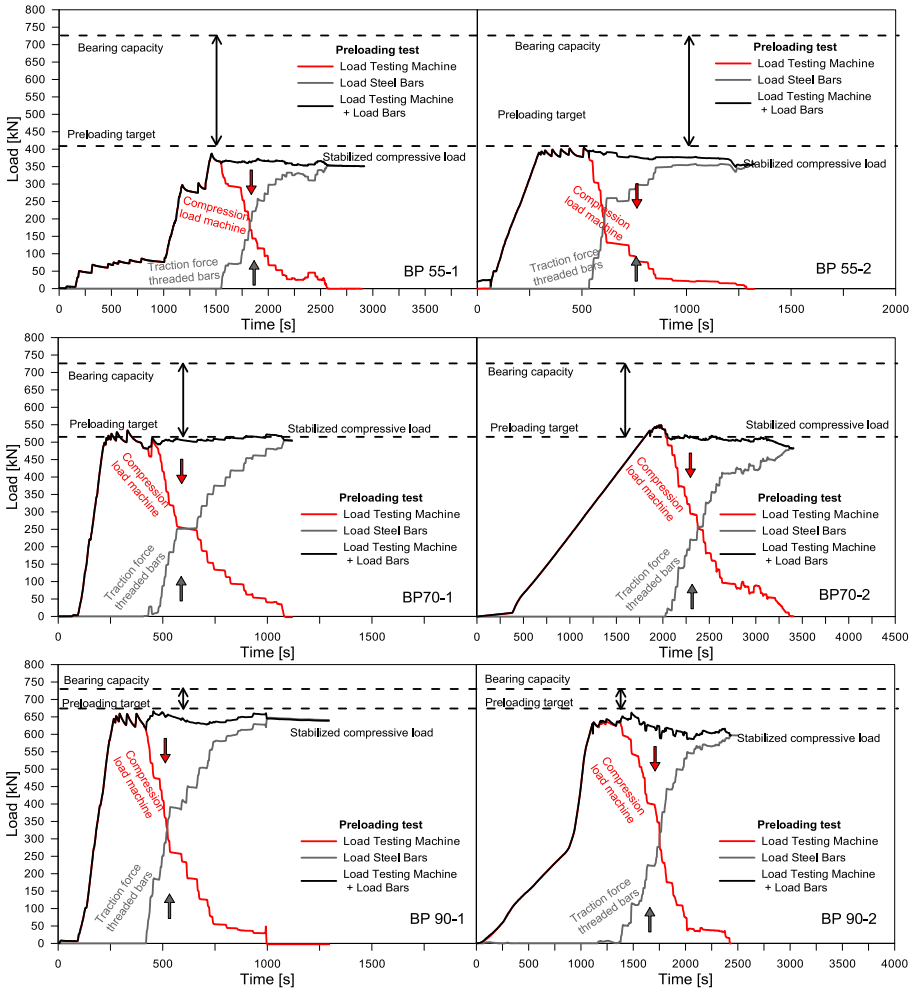

Figure 4.11. Preloading on specimens type B.

Unconfined concrete behavior was completely characterized (by recording axial and lateral strains) during the preloading by strain gauges applied at the middle height of the specimens. For each specimen the load-strain response was subsequently correlated with the results obtained by the failure tests described hereinafter.

Four representative points schematized the chronological process of the preloading up to the failure tests (see Table 4.3):

- The time T1, corresponding to the end of the application of preload;

- The time T2, corresponding to the removing of the strain gauges from the plain concrete and the application of the fiber textile and the epoxy resin;
- The time T3, corresponding to the moment in which the strain gauges were applied to the sheets (in this phase the epoxy resin was in the drying phase);
- The time T4, corresponding to the moment in which the confined specimens were subjected to the collapse tests.

Table 4.3. Temporal sequence of preparation of individual specimens.

Specimen	Age of concrete (hours) at			
No.	End of application of preload (T1)	End of wrapping (T2)	Begin of strain measurement (T3)	Begin of application of breaking load (T4)
AP 40-1	633	651	673	673
AP 40-2	1260	1265	1282	1304
AP 60-1	759	766	779	801
AP 60-2	1308	1328	1336	1353
AP 80-1	754	758	780	802
AP 80-2	1284	1303	1311	1330
BP 55-1	1476	1492	1502	1515
BP 55-2	2171	2176	2198	2212
BP 70-1	2126	2131	2151	2170
BP 70-2	2297	2315	2321	2343
BP 90-1	1814	1832	1837	1855
BP 90-2	2223	2226	2243	2266

For the specimens subjected to lower and medium preload levels (as specimens AP40-1, AP40-2, BP55-1 and BP55-2) after the achievement of the target preload a very stable behavior was found respect to the cylinders subjected to high preloading levels. No damage was observed for the plain concrete and the loss of load due to the creep and relaxation effects was negligible (for the preloaded specimens up to the 55% of the unconfined concrete strength the loss of load was lower than 7%).

Under high preloading conditions (between 55% and 90%) slightly more unstable behavior was observed: for the specimens AP80-1, AP80-2, BP90-1 and BP90-2, micro-cracks occurred in the plain concrete and nonlinear behavior of concrete resulted in a slightly higher loss of load during the

subsequent steps. Despite this, in the worst cases the loss of load did not exceed 18%.

To give a more accurate information about the preloading process Table 4.4 has been created in which the exact value of the preload force experimentally obtained is compared with the preload target force and the force at the moment of the collapse tests.

The behavior of the specimens during the subsequent steps after the preloading is reported in Fig. 4.12 showing the differences in terms of load reduction on the specimens with different preload levels.

Table 4.4. Preloading test results and monitoring.

Specimen	Target preload force (kN)	Experimental preload force at time T1 (kN)	Experimental / target preload deviation	Experimental preload at time T4 (kN)	% loss of load
AP40-1	270	267.29	0.99	261.05	2.33
AP40-2	270	266.81	0.99	256.25	3.96
AP60-1	393	395.9	1.00	366.14	7.52
AP60-2	393	406.7	1.03	368.17	9.47
AP80-1	525	540.11	1.03	443.76	17.84
AP80-2	525	527.34	1.00	433.08	17.87
BP55-1	393	361.5	0.92	354.55	1.92
BP55-2	393	397.97	1.01	371.98	6.53
BP70-1	525	541.19	1.03	468.62	13.41
BP70-2	525	551.94	1.05	477.81	13.43
BP90-1	655	661.84	1.01	564.13	14.76
BP90-2	655	640.04	0.98	544.06	15.00

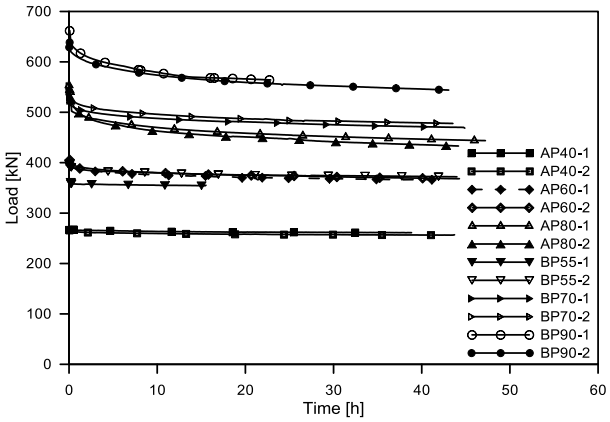

Figure 4.12. Load trend on the specimens during the test stages.

Collapse tests

During the monotonic compression tests in both cases (with and without preload) the load was strictly increased until collapse, exhibiting a bilinear behavior in accordance with the classical formulations of the confining mechanism of circular columns. The failure of all tested specimens was reached in correspondence of the failure strain of the fibers, with an average hoop rupture strains of the FRP obtained from the compression tests smaller than the tensile strains provided from the technical sheets, in agreement with several previous studies (Spoelstra and Monti, 1999, Lam and Teng, 2004).

Respect to the reference specimens (A1 and B1), monotonic tests of the confined cylinders showed an increasing of the compressive strength $k_2=f_{cu}/f_{cm}$ of 2.65 and 1.84 for the type A and B respectively, with a large increasing of the ultimate strain capacity, that, in the case of confined curves with hardening behavior, corresponds to the strain at maximum confining stress ε_{cc}. Results of the compressive tests are summarized in Table 4.5.

Table 4.5. Experimental results of the tested specimens.

Series	Specimen	f_{cm} (MPa)	P_{max} (kN)	f_{cu} (MPa)	ε_{cc} (%)	$\varepsilon_{h,rup}$ (%)
A	A1	38.13	670.20	37.93	0.200	0.092
	AS1	38.13	1800.00	101.85	2.302	1.256
	AS2	38.13	1754.46	99.28	2.262	/
	AS3	38.13	1792.83	101.45	2.254	1.177
	AP40-1	38.13	1748.08	92.22	2.163	/
	AP40-2	38.13	1756.96	99.42	2.391	1.149
	AP60-1	38.13	1718.21	97.23	2.452	/
	AP60-2	38.13	1789.95	101.29	2.605	1.307
	AP80-1	38.13	1742.63	98.61	2.639	1.219
	AP80-2	38.13	1641.54	92.89	2.547	1.130
B	B1	41.70	740.80	41.89	0.180	0.058
	BS1	41.70	1332.40	75.39	1.622	1.04
	BS2	41.70	1391.30	78.71	1.671	1.047
	BP55-1	41.70	1365.62	77.28	1.773	1.067
	BP55-2	41.70	1371.75	77.62	1.789	1.069
	BP70-1	41.70	1433.69	81.29	1.740	1.043
	BP70-2	41.70	1398.09	79.11	1.622	1.056
	BP90-1	41.70	1492.18	84.44	2.172	/
	BP90-2	41.70	1375.33	77.83	1.916	1.079

Some unconfined and confined specimens before and after the compression test are shown in Fig. 4.13. Concrete compression crushing failure was observed for the specimens A1 and B1 with smeared vertical cracking formed near to the crushing load (about 90% of the compressions strength of the material). The very good compaction of the concrete during the casting process provided to the specimens a good compression behavior so that cracking resulted as much as possible reduced and near to the failure conditions. This aspect was utmost of importance for the subsequent preloading tests because the absence of cracks avoided stress concentration of tension on the fibers without causing premature failure.

All the tested specimens having the same characteristics showed a very similar behavior. Therefore the axial behavior of the tested specimens was well identified to investigate the differences compared to the preloaded specimens.

Figure 4.13. Unconfined and confined concrete specimens. Monotonic tests without preload.

The analysis of the results obtained from tests with preload allowed to state that the ultimate capacity of the confined specimens seems to be not particularly affected by the preloading level reached before applying the CFRP sheets. All the tested specimens showed similar behavior at failure characterized by the achievement of the failure strain of the carbon fibers (Fig. 4.14 shows some preloaded confined specimens before and after the tests), and a comparable ultimate load. Instead, a difference between the two types of test was observed in the load-strain behavior.

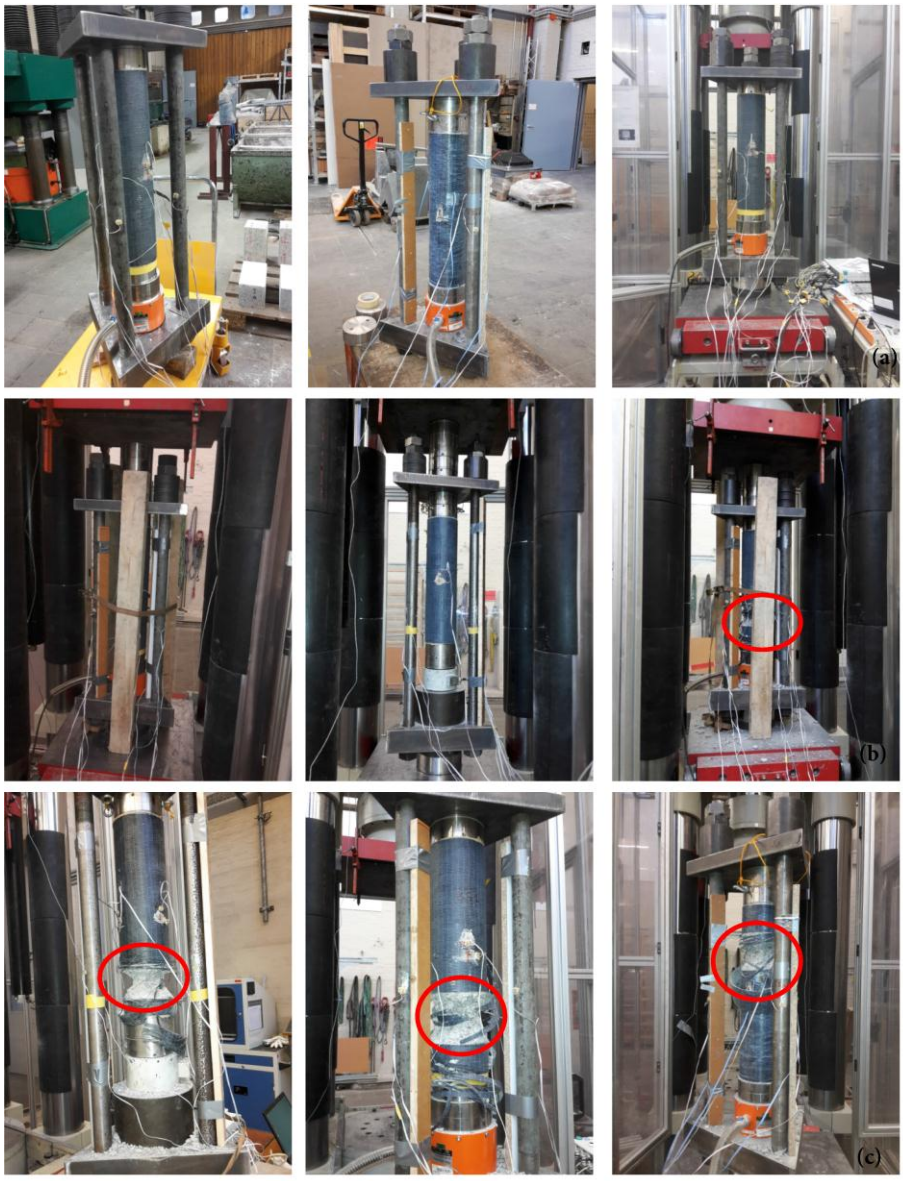

Figure 4.14. Specimen under preload (a); failure test on preloaded specimens (b); specimens at the end of failure tests (c).

Comparisons between the resulting curves (Figs. 4.15) show that the stiffness of the first ascending branch (before the stiffness turning point) is not affected by the preloading. This agree also with the standard case in which it is well known that the ascending branch of FRP-confined concrete does not provide variations respect to the unconfined concrete response up to stresses near to the unconfined concrete strength. Indeed, since the preload forces were in every cases lower than the unconfined concrete strength, the unconfined and confined concrete responses had to be the same regardless the presence or not of the preload. Conversely, a change of the stiffness (slight decrease in slope with increasing of the preload levels) in the second ascending branch was observed in some cases, while in the other cases a slope similar to that obtained from the monotonic tests, but with reduced values, was obtained. This reduction in the secant stiffness could be justified by the fact that the lateral confinement pressure at the same axial strain was lower due to the strain-lag that causes, for the same value of lateral strain of the concrete, lower values of lateral pressures. The reason is the lower strain of the fibers, as in detail explained below.

In particular, the ultimate strength and strain capacity is associated with the rupture of the fibers. Consequently, when the column is wrapped under a certain stress/strain level, the fibers start to stretch after with respect to the case in which the confinement is applied at zero stress/strain levels. Therefore, at the same level of axial strain, the preloaded specimens provide a lower load because of the lower strain of the fibers. For example, by analyzing the resulting curves of Fig. 4.16, if specimens AS1-2 at 0.01125 of axial strain and the corresponding lateral strain of 0.006 are compared the non preloaded response with the preloaded one, to give the same value of lateral strain, specimen AP60-2 needs to reach 0.0121 of axial strain and specimens AP80 1-2 need to reach 0.0134 of axial strain. The same effect can be observed for specimens type B. An other way to highlight this particularity is to observe the behavior in terms of secant dilation angle, as will be described in the next section.

The above discussed phenomenon allows reaching slightly higher ultimate axial strain at the same ultimate compressive strength.

It is important to underline that the reduction of the load-strain response respect to the non-preloaded cases resulted more evident in the case of specimens of type A. For the specimens of type B the experimental results showed a very similar behavior, independently from the preloading level.

Moreover, increasing of the ultimate compressive strain, caused by the delayed CFRP wrapping, was more evident also for the specimens of type A.

Results regarding the lateral strains of specimens AS2, AP 40-1 and BP90-1 are not included in the analysis because of an anomalous behavior recorded by the horizontal strain gauges.

The loss of load and the increasing of axial strain on specimens subjected to high preloading levels modified experimental load-strain response so that in the first phase of the collapse tests, the previous unloading determined a semi-cyclical response whereby the ascending branch showed a higher stiffness, as a reloading, and then continued with the desirable monotonic response. Specimens AP80-1, AP80-2, BP90-1 e BP90-2 showed a noticeable semi-cyclical behavior, as it is possible to observe in Fig. 4.15.

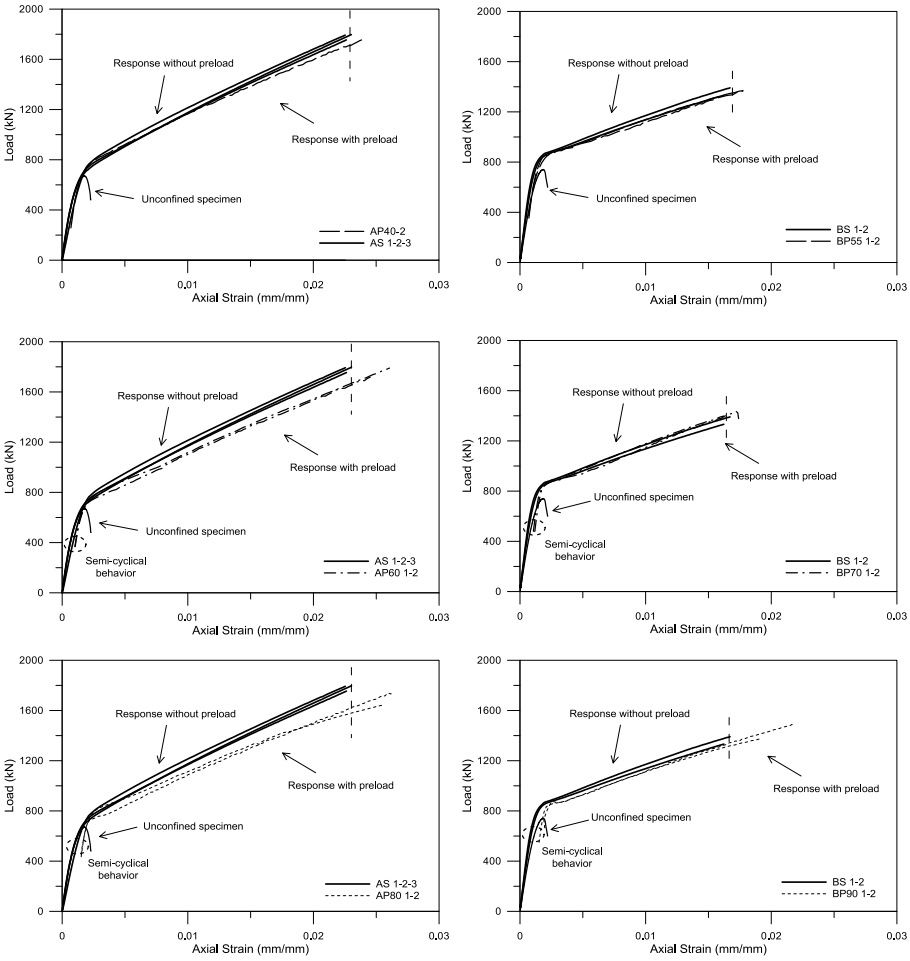

Figure 4.15. Experimental load-axial strain response: comparisons between non-preloaded and preloaded specimens.

Lateral strain to axial strain response and dilation angle

Several previous studies investigated with different approaches the lateral strain to axial strain response of FRP confined concrete under monotonic compressive loads. In some cases, explicit relationships were used to describe the lateral strain and axial strain behavior through the secant or tangent dilation angle, or the secant strain ratio of the confined concrete (Mirmiran and Shahavy, 1997, Binici, 2005, Lam and Teng, 2007). In other cases, an implicit relationship was adopted as a result of increasing of the area strain (Benzaid et al., 2010). Other authors provide closed form

equation to obtain the entire lateral strain to axial strain response of the confined concrete subjected to passive and active lateral pressure (Teng et al., 2007, Lim and Ozbakkaloglu, 2014). In this study, the secant dilation angle η, defined as the ratio of the secant slope of the lateral-to-axial strain curve of FRP-confined concrete ($\varepsilon_l/\varepsilon_c$), is adopted to show the deformational behavior of the non-preloaded and preloaded tested specimens. Lateral strains and axial strains are assumed to be positive.

In this section, load-strain response is analyzed by comparing all the tested specimens (Fig. 4.16 a (1-2). As mentioned in the previous section, reduction of the load capacity for a given value of axial strain appears to be more evident in the case of high confinement ratio (as in the case of specimens of type A), while this effect seems to be less marked for medium confinement ratio (as in the case of specimens of type B).

In Fig. 4.16 b (1-2), experimental lateral-to-axial strain response shows appreciable differences of the preloaded specimens respect to the case of standard monotonic tests. Differences are denoted in the second branch of the lateral-to-axial strain curves. The first branch is the same for all the tested specimens, while, in the second branch, the preloaded specimens provided a "delayed confined response" with a lower slope when the confinement become significantly relevant on the load-strain response (in agreement with Pan et al., 2017a, Pan et al., 2017b).

This effect is also highlighted in the Fig. 4.16 c (1-2) where the secant dilation angle of the confined concrete was lower respect to the standard monotonic tests. In particular, the reduction of η seems to be more evident with the increasing of the preloading levels.

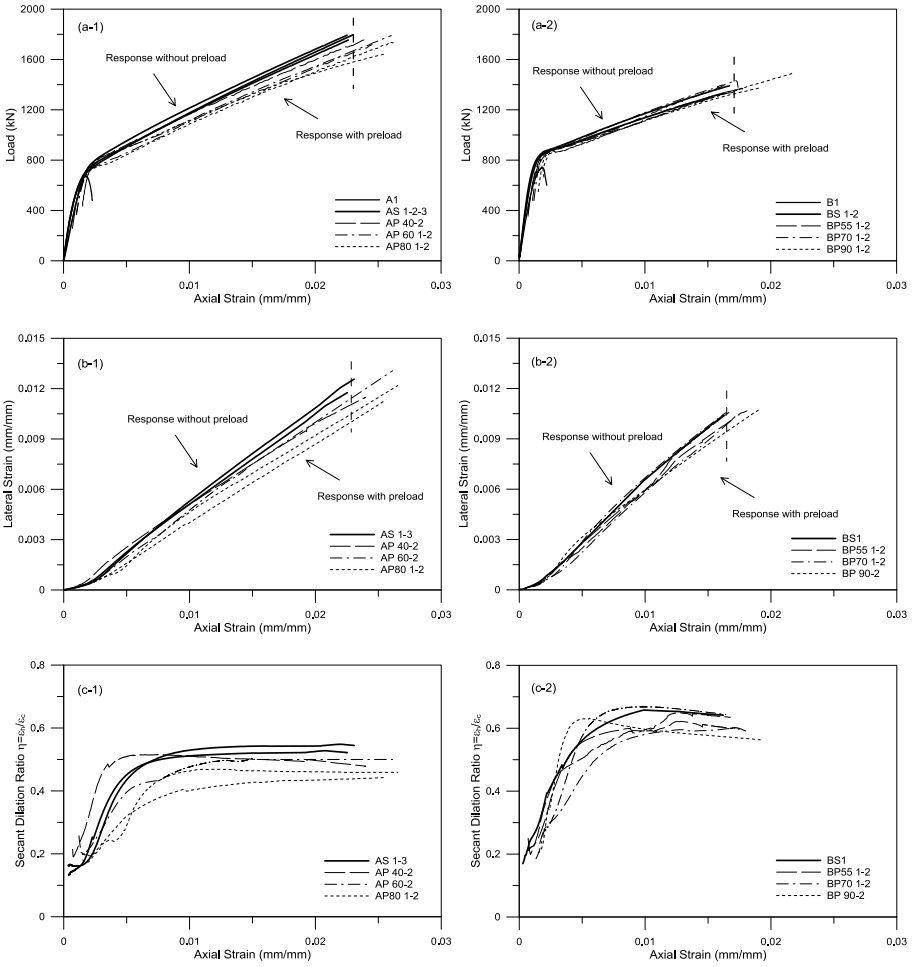

Figure 4.16. Experimental responses: (a-1) load-strain curves - concrete type A, (a-2) load-strain curvesc- concrete type B, (b-1) lateral strain-axial strain curves - concrete type A, (b-2) lateral strain-axial strain curves - concrete type B, (c-1) secant dilation ratio - concrete type A, (c-2) secant dilation ratio - concrete type B.

Evaluation of the lateral confinement pressure provided by CFRP sheets

It is well known from the literature (Spoelstra and Monti, 1999, Lam and Teng, 2003) that ultimate hoop strains of the fibers are smaller than the nominal values and also in this experimental work this phenomenon was observed for the strengthened specimens. Usually, basing on experimental

observations, reductive factors are provided in order to obtain the lower value to compute lateral confinement pressure of the FRP jackets. Here, the average of the ultimate hoop strains at collapse was computed and compared with the nominal value provided by the technical sheets, defining the effective strain factor k_f. In the case of specimens with three CFRP sheets (specimens of type A) the average value of $\varepsilon_{h,rup}$ was equal to 1.206% and the corresponding value of k_f became 0.670. While, for the specimens with two CFRP sheets (specimens of type B) the values of $\varepsilon_{h,rup}$ and k_f were 1.057% and 0.587 respectively.

In addition to the classical considerations, lateral confinement pressure in the case of preloaded specimens fl_P is affected by the lateral strain configuration of the specimens at the moment in which confinement jackets are applied. Therefore, ultimate effective lateral confinement pressure is not associated with the ultimate strain value experimentally recorded but rather to the confined load-strain history. To evaluate the exact value of the lateral confinement pressure it is necessary to detract from the ultimate hoop strain $\varepsilon_{h,rup}$ the strain value ε_h^* corresponding to the moment in which the specimens became "confined" by the application of the unidirectional carbon fiber textile. Here, this value is assumed equal to the strain corresponding to the beginning of the failure tests. In this way, reduced hoop strain $\varepsilon_{h,eff}$ was used to evaluate the respective ultimate lateral pressure, that is:

$$fl_P = \frac{2 \cdot t_j \cdot E_{jm} \cdot \varepsilon_{h,eff}}{D} = \frac{2 \cdot t_j \cdot E_{jm} \cdot \left(\varepsilon_{h,rup} - \varepsilon_h^*\right)}{D} \qquad (4.2)$$

Results are shown in Table 4.6. Even the value of fl_P is associated with the collapse conditions, the "step-by-step" value of the load-strain response is lower with respect to the case without preload, and this phenomenon could justify the reduced step-by-step axial capacity of the preloaded specimens. However, the value of maximum lateral confinement pressure obtained for all the tested specimens resulted the same independently from the applied preload level. This means that the failure conditions correspond to an equal strength value but to different ultimate strains due to the delayed application of the fiber composite textile.

Table 4.6. Lateral pressure experimentally determined.

Series	Specimen	$\varepsilon_{h,rup}$ (%)	$\varepsilon_{h,eff}$ (%)	Lateral pressure (MPa)
A	A1	0.092	-	-
	AS1	1.256	1.256	15.408
	AS2	/	/	/
	AS3	1.177	1.177	14.432
	AP40-1	/	/	/
	AP40-2	1.149	1.139	13.965
	AP60-1	/	/	/
	AP60-2	1.307	1.292	15.844
	AP80-1	1.219	1.163	14.267
	AP80-2	1.130	1.079	13.238
B	B1	0.058		-
	BS1	1.040	1.040	8.501
	BS2	1.047	1.047	8.558
	BP55-1	1.067	1.049	8.578
	BP55-2	1.069	1.054	8.616
	BP70-1	1.043	1.017	8.314
	BP70-2	1.056	1.030	8.423
	BP90-1	/	/	/

To confirm further the above statement, Fig. 4.17 shows the comparisons between the maximum lateral confinement pressure provided by the CFRP jackets for both types of reinforced specimens. After the evaluation of the lateral pressure by the compression test without preload, the obtained average value is assumed as a reference value to compare the values coming from the tests under preload conditions. In the case of equal strength of the confined concrete, of course, equal value of the lateral confinement pressures has to be obtained for each level of applied preload. This phenomenon is confirmed in all the examined cases (specimens AS-AP and BS-BP). In detail, specimens AP40-2 and AP80 1-2 show a slightly lower confinement pressure respect to the average value, while specimen AP60-2 shows a slightly higher confinement pressure, indicating therefore that the similar values of the compressive strength of all the tested specimens depend on the similar value of the maximum lateral confinement pressure. For the case of specimens with concrete type B strengthened with two CFRP sheets, very near values respect to the average lateral pressure are observed. This phenomenon is obviously connected also in this case to the comparable ultimate load experimentally observed for all the tested specimens.

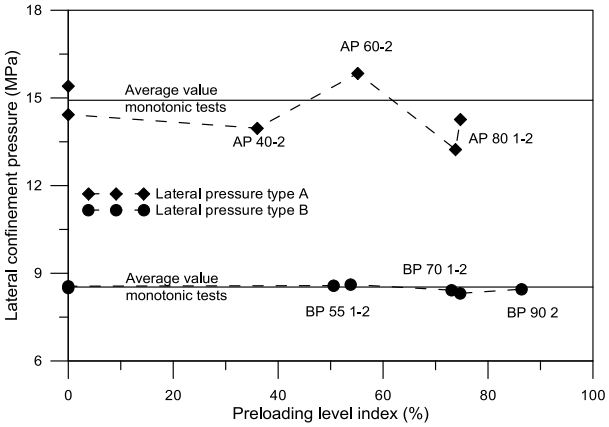

Figure 4.17. Maximum lateral confinement pressure of the tested specimens.

Consideration on the ultimate conditions and comparison with the available data

In order to better understand the differences of the results, an effective preloading strength factor $k_{s,prel}=f_{cu,p}/f_{cu}$, was defined as the ratio between the ultimate confined compressive stress of a preloaded specimen $f_{cu,p}$ and the ultimate confined compressive stress obtained from standard compression tests f_{cu}. Similarly, considerations on the strain capacity were analyzed by the effective ultimate strain ratio $k_{\varepsilon,prel}=\varepsilon_{cc,p}/\varepsilon_{cc}$, defined as the ratio of the ultimate confined compressive strain of a preloaded specimen $\varepsilon_{cc,p}$ and the ultimate confined compressive strain obtained from the standard tests ε_{cc}. Results were also compared with the experimental investigation carried out by He and Jin (2011).

As depicted in Fig. 4.18, results of the current study present a little scatter with a regular trend for both efficiency factors. Regarding the strength capacity, the values of $k_{s,prel}$ are around the unit value, indicating, as mentioned before, that preloading levels do not influence the failure load. The scatter assumes a maximum values of ± 6% and a standard deviation σ=0.0339 (differently from what found by He and Jin, 2009, that is σ=0.0727), and these variations can be attributed to experimental uncertainties (small eccentricity in the specimens, non-homogeneity of the concrete and small imperfections during the bonding of the fiber textiles to the specimen). Furthermore, ultimate strain capacity factor $k_{\varepsilon,prel}$ shows an

increasing trend with the increasing of the preloading level index in agreement with the above considerations. More regular trend for the concrete "type A" was observed, with a maximum value $k_{\varepsilon,prel}$ of 1.161 (corresponding to an increase of 16.10% of the ultimate confined compressive strain) in the case of preloading force of 80%. Although the trend is less regular for the concrete type B, also, in this case, a higher ultimate strain was observed for all the preloaded specimens (except specimen BP70-1) with a maximum value equal to 1.163 for the specimen BP90-1 (in agreement with specimens AP 80 1-2).

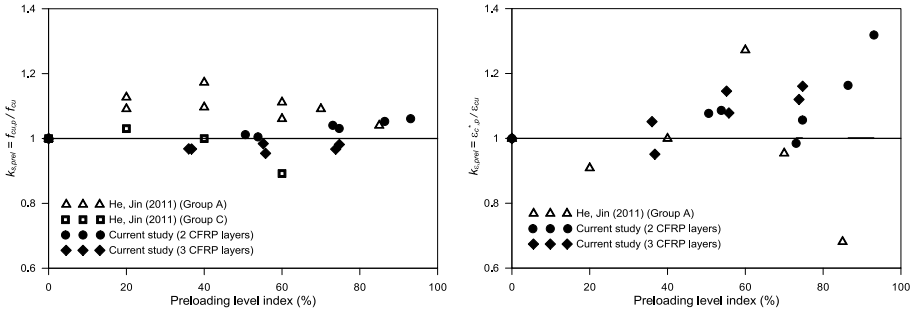

Figure 4.18. Effective preloading factors.

4.4 Comparisons between experimental results and FE model

A FE model has been developed on the basis of the formulations described in chapter 3.4 with regard to the monotonic compressive behavior without preload and chapter 3.5 for simulations that take into account the effects of preload. The FE model is also based on the mechanical characteristics of the materials (concrete and FRP) obtained from the above experimental study.

Moreover, comparisons between FE model and experimental results are basic for the validation of the FE strategy discussed in the previous chapter.

In this regards, Fig. 4.19 shows that good agreement was found between experimental results and numerical simulations. A very small reduction of the axial stress vs axial strain curve was obtained by assigning the preloading level on the plain concrete model. In details, in the case of a preloading level up to 40% f_{c0}, the effect of preloading may be neglected entirely. As long as the unconfined concrete is elastic, the response of the preloaded configuration overlaps the monotonic response. When the

preloading level increases, a reduction of the axial stress vs axial strain response becomes significative.

The important aspect to focus on is also that the numerical model previously developed reproduces the same experimentally observed phenomenon. Although the preload level in the specimens may change, the strength corresponding to the collapse after the confinement results unchanged. Also, it corresponds to the ultimate deformation of the carbon fibers. Specimens confined after different preload are able to carry the same collapse load, showing a reduction in the secant stiffness of the stress-strain law, in both experimental and numerical cases. Fig. 4.19 shows that this reduction increases with the increasing of the preload level.

Regarding the results obtained from the finite element modeling it is important to state that the only parameter that defines the relationship between the evolution of the axial and the lateral strain is the dilation angle.

The ratio between lateral and axial strain exhibited by confined concrete follows the same law of the unconfined concrete until reaching a constant[8] value, depending on the stiffness of the bandage. In case of specimens subjected to preloading, the first load stage is not affected by the presence of the bandage, while when the fibers start to give their contribute, the relationship between the strains (axial and lateral) is almost linear, and the trend is similar to that exibited by the specimens without preload (Fig. 4.20).

Comparisons between the numerical and experimental results show a good agreement confirming the reliability of the FE model in the prediction of both the trend of the strains connected to the lateral confining pressures and finally of the confined concrete strength and of the strain capacity.

Even though the lateral strain vs axial strain response remains almost unchanged, differences are observed in terms of lateral confinement pressure evolution in the comparison between preloaded and non-preloaded specimens. From the moment in which the fibers are applied to the model under deformed shape, the fibers themselves follow the lateral concrete strain and the axial concrete strain development. Depending on the strain level of the concrete, the lateral confinement pressure may increase more or

[8] It was demonstrated (Hany et al., 2016), as also explained in the Chapter 3, that by using a constant dilation angle the lateral strain-to-axial strain relationship is not affected by a change in slope after the turning point of the axial stress-axial strain relationship of the FRP-confined concrete.

less rapidly. For instance, as given in Fig. 4.21, it is possible to observe that, after preload levels of 50%, lateral pressure shows almost a linear behavior.

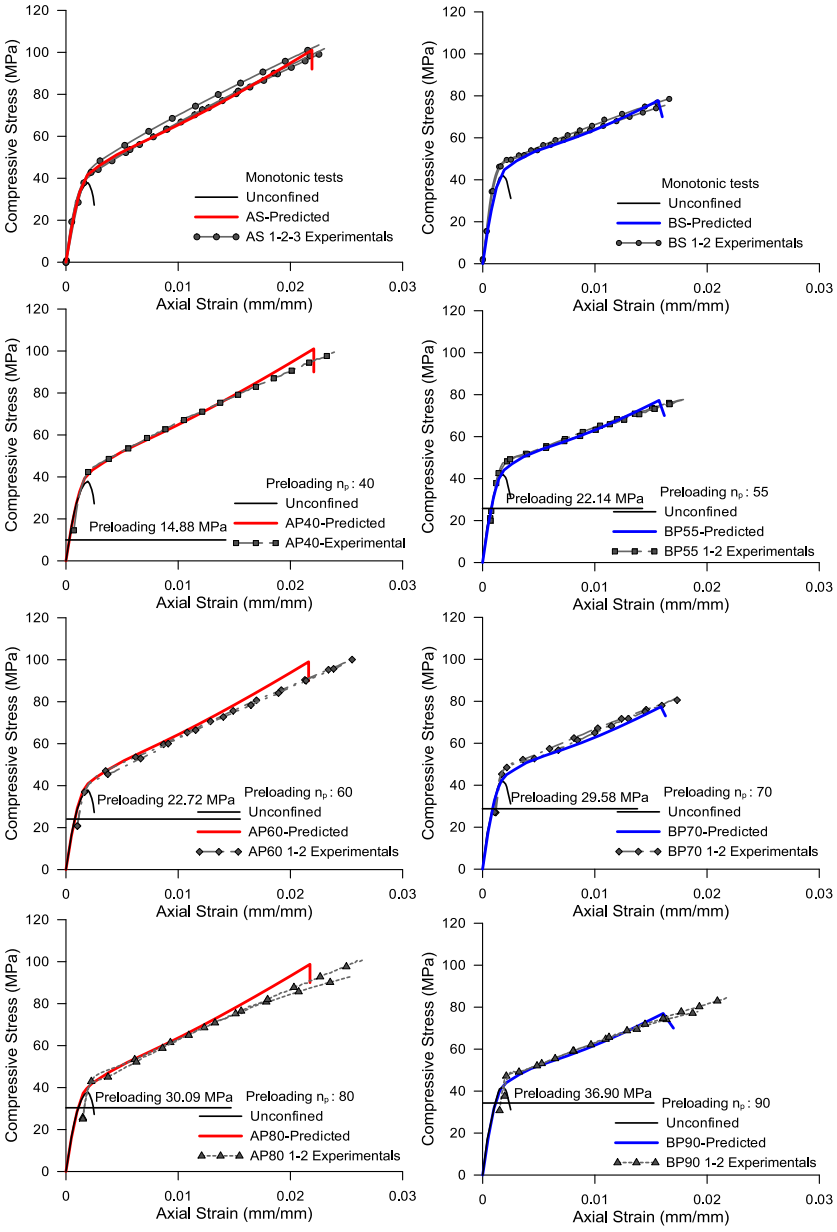

Figure 4.19. Axial stress-to-axial strain responses: experimental-FEM comparisons of non-preloaded and preloaded specimens.

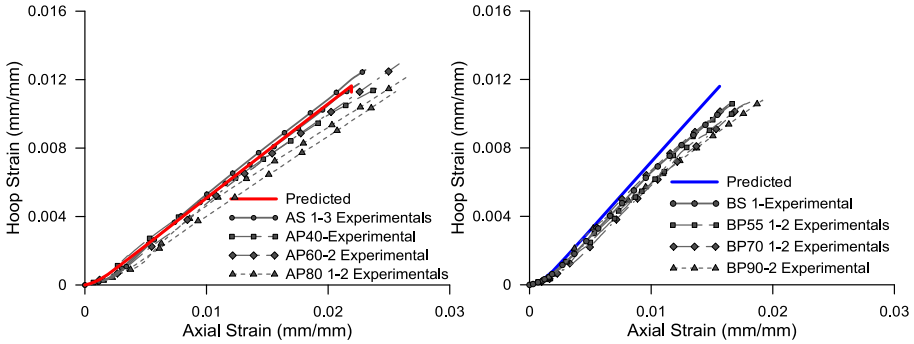

Figure 4.20. Lateral strain-to-axial strain response: experimental-FEM comparisons.

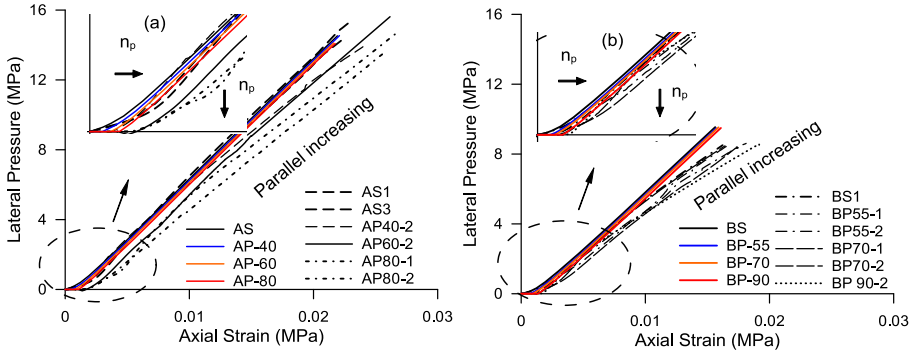

Figure 4.21. Lateral pressure in the case of preloaded specimens: experimental-FEM comparisons of specimens type A (a) and specimens type B (b).

4.5 Analytical modeling

Above it has been shown that through an accurate FE modeling it is possible to reproduce the compression behavior of concrete specimens confined with FRP subjected to monotonic load, preloaded or not preloaded.

However, FEM modeling involves a significant computational effort and, above all, requires the case by case definition of specific parameters.

In order to have a reliable and easy-to-manage computational tool to predict the compression behavior of confined concrete, the analytical analysis-oriented type models (treated in chapter 2 dedicated to the state of

the art of them) are suitable. These models allow obtaining the complete response in compression through an incremental process that governs the response depending on few parameters easily manageable.

4.5.1 Analysis-oriented model for the compressive behavior of FRP-confined concrete under monotonic load conditions

Here, a modification of the parameters of the analysis-oriented stress-strain model provided by Teng et al. (2007) to reproduce the experimental results is presented before introducing new concepts regarding the response under preloading conditions. In particular, the lateral-to-axial strain relationship and the failure criterion is modified to obtain a better prediction of the deformational behavior in function of the mechanical parameters of the confined concrete.

Lateral confinement pressure

According to the traditional formulations available in the literature, in case of circular sections, the ultimate lateral confinement pressure can be obtained by the following relationship:

$$f_{l,\max} = \frac{2 \cdot t_j \cdot E_j \cdot \varepsilon_{h,rup}}{D} \tag{4.3}$$

in which t_j is the thickness of the bandage, E_j is the actual elastic modulus of the fibers, D is the diameter of the section and $\varepsilon_{h,rup}$ is the hoop strain corresponding to the rupture of the fibers. Several previous works demonstrated that the value of $\varepsilon_{h,rup}$ results greatly reduced respect to the nominal value ε_{ju} provided by the data sheets. Here, the effective value of the rupture hoop strain is evaluated as a function of the concrete strength at the ultimate nominal value, by the relationship proposed by Lim and Ozbakkaloglu (2015).

$$\frac{\varepsilon_{h,rup}}{\varepsilon_{ju}} = k_f = 0.9 - 2.3 \cdot f_{c0} \cdot 10^{-3} - 0.75 \cdot E_j \cdot 10^{-6} \tag{4.4}$$

in which k_f is the strain reduction factor, and f_{c0} is the unconfined peak strength of the concrete.

Lateral strain-to-axial strain relationship

The original formulation proposed by Teng et al. (2007) results useful because it is applicable to unconfined, actively confined and FRP-confined concrete. The axial deformation – lateral deformation law assumes the form:

$$\frac{\varepsilon_c}{\varepsilon_{c0}} = \Phi\left(\frac{-\varepsilon_h}{\varepsilon_{c0}}\right) = A\left\{\left[1+B\left(\frac{-\varepsilon_h}{\varepsilon_{c0}}\right)\right]^C - \exp\left[D\left(\frac{-\varepsilon_h}{\varepsilon_{c0}}\right)\right]\right\} \tag{4.5}$$

in which ε_c is the current axial strain, ε_{c0} is the unconfined peak strain, and A, B, C, D are constants originally proposed equal to 0.85, 0.75, 0.7 and 7 respectively. Moreover, the relation between axial strain and lateral pressure f_l is:

$$\frac{\varepsilon_c}{\varepsilon_{c0}} = \left[\Phi\left(\frac{-\varepsilon_h}{\varepsilon_{c0}}\right)\right]\left(1+\beta\frac{f_l}{f_{c0}}\right) \tag{4.6}$$

in which β is a coefficient with a proposed value equal to 8.

This equation results an efficient tool to predict the sectional behavior, conversely, it is not able to capture the tri-dimensional behavior of confined cylinders. In the present study, the constant B of Eq. 4.5 and the parameter β of Eq. 4.6 have been recalibrated to give a better agreement with the test results. In details the proposed values are 0.8 and 10, respectively.

Axial stress-strain relationship

As it was suggested in the previous studies, the "step-by-step" response can be obtained through an incremental process in which for a given value of axial or lateral strain, the corresponding stresses are determined with reference to an equivalent active confinement state. The entire process is represented up to the failure of the specimens, that corresponds to the rupture of the fibers. In order to represent the entire load/strain process, an iterative process is required if the incremental step is performed for a given axial strain value, because the corresponding value of lateral strain has to be determined in such a way the equilibrium conditions are satisfied. On the other hand, if the incremental process is performed for a given value of lateral strain, the corresponding value of axial strain can be easily determined.

The axial stress-strain law of the confined concrete is represented by the original equation proposed by Popovics (1973) for unconfined concrete and

used later by several authors to reproduce the behavior of steel and FRP-confined concrete:

$$\frac{\sigma}{f_{cc}} = \frac{x \cdot \gamma}{\gamma - 1 + x^{\gamma}} \quad \text{for} \quad 0 \le \varepsilon_c \le \varepsilon_{cu} \tag{4.7}$$

$$x = \frac{\varepsilon_c}{\varepsilon_{cc}}, \gamma = \frac{E_c}{E_c - \frac{f_{cc}}{\varepsilon_{cc}}} \tag{4.8}$$

Moreover, the following equations are proposed to determine the peak strength f_{cc} and the strain ε_{cc} at the peak stress of the confined concrete corresponding to a certain value of lateral confinement pressure:

$$\frac{f_{cc}}{f_{c0}} = 1 + k_1 \left(\frac{f_l}{f_{c0}} \right)^{A_1} \tag{4.9}$$

$$\frac{\varepsilon_{cc}}{\varepsilon_{c0}} = 1 + 5k_1 \left(\frac{f_l}{f_{c0}} \right)^{A_1} \tag{4.10}$$

with k_1 and A_1 equal to 4.1 and 1.025 respectively.

4.5.2 Analysis-oriented model of preloaded FRP-confined concrete

Axial-lateral strain relationship of unconfined concrete

When the concrete section is subjected to a certain stress level, the corresponding axial and lateral strains can be obtained if the constitutive relationships are assumed. In the present study, the constitutive law proposed by Popovics (1973) is adopted to describe the axial compressive behavior of the unconfined concrete.

$$\frac{\sigma}{f_{c0}} = \frac{x \cdot r}{r - 1 + x^{r}} \quad \text{for} \quad 0 \le \varepsilon_c \le \varepsilon_{cu} \tag{4.11}$$

$$x = \frac{\varepsilon_c}{\varepsilon_{c0}}, \qquad r = \frac{E_c}{E_c - E_{\sec}}, \qquad E_{\sec} = \frac{f_{c0}}{\varepsilon_{c0}} \tag{4.12}$$

For a given value of axial strain, the corresponding lateral strain of the can be determined if the relationship between the two strains is known. To correlate the current lateral strain corresponding to the preload state, the relationship proposed by Kupfer et al. (1969) allows obtaining the variation of the Poisson ratio ν of concrete under biaxial stress state and consequently the value of ε_h:

$$\varepsilon_h = \varepsilon_c \cdot \nu(\varepsilon_c) \tag{4.13}$$

$$\nu(\varepsilon_c) = \nu_0 + 1 + 1.38\left(\frac{\varepsilon_c}{\varepsilon_{c0}}\right) - 5.36\left(\frac{\varepsilon_c}{\varepsilon_{c0}}\right)^2 + 8.59\left(\frac{\varepsilon_c}{\varepsilon_{c0}}\right)^3 \tag{4.14}$$

Lateral confinement pressure under preloaded conditions

To evaluate the exact value of the lateral confinement pressure, it is necessary to detract from the current hoop strain ε_h normally exhibited in an unconfined state, the strain ε_h^* prevented by the confinement. In this way, the "step by step" value of the lateral pressure is correlated to the strain compatibility of the preloaded stress/strain state.

$$fl_p = \frac{2 \cdot t_j \cdot E_j \cdot \varepsilon_{hp}}{D} = \frac{2 \cdot t_j \cdot E_j \cdot \left(\varepsilon_h - \varepsilon_h^*\right)}{D} \tag{4.15}$$

and consequently, the confined strength and corresponding strain can be determined by using Eqs 4.9-4.10 as:

$$\frac{f_{cc}}{f_{c0}} = 1 + k_1\left(\frac{fl_p}{f_{c0}}\right)^{1.025} \tag{4.16}$$

$$\frac{\varepsilon_{cc}}{\varepsilon_{c0}} = 1 + 5k_1\left(\frac{fl_p}{f_{c0}}\right)^{1.025} \tag{4.17}$$

Considering what above described, the stress-strain curve can be obtained by the following simple procedure:

- Fix the preloading ratio index n_p;
- evaluate the preloading axial stress of the unconfined concrete through Eq. 4.1;
- evaluate unconfined axial and lateral strain at the fixed stress level Eqs. 4.11-4.14; to this point, at each increment of lateral strain $\varepsilon_{hp} = \left(\varepsilon_h - \varepsilon_h^*\right)$ evaluate the actual value (fl_P) using Eq. 5.15;
- calculate the actual confined concrete strength and axial corresponding strain by Eqs. 4.16-4.17;
- determine the confined current stress and strain by Eqs. 4.7-4.8;

The procedure is developed until ε_{hp} reaches the rupture value, defined by Eq. 4.4.

4.5.3 Experimental-analytical comparisons

The stress-strain response obtained from the analysis oriented model agree well with the experimental results. Indeed, as the preloading level index increases, a reduction of the confined compressive stress value, corresponding to the step-by-step value of the lateral confinement pressure occurs ($f_{lP}<f_l$ for each incremental step).

In the first phase (corresponding to the preloading), unconfined and confined response results very similar, because, as it is well known from the mechanism of passive confinement, there are no difference between the stress-strain curves up to relevant values of the lateral confinement pressure and, therefore, the confined concrete is not affected by an effective confinement level. This effect is also noticed in the lateral strain-to-axial strain relationship, that shows an analog trend for the unconfined and confined concrete.

In the second branch (for compressive stress higher than f_{c0}), the curves of non-preloaded and preloaded elements follow almost a parallel trend with hardening stress-strain behavior. This branch is characterized by lower values of the compressive stress for an assigned strain in the presence of preloading due to the reduction of the secant stiffness of concrete caused by the preloading itself. Finally, failure conditions are identified from the same value of the lateral confinement pressure, and consequently, the same value of the compressive strength of the confined concrete. The value of ultimate axial confined strain results improved in order to allow the achievement of the rupture hoop strain $\varepsilon_{h,rup}$.

In Figs. 4.22 and 4.23, comparisons between analytical and experimental results in terms of lateral confinement pressure and axial compressive stress-strain curves are shown in the case of low, medium and high preloading levels. It is important to state that in the case of low preloading levels (for a preloading stress ranging from 40% and 55% of f_{c0}), differences between preloaded elements' response and non-preloaded elements' response are negligible. Differences are denoted starting from medium preloading levels (specimens AP 60, BP 70, AP 80, BP 90).

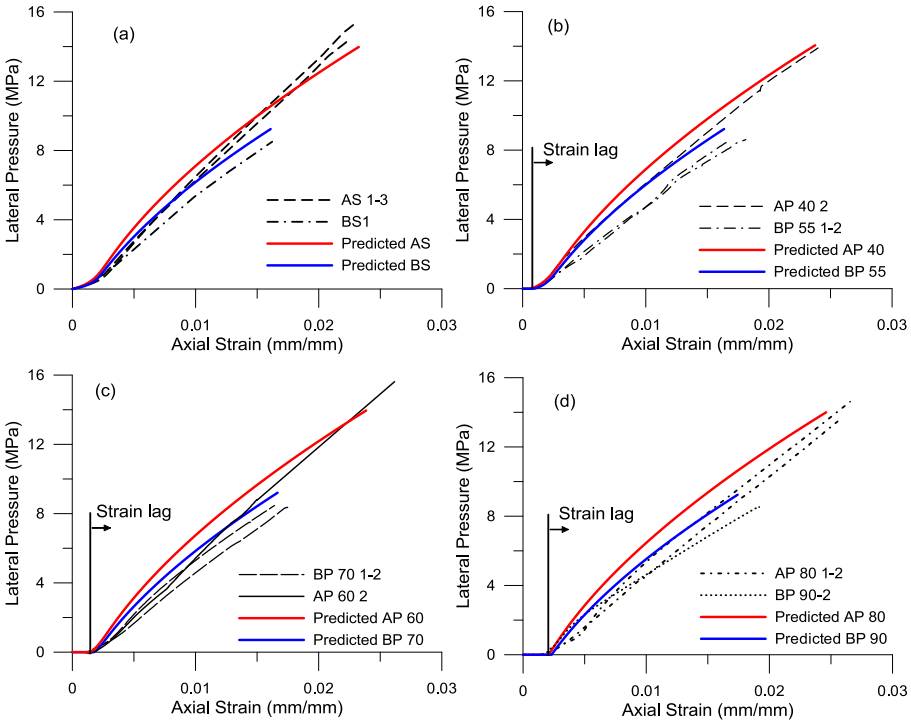

Figure 4.22. Comparisons between experimental and analytical lateral confinement pressure for (a) confined non preloaded specimens; confined specimens after (b) low, (c) medium, (d) high preloading levels.

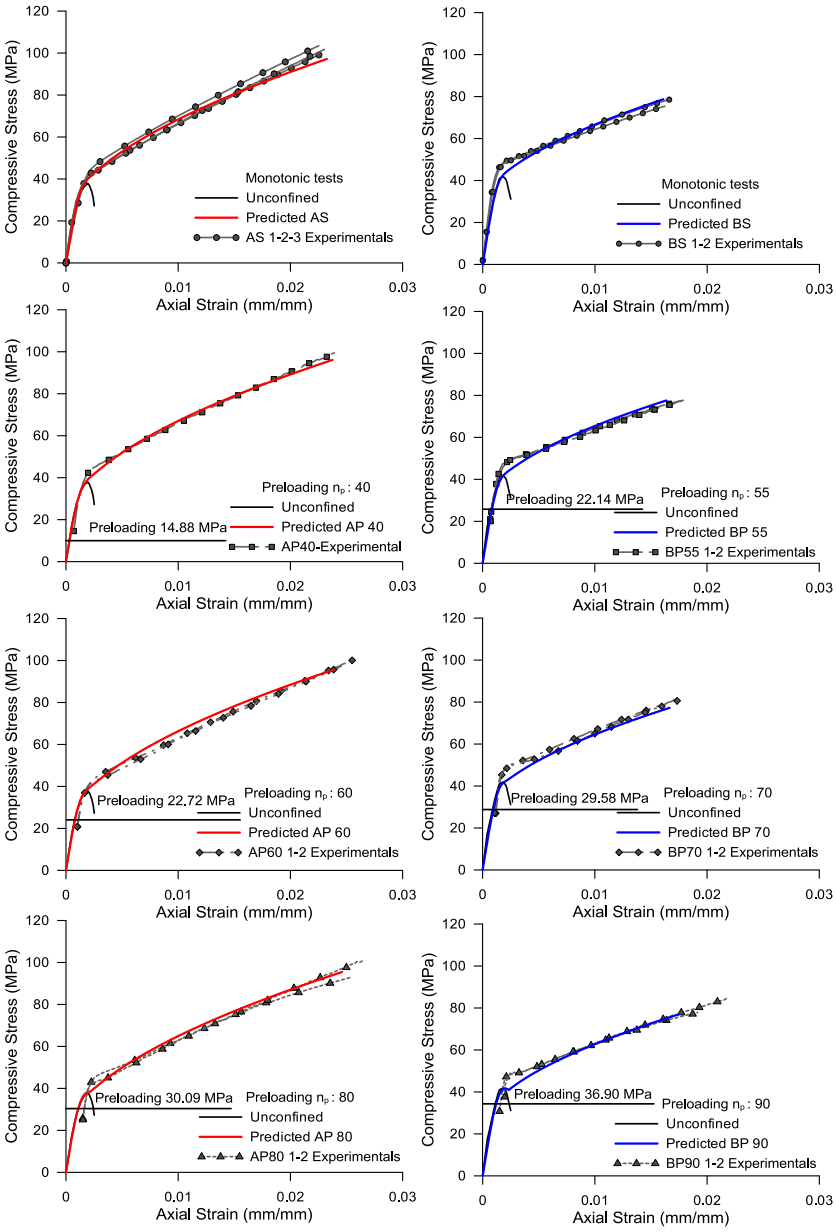

Figure 4.23. Comparisons between experimental and analytical axial stress-to-axial strain curves for (a) confined non preloaded specimens; confined specimens after (b) low, (c) medium, (d) high preloading levels.

5. AXIALLY PRELOADED STEEL JACKETED SUBSTANDARD CONCRETE COLUMNS: EXPERIMENTAL INVESTIGATION AND MODELING

5.1 Introduction

The findings of Chapter 4 are here extended to the case of confinement by means of steel cages composed by angles and battens. Differently from the FRP wrapping that provides elastic confinement up to the failure of the composite jackets, the mechanical behavior of the steel confining device involves elasto-plastic confinement response, with maximum lateral confining pressure achieved in correspondence to the yielding of the steel. It should be noted that the non-uniform distribution of the axial and consequently the lateral strains along the element confined translates into a complex compression response because the yielding of the external steel reinforcement is not reached at the same time by all the components. Moreover, in the case of jacketing by steel angles and battens, more attention needs for the evaluation of the axial load-bearing contribute given by the confined concrete and the steel angles.

As a preliminary consideration it could be expected that loading before application of the reinforcement, delay of the confinement and delayed activation of the angles translate into a considerable reduction of the capacity with respect to the case of members not loaded before the reinforcement. However, since there are no available studies on this subject, this statement needs to be accurately proved by experimental observations.

This chapter presents an experimental investigation aimed to verify this. All the procedures adopted to simulate the strengthening process under service conditions (that is under preexisting loads) and the evaluation of the compressive response will be described. Finally, an analytical model able to consider the preloading effects is developed on the basis of the experimental observations.

5.2 Experimental program

The experimental program consisted in compression tests on ten columns strengthened by means of steel cages under different load conditions. Tests on unreinforced, reinforced before any loading and reinforced after axial loading at a fixed rate of the capacity were provided.

Concrete prismatic specimens having dimension of 200x200x750 mm (aspect ratio 1:3.75) were made by means of wooden formworks. At the top and the bottom two steel grid were inserted to provide an over strength to the far ends of the specimens avoiding potential brittle failure during compression tests. During the casting process, soft vibration ensured a minimum void content in the cementitious matrix. Leveling of the end cross-sections of the specimens was performed to guarantee a uniform contact during the compression tests between machine loading plate and specimen.

The steel cage was composed by angles and strips, of type S275 steel, having dimension of 50/50/5 and 40/4 respectively connected with each other by welding (see details in Figs. 5.1-3). For both angles and battens, no mortar was uses at the contact surfaces with the concrete columns.

The effect of a load preexisting at the time of the reinforcement was investigated experimentally by applying the steel jacketing on loaded specimens and subsequently performing collapse tests. As discussed in the previous chapter, the compressive response of the confined concrete was evaluated for low, medium and high level of the preload.

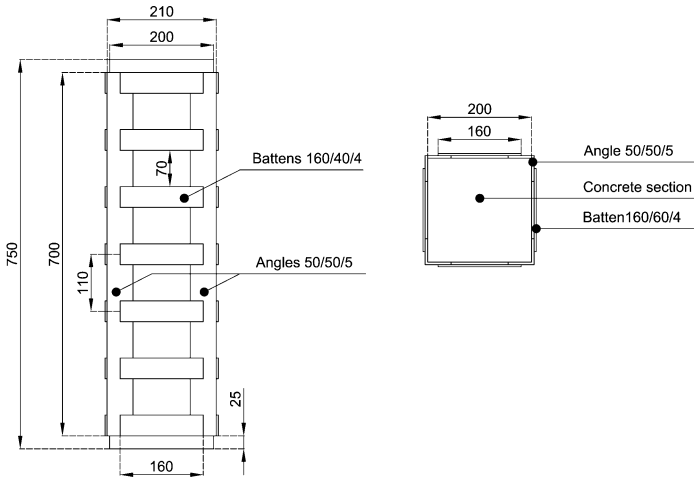

Figure 5.1. Geometrical details of the steel jacketed specimens.

(a) (b)

Figure 5.2. Casting of concrete (a); leveling of the specimen end-cross sections.

(a) (b) (c) (d)

Figure 5.3. Plain concrete specimens (a); component of a steel jacket before the application (b); fixing of a steel jacket to a concrete specimen before final welding (c); welded jacket in the final configuration.

Test set up and instrumentation

The monotonic compression tests were carried out using a compression machine with a nominal maximum loading capacity of 4000 kN. The assigned displacement speed was 0.3 mm/min. The displacements were imposed by a servo-hydraulic system electronically controlled by the user from a computer.

Axial strains on the column specimens were measured by means of two systems of digital transducers. Four of these had a gauge length equal to the internal length of the specimen (750 mm) and were placed at the corners. Further, four transducers were placed on the lateral faces of the column at the middle height, with a gauge length of 220 mm. The double system of transducers allowed the recognition of strain concentration in the middle of the specimens. Strains on the steel cages were also recorded by means of "linear type" strain gauges with gauge length of 13 mm. Horizontal and vertical strain gauges were bonded to the steel battens in correspondence of the middle height of the column and of the external surface of the steel angles at the top, the middle and the bottom respectively. This measurement layout allowed to obtain average strains and stresses of the battens (controlling therefore the evolution of the lateral pressure) and average strains and stresses of the angles (obtaining the axial load carried out by the angles). Details of the measurement setup are reported in Fig. 5.4.

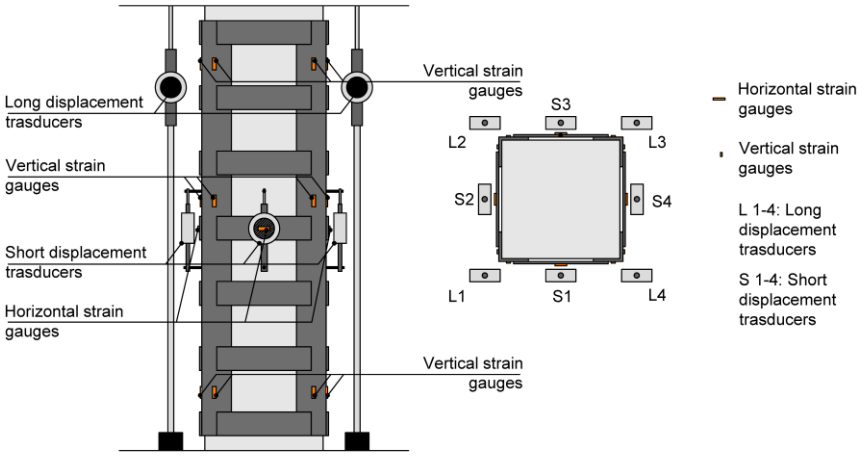

Figure 5.4. Arrangement of measurement devices.

Preloading was applied in a special three-dimensional steel testing frame system composed by three rigid steel beams and four steel bars (diameter of 80 mm) fixed to the lower floor structure. Hydraulic jack and a load cell were placed between the central steel beam and the concrete specimen in order to apply the compressive force monitored by digital data acquisition system.

The welding of the steel cages was done while specimens were under a certain assigned stress/strain state. The apparatus for the preloading is shown in Fig. 5.5.

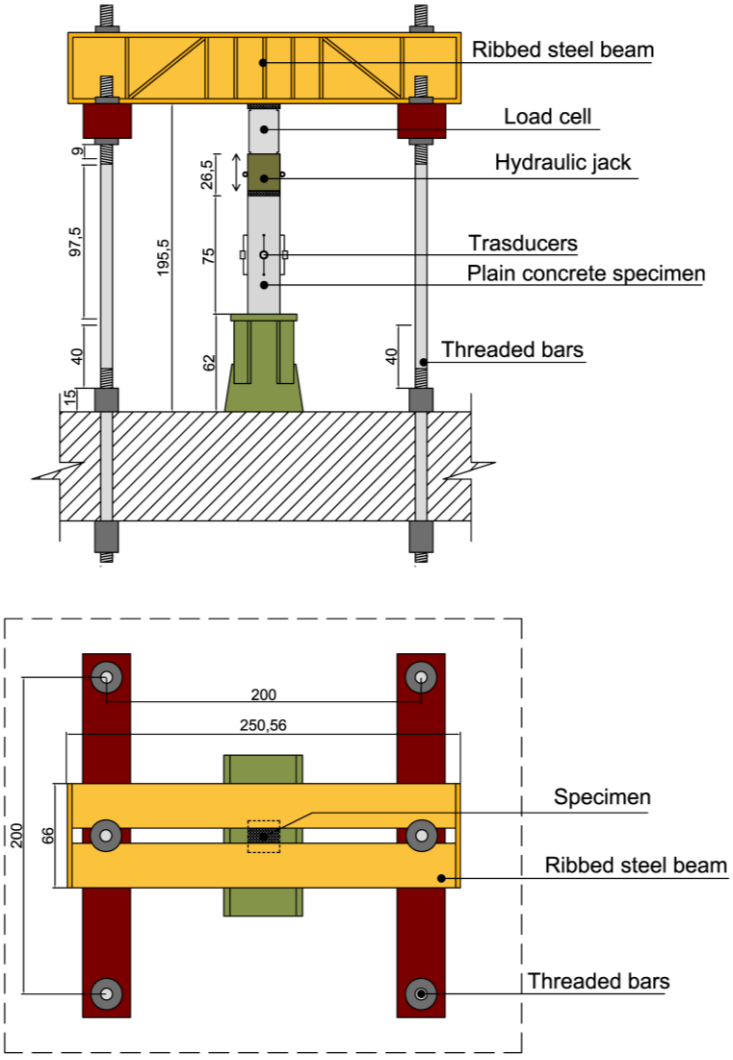

Figure 5.5. Preloading apparatus.

Compression tests on steel jacketed concrete specimens not preloaded were performed to obtain an upper bound that identifies the standard conditions in which laboratory tests are performed, and then to observe the differences with the response of the specimens reinforced while loaded. During loading, concrete is subjected to a lateral confinement pressure while angles are subjected to frictional forces caused by the sliding between the column-angles contact surfaces.

During the monotonic tests, the axial strains on the angles, the shortening of the column, the shortening along the height of the specimens and the strains of the battens were recorded. Steel jacketed non preloaded columns subjected to compression are shown in Fig. 5.6.

Figure 5.6. Steel jacketed specimens before compression (no preloading).

Compression tests on preloaded specimens were performed under established preload forces. After the strengthening, the specimens were unloaded and moved to the load testing machine to perform the failure load test. By unloading the specimens after wrapping the concrete went back to a zero stress state coupled to a residual plastic strain. Conversely, the steel cage (that was welded when the column was in a deformed shape) kept its configuration. When the strengthened specimens were reloaded for the collapse test, the first stage of loading interested only the concrete without any contribution of the jackets which became effective when the concrete reached the load/strain configuration corresponding to the level of the preload. Fig. 5.7 shows the preloading and a step of the strengthening of a specimen.

Figure 5.7. Preloading of a specimen and welding/application of the steel jackets after loading.

The steps of the tests of the preloaded specimens are listed hereinafter:

- Preloading: during this stage, the measuring of the shortening in the middle height of the specimens allowed to identify the stress-strain behavior of the unconfined concrete. Once the target preload was reached, stabilization of the load and acquisition of creep strains evolution were performed;
- Strengthening: After preloading, digital transducers were removed from the concrete specimens and steel jackets were applied by welding;
- Unloading: specimens were unloaded and transferred to the load testing machine, strain gauges were applied to the steel cages and the digital transducers to the concrete specimens as in the case of the preload tests. Moreover, long digital transducers were assembled at the four corners of the specimens;
- Collapse test: the specimens were loaded up to collapse, recording axial strains of the columns and axial and lateral strains on the steel jackets.

Fig. 5.8 shows the scheme of the test procedure.

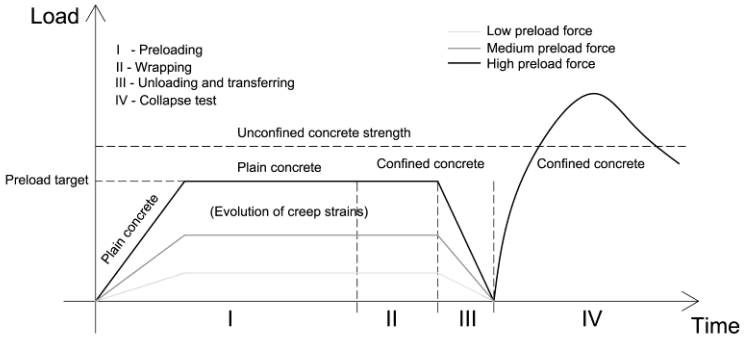

Figure 5.8. Specimen loading history.

Mechanical characterization of the materials and preloading level index

The target strength for the concrete was 20 MPa. Concrete mixture was composed by CEM I 32.5 R, water, sand and aggregate with size varying from 0 to 20 mm, having proportion in weight 1:1.51:0.384:0.353. Concrete cubes having size of 150 mm were made during the concrete casting, testing the compression strength after 28 days. The tests were performed according to *UNI EN 12390* Standards. Test results are given in Table 5.1, while some pictures of the mechanical characterization of the concrete are shown in Fig. 5.9.

Table 5.1. Mechanical properties of the concrete.

Cube (150 mm)	Max load (kN)	Strength (MPa)	
1	476.90	21.195	Average cubic strength (MPa) 19.986
2	457.00	20.311	
3	494.30	21.968	
4	494.10	21.960	Standard Dev. 2.2936
5	423.90	18.840	
6	396.50	17.622	
7	442.60	19.671	
8	375.30	16.680	Average cylinder strength f_{c0} (MPa) 16.59
9	399.40	17.751	
10	536.90	23.862	

The preload level, defined as the ratio between the compression stress applied to the specimen and the compression strength of the unconfined concrete (Eq. 1.1), was chosen depending on the strength obtained by the

compression tests on cubes (mean cylindrical strength f_{c0} =16.59 MPa) and from compression tests on two plain concrete specimens. Considering that maximum loads for the two specimens were of 633.94 kN and 715.27 kN (average max load and stress of 674.58 kN and 16.86 MPa respectively) the target strength f_{c0} was therefore considered equal of 16.75 MPa.

Figure 5.9. Compression tests on concrete cubes.

Specimens were labeled depending on the type of preload (P#), the type of reinforcement (S) and the number of the specimen #. For example, specimen P0S1 referred to 0 preload force, specimen strengthened with steel jackets (S), specimen n°1, while specimen P40S2 referred to a preload force nominally equal to the 40% of the strength, specimen strengthened with steel jackets, specimen n°2. Table 5.2 lists the details of each test.

Table 5.2. Type of tests.

Specimen	f_{c0}, ε_{c0}, E_c	Type	Preload level (%)	Preload force (kN)
NC1	16.75 MPa 0.002 19358.36 MPa	Plain	/	0
NC2		Plain	/	0
P0S1		Confined	/	0
P0S2		Confined	/	0
P40S1		Preloaded and confined	40	270
P60S1		Preloaded and confined	60	402
P60S2		Preloaded and confined	60	402
P72S1		Preloaded and confined	72	483
P80S1		Preloaded and confined	80	530
P80S2		Preloaded and confined	80	530

5.3 Discussion of the results

Preloading tests

Load-strain response of specimens during preloading tests was monitored to obtain the unconfined concrete behavior before the application of the external reinforcement. Fig. 5.10 shows the compressive response of the specimens loaded at 40%, 60%, 72% and 80% of f_{c0}. The responses were also compared with the results of monotonic tests up to collapse for the unconfined specimens NC1 and NC2 and the corresponding theoretical unconfined concrete stress-strain law according to Popovics (1973).

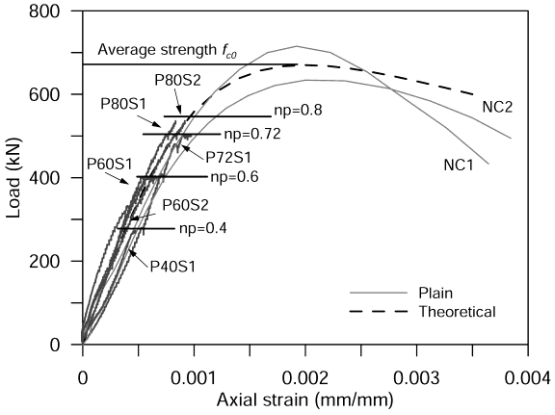

Figure 5.10. Load-strain curves of the plain concrete specimens.

Preload tests had variable duration depending on the evolution of creep strains after the maximum load was reached. In Table 5.3, the results of the preload tests are reported. In details, the strains of the specimens at the end of the application of the preload force ε_{c1}, the strains at the time of application of the steel cages ε_{c2} and the corresponding concrete ages are listed. The results are also compared with the analytical predictions according to Eurocode 2 *EN 1992-1-1* (Fig. 5.11). Eurocode 2 relationships resulted suitable to an overall prediction on the evolution of strains as confirmed by analytical-experimental comparisons.

Table 5.3. Strain at the end of the preload monotonic ramp (T1) and at the end of the constant preloading time corresponding to the application of the steel jacket (T2).

Specimen	Age of concrete T_1 (hours)	Strain ε_{c1}	Age of concrete T_2 (hours)	Strain ε_{c2}
P40S1	6120.0	0.000194	6130.0	0.000289
P60S1	5040.0	0.000556	5051.0	0.000872
P60S2	5340.0	0.000684	5350.0	0.000796
P72S1	5760.0	0.000799	5766.5	0.001050
P80S1	7380.0	0.000854	7387.5	0.001159
P80S2	7560.0	0.000798	7565.0	0.001430

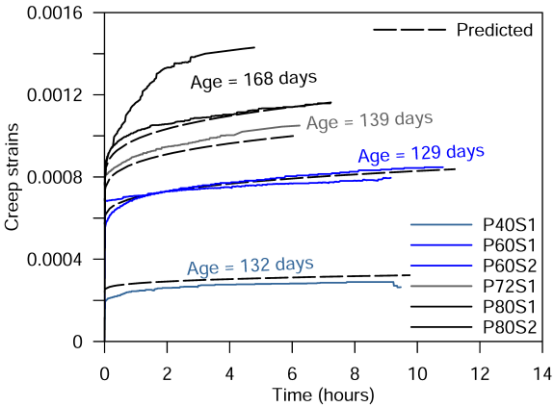

Figure 5.11. Evolution of creep strains on the preloaded specimens.

In the case of low preload levels, i.e. for preloaded specimens at 40% and 60% of the strength, creep strains evolution was restricted and stable. In fact, axial strains increased about 48.96% after 10 hours of load for specimens P40S1, while the creep strain increasing was of 56.83 % and 33.33% after about 10 hours of load for specimens P60S1 and P60S2 respectively. Otherwise, for high preload forces, higher creep strains evolution was observed followed by smeared cracking of the specimens (see Fig. 5.12). In the latter case, time of preload was limited to avoid excessive damage. For example, creep strain increase was of 31.41% for the specimen P72S1 after 6.5 hours of preload and of 36% after 7.5 hours of load for specimen P80S1. Anomalous behavior was observed by specimen P80S2 for which creep strain increasing was 79.20 % after only 5 hours of preloading.

Figure 5.12. Evolution of cracking strain on specimen P80S2.

Collapse tests

Load-strain response of the strengthened specimens was characterized by load increasing behavior up to the maximum load capacity, followed by a strain-softening behavior. Compression tests were terminated in correspondence to a reduction of 85% of the maximum load. In some case a premature failure of the confinement device occurred by failure of the welding between steel angle and strip causing a high loss of load (as for specimen P0S2).

The results showed a significant increase in load and deformational capacity compared to the compression response of unconfined specimens. In details, the maximum load of the P0S1 and P0S2 (non-preloaded) specimens was 1364.8 kN and 1402.97 kN respectively, with an average strength increasing of 105.14 % respect to specimens NC1 and NC2. It is important to note that this increase in the load capacity was due to the global contribution provided by the response of the confined concrete and the angles. Analogous reasoning has to be done also for the increase of strain at the peak stress; P0S1 and P0S2 showed a peak strain of 1.721% and 1.813%, respectively, with an average increasing of 772.59% respect to the plain concrete.

Compression tests of preloaded specimens showed differences respect to the non-preloaded ones. Load-strain curves were affected by reduction of the maximum load bearing capacity and a significant reduction in the secant stiffness. This effect was caused by the delayed response of the confined concrete (lower confinement lateral pressure for a given value of axial strain respect to the non-preloaded specimens) directly proportional to the applied preload level as for the load carried out by the angles. These reductions can be observed in Table 5.4 that summarizes the experimental results in terms of maximum axial load capacity P_{max}, strain at peak stress ε_{cc}, ultimate load P_u and the corresponding strain ε_{cu}. Moreover, load strain response is shown in Figure 5.13.

Table 5.4. Experimental results of the tested specimens.

Specimen	f_{c0} (MPa) ε_{c0}	P_{max}	ε_{cc}	P_u	ε_{cu}
NC1		715.227	0.00202	589.006	0.00300
NC2		633.936	0.00203	494.777	0.00387
P0S1		1364.800	0.01721	1165.333	0.03236
P0S2		1402.970	0.01813	1347.733	0.02003
P40S1	16.75	1297.300	0.01519	1061.330	0.02688
P60S1	0.002	1274.137	0.01988	1118.988	0.03180
P60S2		1237.306	0.01426	1078.410	0.02784
P72S1		1179.805	0.01902	1051.200	0.02774
P80S1		1203.005	0.014500	973.8667	0.03825
P80S2		1323.125	0.019193	1059.204	0.03781

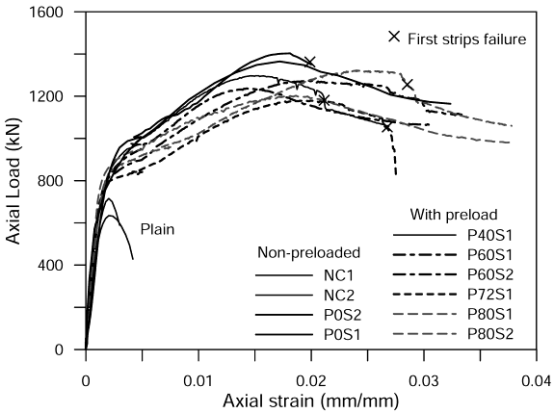

Figure 5.13. Load-strain response of the tested specimens.

In order to better understand the effects of preload on the compression response it is useful to differentiate the concrete response from that of the angles; in this way, the single contribute to the load-bearing capacity can be identified adequately.

By the strain gauges applied to the angles, the average stress of the angles was obtained (readings at the top, at the bottom and at the middle height). By the mean strain the corresponding axial load was calculated. Finally, the axial load was correlated to the axial strain of the specimens to obtain the load strain response.

In the case of monotonic tests without preload, the response of the angles was activated from the initial loading phases exhibiting a linear increasing behavior until a load of about 418 kN corresponding to about 1.5% of axial strain of the specimens (axial stress of about 220 MPa lesser than the yield stress of steel that in the present case is 275 MPa), after which no significant increase in stress was observed until the failure of the specimens.

This behavior confirms the findings of Chapter 2.[9]

Also for the case of preloaded specimens the maximum load obtained for the angles was comparable, with desirable bilinear behavior in terms of load-strain response. Only for the P80S1 and P80S2 specimens the yield stress was reached. Since the strain distribution along the height of the specimen is

[9] In Chapter 2 it was demonstrated that after the achievement of the maximum frictional forces along the contact surfaces between steel angles and concrete, only sliding occurred without further stress increasing.

not uniform, this difference could be attributed to strain concentration with the result that the local stress increased.

On the other hand, the delay in activation of the angles response with respect to the case without preload was observed for all the specimens. Apart from the specimen P40S1 subjected to a preload of 40% of f_{c0} for which the response in the early stages was similar to the specimens without preload, the other tests showed different load-strain curves. In fact, the global response was characterized by a reduction in capacity also due to the lower contribution of angles in the early stages of loading. Fig. 5.14 shows the experimental response of the angles.

Concrete contribution was then obtained by subtracting the load-strain response of the angles from the global load contribution of the specimens. Figure 5.15 shows the load-strain curves of the confined concrete. In this figure the responses of the unconfined concrete are included too. The effect of the reinforcement resulted in an increase in the strength of the concrete and a considerable increase in ductility.

As regards to preloaded specimens, the contribution of the concrete shows variations in both stress and deformation limits. Preloading therefore affects ductility, resulting in a reduction of the latter, because of a higher stress degradation in softening branch (Fig. 5.15).

In Fig. 5.16 the experimentally observed capacities versus the preload levels are proved by showing the increasing strength factor k(np), defined as the ratio between the capacity of the strengthened specimens and the capacity of the not reinforced specimens, versus the applied preload level index np.

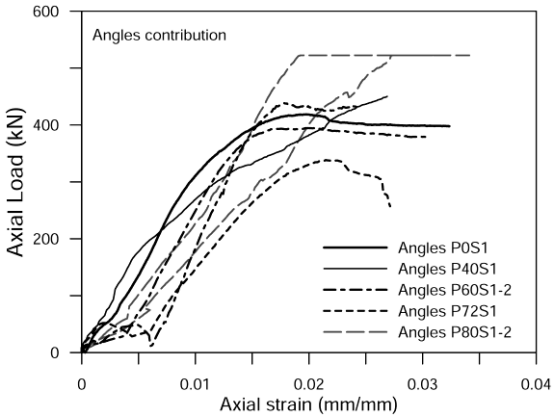

Figure 5.14. Load-strain response of the steel angles.

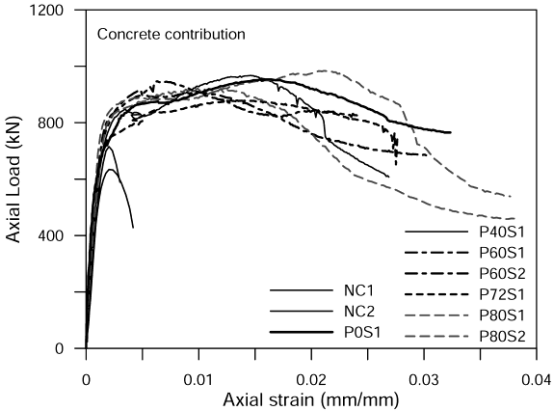

Figure 5.15. Load-strain curves of the confined concrete.

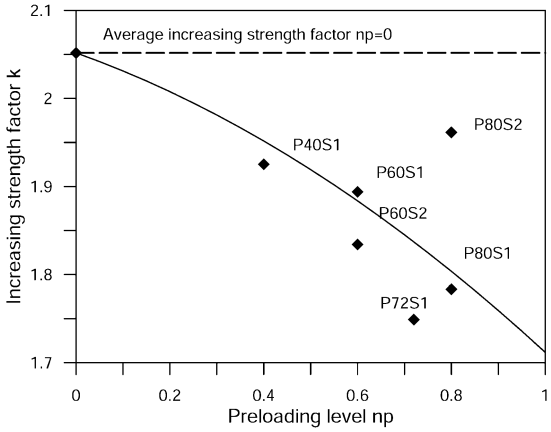

Figure 5.16. Increasing strength factor depending on the applied preload level.

5.4 Analytical model

The reproduction of the compressive behavior experimentally observed requires an accurate definition of the physical phenomenon. In fact, in the first phase in which the concrete columns -subjected to preload- reached the target preload level, a certain stress-strain state was exhibited. Subsequently, especially for substandard concrete type, creep strains occurred. After the reinforcement phase, the columns subjected to discharge (because of the transferring to the load testing machine) were affected by the loss of the Poisson effects except for residual deformations due to the cyclic behavior. Then, the specimens were re-loaded until collapse providing behavior of "plain concrete type" until the deformed configuration was reached at the moment of unloading and subsequently affected by the confinement phenomena.

The analytical model presented hereinafter is able to reproduce both the compressive behavior of confined concrete under standard conditions (monotonic response without preload) and the compressive behavior with preload. The cyclic behavior of the plain concrete is not considered in the model. On the other hand, the model is capable to account for the time-dependent effects when they are not negligible in the evaluation of the compressive response.

5.4.1 Stress-strain behavior of the confined concrete

The compressive response of concrete columns confined by steel jacketing reveals a "semi-active" confinement state of concrete. Differently from active or passive confinement, where confinement pressure is constant or variable throughout the load path, this kind of phenomenon is a hybrid situation between the two cases above mentioned. It is characterized by an elastic response in the early stages of loading, providing a variable confinement pressure by increasing the axial and lateral deformations of the confined concrete up to the achievement of the yielding of the steel, after which the confining pressure does not increase more (elasto-plastic behavior of the steel).

However, in the past, many studies assumed simplified hypothesis of active confinement based on the maximum contribution that the transverse steel is capable of conferring to the concrete. The axial stress-strain curve of the confined concrete was therefore connected to the steel mechanical limits[10]. This simplified assumption can be suitable to reproduce the behavior of concrete reinforced with internal reinforcements according to the classical approaches for assessing the strength and deformational capacity of RC sections without external reinforcement. The preloading further complicates the approach since in the first loading stages, until the stress/strain conditions related to the preloading are achieved, the concrete behavior is of a non-confined type and the hypothesis of active or passive confinement is not adequate, causing errors in the capacity evaluation as well as it was experimentally confirmed. These considerations necessitate the definition of an appropriate confinement model that can take into account all of the above-mentioned phenomena. The proposed approach is described below.

In the case of semi-active confinement, it is useful to consider the concrete response at every load steps characterizing the evolution of the confining pressures both in the elastic phase and after the yield of the steel.

As in the previous chapter, a relationship that links the trend of axial and lateral deformations depending on the confinement pressure is adopted

[10] The studies introducing this theory date back to the last century. Among the first important contributes there are Richart et al. (1928), Kent and Park (1971), Mander et al. (1988), Saatcioglu and Razvi (1992).

according to Teng et al. (2007). The original relationship proposed by the authors is reported below:

$$\varepsilon_c = 0.85\varepsilon_{c0}\left\{\left[\left(1+8\frac{f_l}{f_{c0}}\right)\left(1-0.75\left(\frac{-\varepsilon_l}{\varepsilon_{c0}}\right)\right)^{0.7} - \exp\left(-7\left(\frac{-\varepsilon_l}{\varepsilon_{c0}}\right)\right)\right]\right\} \quad (5.1)$$

in which ε_c is the axial strain of the concrete, ε_l is the lateral strain, ε_{c0} is the unconfined peak strain, and f_l is the current lateral confinement pressure provided by the confining device.

It should be noted that the relationship described above refers to the sectional behavior of circular columns, therefore, in the present study, an equivalent circular section according to the assumption made by various authors such as Hany et al. (2016), Pan et al. (2016a) is made. In this regard, equivalent diameter of the square cross-section was evaluated as:

$$D_e = \sqrt{2}b \quad (5.2)$$

with b being the side length of the square cross-section.

The lateral confinement pressure provided by the steel angles and battens can be determined according to the assumptions of Badalamenti et al. (2010), which consider a uniform equivalent confinement pressure acting on the confined concrete core. A brief description of the model to give an idea of the assumptions adopted by the authors and the way in which they treated the resolution of the problem is provided in the following.

For the determination of the stress state of a section confined with steel angles and plates, a plane stress model was assumed, with the subsequent simplification of a uni-dimensional elastic beam on elastic springs. The latter simulate the interaction between the steel and the confined core, while the angles are identified by rigid beams due to the higher inertia with respect to the battens (Fig. 5.17).

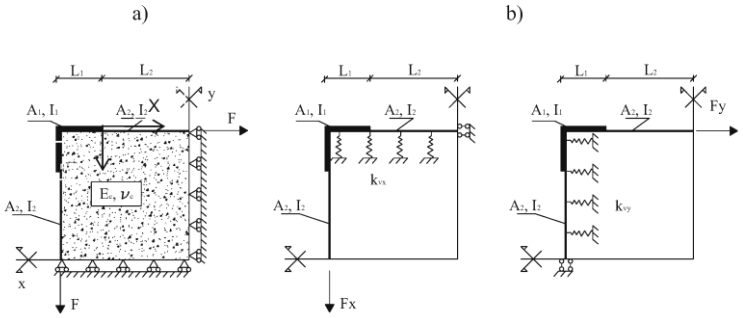

Figure 5.17. Plane stress model (a); beam model. (Badalamenti et al., 2010).

The problem involves the resolution of a differential equation of an elastic beam on elastic soil in a deformed configuration, calculating the uniform confinement pressure taking into account the discontinuity between two consecutive battens by means of an efficiency coefficient k_e. Moreover, it was considered that the confinement pressures exercised by the angles are accompanied by shear friction acting on the legs perpendicular to the beam on elastic springs parallel to the force F. This shear action can be assumed proportional to the confining pressure and to a frictional coefficient μ assumed equal to 0.5.

If the influence of the confinement pressure along the battens is negligible or absent (this assumption also reflects the configuration adopted in the experimentation discussed in the previous chapter characterized by no contact between battens and concrete), the expression for the evaluation of the force F is:

$$F = \frac{b \cdot \varepsilon_l}{(1+\mu)\left[\frac{1}{E_s}\left(\frac{L_1}{s_b \cdot t_1} + \frac{(b-L_1)}{s_2 \cdot t_2}\right) + \left(\frac{b(1-\nu)}{E_c \cdot L_1}\right)\right]} \exp\left(-1.5\frac{s_b}{b}\right) \qquad (5.3)$$

in which L_1 and t_1 are the side length and the thickness of the angles, s_2 is the width of the battens, E_s is the elastic modulus of the steel and s_b is the spacing considered between the center of two consecutive battens.

According to the uniform lateral confining pressure defined by Mander et al. (1988), referring to F value of Eq. 5.3, it can be assumed that:

$$f_l = \frac{2 \cdot F}{b \cdot s_b} \qquad (5.4)$$

obtaining therefore the lateral confining pressure provided by the steel jacket depending on steel angles and battens. Here, it is assumed that the lateral strain of the concrete is related to the axial strain by the Eq. 5.1 and the lateral confinement pressure (Eq. 5.3). Moreover, since the product of E_c by L_1 makes the ratio b(1-ν)/(E_c L_1) negligible compared to the other terms of the Eq. 5.3, finally the expression adopted for the confinement pressure is:

$$f_l = \frac{2 \cdot E_s \cdot \varepsilon_{l(\varepsilon_c, f_l)}}{(1+\mu)\left[\left(\frac{L_1}{t_1} + \frac{s_b(b-L_1)}{s_2 \cdot t_2}\right)\right]} \exp\left(-1.5\frac{s_b}{b}\right) \quad \leq f_{l,\max} \tag{5.5}$$

Taking ε_l as the lateral strain of the battens, the value of the lateral confinement pressure linearly increases up to the yielding of the steel, reaching therefore the maximum achievable value $f_{l,\max}$.

The solution requires an iterative procedure for the determination of ε_l depending on f_l for a given axial deformation. On the other hand, if the procedure is performed defining lateral strain increment, the solution is determined at each imposed ε_l, obtaining the axial strain in function of the current confining pressure.

For preloaded members, the concrete exhibits a certain stress-strain configuration. In terms of axial compression stress-strain curve, the first branch of the curve is characterized by the behavior of unconfined concrete until the preload level is reached. Then, the application of the confinement device implies the variation of the axial and lateral deformation as a function of the level of confinement pressure that is generated by continuing to give shortenings and therefore lateral expansions to the column. The confinement pressure, according to the compatibility conditions is therefore referred to an ε_{lp} determined by subsequent increments.

As for the case of confinement with FRP, by means of the Eq. 4.15 it is obtained the confinement pressure, that is:

$$f_l = \frac{2 \cdot E_s \cdot \varepsilon_{lp}}{(1+\mu)\left[\left(\frac{L_1}{t_1} + \frac{s_b(b-L_1)}{s_2 \cdot t_2}\right)\right]} \exp\left(-1.5\frac{s_b}{b}\right) \quad \leq f_{l,\max} \tag{5.6}$$

with:

$$\varepsilon_{lp} = \varepsilon_l - \varepsilon_l^* \tag{5.7}$$

imposing:

$$\varepsilon_{lp} = 0 \text{ if } \varepsilon_l - \varepsilon_l^* < 0 \tag{5.8}$$

$$\varepsilon_l^* = \varepsilon_{l,el}(np) + \varepsilon_{l,t}(np) \tag{5.9}$$

In Eq. 5.9, the terms $\varepsilon_{l,el}(np)$ $\varepsilon_{l,t}(np)$ refer to the instantaneous and the time-dependent lateral strain of concrete respectively.

Lateral strain-to-axial strain and confinement pressure with no time-dependent effects

A simplified estimation of the lateral strain $\varepsilon_{l,el}$ of the plain concrete can be done in function of the axial strain of the concrete at the moment of preloading ε_{cp} assuming the relationship of Kupfer (1969):

$$\varepsilon_l = \nu(\varepsilon_c) \cdot \varepsilon_{cp} \tag{5.10}$$

with:

$$\nu(\varepsilon_{cp}) = \nu_0 \left[1 + 1.38\left(\frac{\varepsilon_{cp}}{\varepsilon_{c0}}\right) - 5.36\left(\frac{\varepsilon_{cp}}{\varepsilon_{c0}}\right)^2 + 8.59\left(\frac{\varepsilon_{cp}}{\varepsilon_{c0}}\right)^3 \right] \tag{5.11}$$

in which ε_{c0} is the peak unconfined concrete strain, ν_0 is the initial Poisson coefficient (in absence of accurate evaluation, it can be assumed 0.2) and ε_{cp} is the axial strain of concrete at the target preload, evaluated with good approximation as:

$$\varepsilon_{cp} = \begin{cases} \dfrac{n_P f_{c0}}{E_c} & 0 < np \le 0.4 \\ \dfrac{n_P f_{c0}}{avg(E_c, E_{\text{sec}})} & 0.4 \le np \le 0.7 \\ \dfrac{n_P f_{c0}}{E_{\text{sec}}} & 0.7 \le np \le 1 \end{cases} \tag{5.12}$$

considering therefore the axial strain ε_{cp} as a linearly function of the longitudinal elastic modulus E_c of concrete if the preload force is 40% of f_{c0} (linear elastic branch), an average value between E_c and the secant modulus of concrete E_{sec} if the preload force is in the inelastic branch up to 70% of f_{c0}, as a linear function of E_{sec} for a preload between 70% of f_{c0} and f_{c0}.

Referring to the geometrical characteristics of the reinforced cross-section described in Figure 5.1 and to the mechanical properties of the concrete and of the reinforcement used to make the specimens (f_{c0}=16.75 MPa, ε_{c0}=0.002, f_{yb}=275 MPa), the behavior of concrete under active,

passive and semi-active confinement in terms of lateral strain-vs-axial strain relationships and lateral confining pressure-vs-axial strain was evaluated in the case of np=0.4, 0.6 and 0.8 (Fig. 5.18).

In the case of preload, the lateral confinement pressure starts at a certain value of axial strain. Then, the confinement pressure is variable up to the yielding of the steel. Lateral strains follow the lateral strain-vs-axial strain law that characterizes the unconfined concrete up to strain state produced by the preload, then it changes according to the elastic-confinement mechanisms up to the yielding of the steel; at this point, the relationship is equal to the curve of active confined concrete.

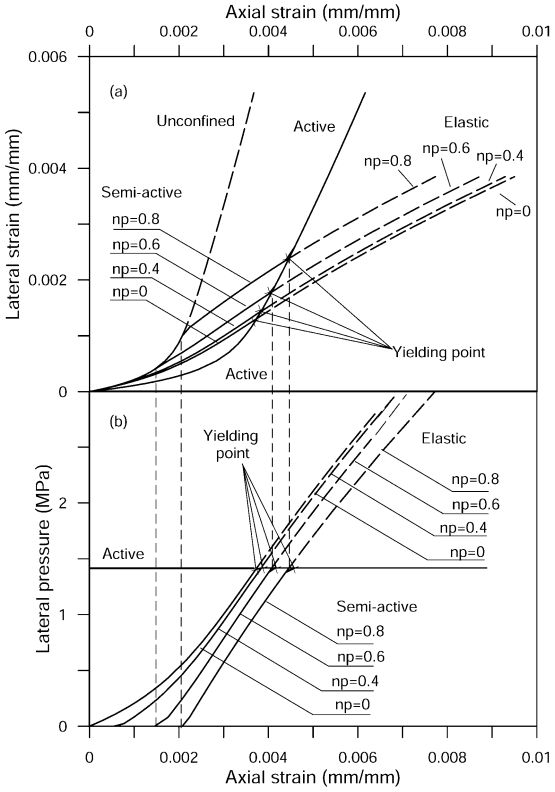

Figure 5.18. Lateral-vs-axial strain (a) and lateral confinement pressure-vs-axial strain (b) laws depending on the preload level np.

Simplified evaluation of the lateral strain of concrete considering time-dependent effects

A simplified evaluation of the lateral strain of concrete can be done starting from the axial strains at the end of the preload $\varepsilon_{cp,t}$. This one can be obtained as sum of the instantaneous strains $\varepsilon_{cp}(np)$ and the creep strain $\varepsilon_{cp}(np,t)$ according to the Eurocode 2 model:

$$\varepsilon_{cp,t} = \varepsilon_{cp}(np) + \varepsilon_{cp}(t, np) \tag{5.13}$$

Once the total axial strain $\varepsilon_{cp,t}$ is obtained, it can be assumed that an empirical estimation of the lateral strain $\varepsilon_{l,t}(np)$ can be obtained in function of the Poisson coefficient assumed in the elastic branch (ν_0=0.2). That is:

$$\varepsilon_{l,t}(np) = \nu_0 \cdot \varepsilon_{cp,t} \tag{5.14}$$

Axial stress-strain law of the confined concrete

Following the incremental procedure, for a given lateral strain as input value, the mechanical properties of the confined concrete can be easily determined considering the strength f_{cc}, the strain at peak stress ε_{cc}, the secant modulus E_{sec}, the compressive stress corresponding to the curve of passive-confined concrete $f_c(\varepsilon)$ before reaching yield stress of the battens, or corresponding to the curve of active confinement when the value of $f_{le,max}$ is reached.

The strength of the confined concrete $f_{cc,p}$ can be evaluated starting from the model of Eurocode 8 properly modified to take into account the effect of a preexisting load:

$$f_{cc,p} = f_{c0}\left[1 + 3.7\eta\left(\frac{f_{le}}{f_{c0}}\right)^{\frac{0.87}{\eta}}\right] \tag{5.15}$$

with η being the reduction coefficient depending on the preload ratio np. The following equation is here proposed based on a regression analysis:

$$\eta = 1 - \frac{f_{c0} \cdot np \cdot (0.165 + 0.034np)}{f_{cc(np=0)}} \quad 0 \le np \le 1 \tag{5.16}$$

The strain at peak stress ε_{cc} variable at each strain increment before reaching the yield stress of the battens and assuming constant value after $f_{le,max}$ is therefore:

$$\varepsilon_{cc} = \varepsilon_{c0} + 5\left(\frac{f_{cc,p}}{f_{c0}} - 1\right) \tag{5.17}$$

Finally, the axial stress-strain relationship of the confined concrete can be obtained according to Mander et al. (1988):

$$f_c(\varepsilon) = f_{cc,p} \frac{\frac{\varepsilon}{\varepsilon_{cc}} \cdot \gamma}{\gamma - 1 + \left(\frac{\varepsilon}{\varepsilon_{cc}}\right)^{\gamma}} \tag{5.18}$$

where γ is the shape factor evaluated as:

$$\gamma = \frac{E_c}{E_c - \frac{f_{cc,p}}{\varepsilon_{cc}}} \tag{5.19}$$

5.4.2 Contribution of the steel angles

To take into account tangential stresses along the contact surfaces between steel angles and concrete Mohr-Coulomb criterion was adopted according to the findings of Chapter 2, considering the frictional forces depending on the lateral confinement pressure. In detail, in section 2.2.2, it was considered that the interface mortar between steel angles and concrete provides a cohesive strength c_0 along the contact surface, and frictional forces are also developed and depend on the lateral confinement pressure f_{le} (exerted by the steel jacketing because of the core expansion) through the friction coefficient μ. Because of these tangential stresses between angles and concrete, the angles are able to carry vertical load P^*_a evaluable by equilibrium along the contact surface (Eq. 2.10). The maximum achievable value for P^*_a was related to the maximum tangential stresses τ_{max} (Eq. 2.7).

In this case, since no interface mortar was used, the Mohr-Coulomb criterion starts from the origin (no cohesive strength c_0) and follows linear relationship depending of the friction coefficient μ that, according to Badalamenti et al. (2010), is assumed 0.5. Moreover, the hypothesis that the lateral confinement pressure developed at the angles is affected by the maximum achievable value without considering the effectiveness coefficient factor (used to evaluate the effectively confined area for the concrete core in order to obtain the confined compressive strength) yields to replace the value $f_{le,max}$ with $f_{l,max}$.

Finally, the maximum normal stress f^*_y acting on the cross section of angles due to the friction is:

$$f_y^* = \frac{2 \cdot na \cdot l_1 \cdot l_0 \cdot \left(\mu \cdot f_{l,\max}\right)}{na \cdot t_1 \cdot \left(L_1 + l_1\right)} = \frac{l_1 \cdot l_0 \cdot f_{l,\max}}{t_1 \cdot \left(L_1 + l_1\right)} \tag{5.20}$$

in which n_a is the number of the angles, L_1 and l_1 are the external side and the internal side of the angles in contact with the concrete column respectively, l_0 is the overall vertical length along the columns and t_1 is the thickness of the angles.

Comparisons between experimental results and Mohr-Coulomb type law are provided in Fig. 5.19 in which it is highlighted that in the case of simple contact (without mortar between the angles and the column surfaces) the more suitable conditions are obtained considering the evolution of the tangential stresses depending on a coefficient of friction 0.5 only.

Moreover, differently from the experimental investigation in Chapter 2 in which the equivalent stress-strain law for the angles was proposed assigning equivalent stiffness at the interface between angles and concrete *Es**(1) (Eq. 2.6) on the basis of empirical observation of the global response, in this case the stress-strain law for the angles is directly provided by reading the strain gauges, being able to define a more reliable actual value of *Es**(2) as an average value of the all experimental tests. The differences of *Es** between the two cases can be attributed of course to the type of contact. Specifically, when the mortar is used at the interface between angles and concrete column, stress distribution is certainly more uniform and this means that the efficiency of the angles is better compared to the case of simple contact.

In Fig. 5.20 the differences between the nominal axial stress-strain law for the angles directly loaded are compared with the two equivalent axial stress-strain laws obtained from the two cases above described. Please note that the model proposed on Chapter 2 assumed cohesive stresses c_0 equal to 0.1 MPa and friction coefficient μ equal to 0.4. This involved a slightly lower equivalent yielding stress f_y* compared to the current model for a lateral confinement pressure $f_{l,max}$ evaluated by Badalamenti et al. (2010) rather than Montuori and Piluso (2009) model.

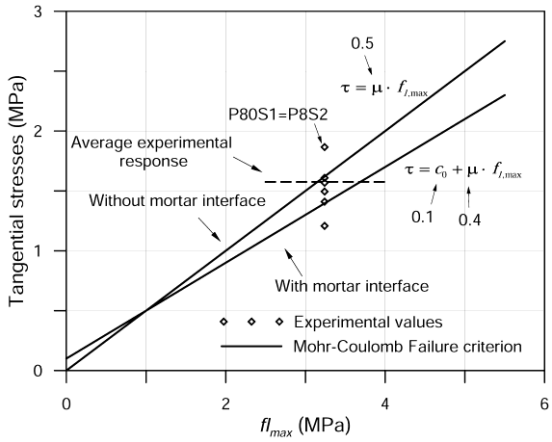

Figure 5.19. Comparisons between experimental results and Mohr-Coulomb model for the evaluation of frictional forces.

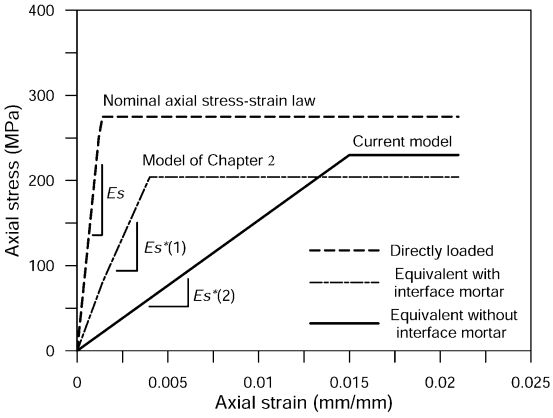

Figure 5.20. Behavior of angles depending on the type of connection and the type of interface with concrete columns.

5.4.3 Experimental-analytical comparisons

In this section, comparisons between experimental results and the proposed analytical model are provided (Figs. 5.21-25). For the above comparisons, the total axial load-axial strain response was obtained

considering the contribution of the steel angles added to the contribution of the confined concrete.

The compressive response is characterized by the reaching firstly of the peak stress for the confined concrete; after this point, the total axial load increases up to the maximum load capacity even if the concrete is in the post-peak branch because of the contribute of the angles in the linear hardening branch. The total maximum load is reached therefore when the angles exhibit the bearing capacity corresponding to the limit friction load. Then the softening occurs as a result of the softening of the concrete associated to the constant contribute of the angles.

In the case of preload, the total axial compressive response is characterized by a lower secant stiffness because of the lower lateral confinement pressure coupled to the axial strains, followed by a lower load contribution of the angles due to their delayed activation.

The model well predict the compressive response compared to the experimental results, showing that for low preload levels, as in the case of P40S1 specimen, no particular reduction in strength are observed respect to the case without preload. Some small inconsistency could be due to the evaluation of the concrete contribute experimentally determined from the total axial load-axial strain curve because of the non-perfect acquisition of the strain gauges and consequently the reproduction of the single contribution (the concrete contribution is obtained subtracting the angles contribution, derived by the strain gauge, to the total reacting axial force).

As the preload level increases the reduction in the global response becomes higher. due to the lower load contribute of the concrete and the delayed activation of the angles response. This fact is more evident in the case of higher preload as for P72S1, P80S1 and P80S2.

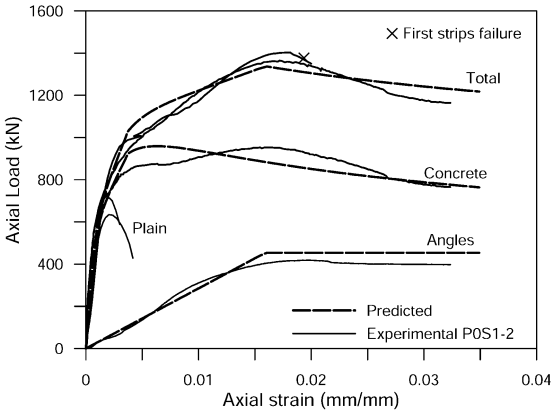

Figure 5.21. Experimental-analytical comparisons for specimens P0S1 and P0S2.

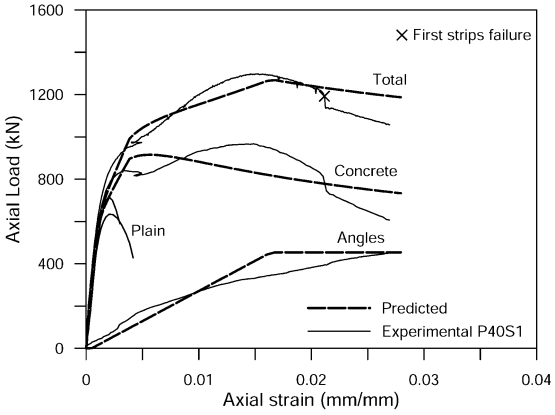

Figure 5.22. Experimental-analytical comparisons for specimen P40S1.

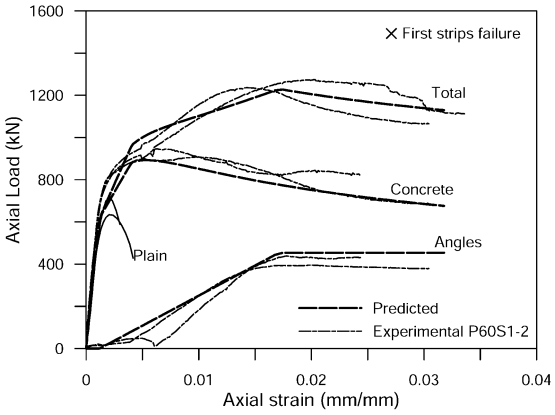

Figure 5.23. Experimental-analytical comparisons for specimens P60S1 and P60S2.

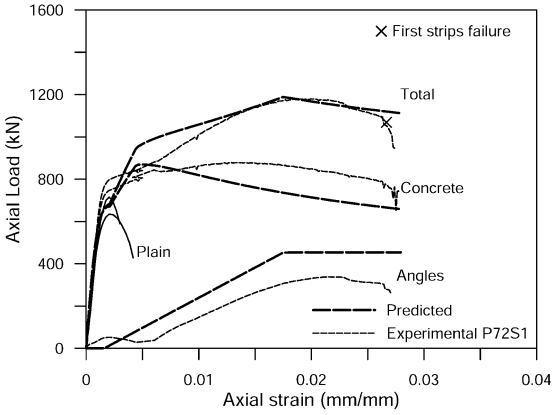

Figure 5.24. Experimental-analytical comparisons for specimen P72S1.

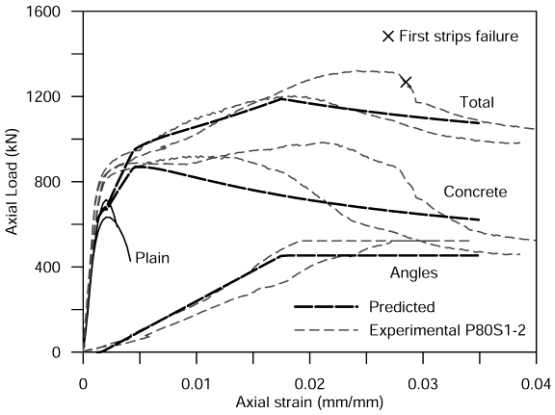

Figure 5.25. Experimental-analytical comparisons for specimens P80S1 and P80S2.

CONCLUSIONS

The present thesis has been aimed to the evaluation of the compressive behavior of externally reinforced concrete columns with two of the most currently used reinforcing devices, that are Steel Jacketing and FRP Wrapping. The reason has been that, although the mechanical behavior of these systems has been widely analyzed by "local approaches", i.e. by the definition of sectional models, the structural behavior of members externally reinforced under service conditions has not been so investigated.

The capacity assessment, that has been one of the primary goals of this thesis, has started therefore by considering new variables within the structural problems by an analysis approach that can be considered as transitional from the "local" to the "global" behavior. In this regard, depending on the type of reinforcement system, different considerations have been done to assess the structural behavior after strengthening.

Firstly, the issue of the load-bearing capacity of RC columns strengthened with steel jacketing under compressive loads have been experimentally investigated focusing also the type of mechanical end-connections of the steel angles. The experimental tests have proved that the assumption provided by the current Technical Codes to neglect the contribution of the steel angles in the load capacity is too conservative. Therefore, numerical and analytical models have been developed to adequately reproduce the behavior experimentally observed. The reasons behind the theoretical assumptions have been explained and discussed.

Subsequently, attention has been focused on the effect of the service loads acting on the columns of buildings while strengthened with external confinement devices. On this issue it has noticed that there are very few studies, both experimental and numerical. In addition, the few available studies concern only the confinement with FRP and all the conclusions pointed out by the authors are frequently in disagreement. In details, some authors state that the effect of preexisting loads is positive, others assess that the preload affects negatively the response in compression of a FRP wrapped member, while others state that preexisting loads are not influent.

As regards to the steel jacketing, it has been noticed the total absence of scientific sources (both experimental and theoretical) facing the case of reinforcing of columns while axially loaded.

This certainly entails confusion for the practical application when instead it would be important to have a solid basis and adequate design recommendations.

In order to try to fill this lack of knowledge, a preliminary numerical approach has been suggested using the Simulia Abaqus software. Two numerical models of concrete columns externally confined with steel jacketing and FRP have been proposed to reproduce the compression response simulating a loading before reinforcement. The compression responses have been then compared to that obtained from the classical approaches not providing, for simplicity, a load acting at the time of the reinforcement.

It has been noticed that, in the case of circular columns wrapped with FRP exhibiting compression strain-hardening behavior, there has been no reduction in the member capacity in presence of preload, while the stress-strain behavior has been characterized by a reduction of the secant stiffness, which has been more evident for higher levels of preload. In the case of FRP-wrapped concrete columns exhibiting a strain-hardening behavior up to the collapse, corresponding to the reaching of the ultimate strain of the FRP textiles, the lateral confinement pressure at collapse does not change varying the level of preload. Consequently, the corresponding strength of the columns have not appeared to undergo variations.

On the contrary, in the case of reinforcement with steel jacketing (producing an elasto-plastic confinement mechanism), by reproducing the compression response of square columns that presented a strain-softening behavior it has emerged that the results may be different. As the preload level has increased, there has also been a reduction in the strength of the confined concrete, accompanied by a reduction in the secant stiffness of the stress-strain curves.

Regarding compressive behavior of preloaded FRP-confined concrete an experimental investigation has been carried out in the laboratory of structures of the Technical University of Munich (DE). The experimental results have been followed the proposal of a numerical modeling approach able to predict both stress-strain response and compressive strength. On the basis of the numerical and experimental observations, a simplified analytical

model has been then proposed for a quick prediction of the capacity of a FRP wrapped column including the effects of preload.

The compressive behavior of columns subjected to preloading and reinforced by steel jacketing has been experimentally observed at the Palermo University laboratory. The experimental campaign has been carried out with the same principles of that carried out on specimens reinforced with FRP. The compression response has been characterized by a reduction in load-bearing capacity increasing when the level of preload increased. As for the case of FRP wrapping, the delay in the activation of the confining device causes a reduction in the lateral confinement pressure at a given load step, reducing also the maximum capacity. The reduction of the load-bearing capacity has been due to the type of the compressive response, that, differing from the case of FRP wrapping, has been characterized by strain-softening behavior.

In this case, it has been also noticed that for substandard concretes with low strength, such as that used for the experimental campaign, the effects of creep are not negligible especially when high levels of preload are considered and they must be included in the assessment of load-bearing capacity.

Finally, on the basis of the experimental observations, an analytical model has been proposed for the reproduction of the compressive behavior of the confined columns in both cases with and without preload considering also time-dependent effects.

The current findings discussed in this thesis strongly encourage a future in-depth development of this kind of approach to properly account the service conditions of structural elements when subjected to reinforcement.

REFERENCES

Aire, C., Gettu, R., Casas, J.R. (2001) "Study of the compressive behavior of concrete confined by fiber reinforced composites." *Proceedings of the International Conference on Composites in Constructions*, 10th-12th October 2001. Balkema Publishers, Porto, Portugal, Proceedings CCC2001, 239-243.

ACI Committee 440. (2002). "Guide for the design and construction of externally bonded FRP systems for strengthening of concrete structures." *ACI 440.2R-02*. Detroit, Michigan.

Adam, J.M., Ivorra, S., Giménez, E., Moragues, J.J., Miguel, P., Miragal, C., Calderón, P.A. (2007). "Behaviour of axially loaded RC columns strengthened by steel angles and strips." *Steel. Compos. Struct.*, 7(5), 405-419.

Albanesi, T., Nuti, C., Vanzi, I. (2007). "Closed form constitutive relationship for concrete filled FRP tubes under compression." *Constr. Build. Mater.*, 21(2), 409-427.

Adam, J.M., Ivorra, S., Pallarès, F.J., Giménez, E., Calderón, P.A. (2009). "Axially loaded RC columns strengthened by steel caging: Finite element modelling." *Constr. Build. Mater*., 23(6), 2265-2276.

Al-Salloum, Y.A., Elsanadedy, H.M., Alsayed, S.H., Iqbal, R.A. (2012). "Experimental and numerical study for the shear strengthening of reinforced concrete beams using textile-reinforced mortar." *J. Compos. Constr*., 16(1), 74-90.

Baltay, P., Gielsvik, A. (1990). "Coefficient of friction for steel on concrete at high normal stress." *J. Mater. Civ. Eng.*, 2(1), 46-49.

Binici, B. (2005). "An analytical model for stress–strain behavior of confined concrete." *Eng. Struct*., 27(7), 1040-1051.

Braga, F., Gigliotti, M. (2006). "Analytical stress-strain relationship for concrete confined by steel stirrups and/or FRP jackets." *J. Struct. Eng. ASCE*, 132(9), 1402-1416.

Badalamenti, V., Campione, G., Mangiavillano, M.L. (2010). "Simplified Model for Compressive Behaviour of Concrete Columns Strengthened with Steel Angles and Strips." *J. Eng. Mech. ASCE*, 136(2), 230-238.

Belal, F.M., Mohamed, H.M., Morad, S.A. (2015). "Behavior of reinforced concrete columns strengthened by steel jacket." *HBRC J.*, 11(2), 201-212.

Campione, G., Miraglia, N., Scibilia, N. (2001). "Comportamento in compressione di elementi in calcestruzzo armato a sezione quadrata e circolare rinforzati con FRP." *Ingegneria Sismica*, 2, 5-12.

Cirtek, L. (2001). "RC columns strengthened with bandage – experimental program and design recommendations." *Constr. Build. Mater.*, 15(8), 341-349.

Cole, C., Belarbi, A. (2001). "Confinement Characteristics of Rectangular FRP-Jacketed RC Columns." *Proceedings of the 5th International Symposium on Fiber Reinforced Polymer for Reinforced Concrete Structures* (FRPRCS-5), 16th-18th July, Cambridge, UK, 823-832.

Chun, S.S., Park, H.C. (2002). "Load Carrying Capacity and Ductility of RC Columns Confined by Carbon Fiber Reinforced Polymer." *Proceedings of the 3th International Conference on Composites in Infrastructure-ICCI*, 10th-12th June. San Francisco, CA, USA, in CD-Rom format.

CEN (European Committee for Standardization). (2004). "Design of concrete structures - Part 1-1: General rules for buildings." *Eurocode 2 EN 1992-1-1*, Brussels, Belgium.

CEN (European Committee for Standardization). (2004). "Design of structures for earthquake resistance – Part 1: General rules, seismic actions and rules for buildings." *Eurocode 8*, Brussels, Belgium.

CNR (Council of National Research). (2004). "Guide for the Design and Construction of Externally Bonded FRP Systems for Strengthening Existing Structures." *CNR-DT 200*. Roma, Italy.

CEN (European Committee for Standardization). (2005a). "Design of composite steel and concrete structures - Part 1: General rules for buildings." *Eurocode 4*, Brussels, Belgium.

CEN (European Committee for Standardization). (2005). "Design of structures for earthquake resistance – Part 3: Assessment and retrofitting of buildings." *Eurocode 8 EN 1998-3*, Brussels, Belgium.

Ciupala, M.A., Pilakoutas, K., Mortazavi, A.A. (2007). "Effectiveness of FRP composites in confined concrete." *Proceedings of the 8th International Symposium on Fiber Reinforced Polymer Reinforcement for Concrete Structures*. Patras, Greece, University of Patras.

Chakrabarti, A., Chandra, A., Bharagava, P. (2008). "Finite Element Analysis of Concrete Columns Confined with FRP Sheets." *J. Reinf. Plastics. Compos.*, 27(12), 1349-1373.

Calderón, P.A., Adam, J.M., Ivorra, S., Pallarès, F.J., Giménez, E. (2009). "Design strength of axially loaded RC columns strengthened by steel caging." *Mater. Des.*, 30(10), 4069-4080.

Campione (2012). "Load carrying capacity of RC compressed columns strengthened with steel angles and strips." *Eng. Struct.*, 40, 457-465.

Csuka, B., Kollár, L.P. (2012). "Analysis of FRP confined columns under eccentric loading." *Compos. Struct.*, 94(3), 1106-1116.

Campione (2013). "RC Columns Strengthened with Steel Angles and Battens: Experimental Results and Design Procedure." *Practice Periodical Struct. Des. Constr.* ASCE, 18(1), 1-11.

De Lorenzis, L., Tepfers, R. (2003). "A Comparative Study of Models on Confinement of Concrete Cylinders with Fiber-Reinforced Polymer Composites." *J. Compos. Constr ASCE*, 7(3), 219-237.

Elwi, A.A., Murray, D.W. (1979). "A 3D hypoelastic concrete constitutive relationship." *J. Eng. Mech. Div. ASCE*, 105(4), 623–641.

Ersoy, U., Tankut, A.T., Suleiman, R. (1993). "Behavior of jacketed columns." *Struct. J. ACI*, 90(3), 288-293.

Fam, A.Z., Rizkalla, S.H. (2001). "Behavior of axially loaded concrete-filled circular fiber-reinforced polymer tubes." *Struct. J.*, 98(3), 280-289.

Feng, P., Lu, X.Z., Ye, L.P. (2002). "Experimental research and finite element analysis of square concrete columns confined by FRP sheets under uniaxial compression." *Proceedings of the 17th Australasian Conference on*

the Mechanics of Structures and Materials (ACMSM17), 12th-14th June, Gold Coast, Australia, 71-76.

Gomes, A., Appleton, J. (1997). "Nonlinear cyclic stress-strain relationship of reinforcing bars including buckling." *Eng. Struct.*, 19(10), 822-826.

Gambarelli, S., Nisticò, N., Ozˇbolt, J. (2014). "Numerical analysis of compressed concrete columns confined with CFRP: Microplane-based approach." *Compos. B Eng.*, 67, 303-312.

Harmon, T.G., Ramakrishnan, S., Wang, E.H. (1998). "Confined concrete subjected to uniaxial monotonic loading." *J. Eng. Mech.*, 124(12), 1303-1309.

Harries, K.A., Kharel, G. (2002). "Behavior and modeling of concrete subject to variable confining pressure." *Mater. J.*, 99(2), 180-189.

Han, L.H., Yao, G.H., Tao, Z. (2007). "Performance of concrete-filled thin-walled steel tubes under pure torsion." *Thin Wall. Struct.*, 45(1), 24-36.

Hassan, M., Chaalal, O. (2007). "Fiber-reinforced polymer confined rectangular columns: assessment of models and design guidelines." *Struct. J.*, 104(6), 693-702.

He, Z., Jin, J.P., Song, J.G. (2009). "Experimental Study on the Expansion Ratio of Preloaded Circular Concrete Columns with CFRP Confinement." *Eng. Mech.*, 26(9), 145-151 (in Chinese).

He, Z., Shi, D. (2009). "Effect of Sustained Load on Static Lateral Responses of CFRP-Confined Columns." *Pacific Science Review*, 11(2), 144-149.

He, Z., Jin, J.P. (2011). "Axial Compressive Behavior of CFRP-Confined Concrete Columns Subject to Short-Term Preloading." *Adv. Mater. Res.*, 163-167, 3830-3837.

Hany, N.F., Hantouche, E.G., Harajli, M.H. (2016). "Finite element modeling of FRP-confined concrete using modified concrete damaged plasticity." *Eng. Struct.*, 125, 1-14.

Ilki, A., Kumbasar, N., Koc, V. (2002). "Behavior of damaged and undamaged concrete strengthened by carbon fiber composite sheets." *Struct. Eng. Mech.*, 13(1), 75-90.

Issa, C.A., Chami, P., Saad, G. (2009). "Compressive Strength of Concrete Cylinders with Variable Widths CFRP Wraps: Experimental Study and Numerical Modeling." *Constr. Build. Mater.*, 23(6), 2306-2318.

Ivorra, S., Estevan, L., Adam, J.M. (2013). "Experimental Study of Axial Stress-Strain Relationship of Cylindrical Concrete Elements Confined by CFRP under a Maintained Preload." In: L. Dezi, G. Marconi, R. Realfonzo (ed.) *2nd Workshop on "The new boundaries of structural concrete"*, 15th-16th September, 2011. Published by Ed. IMREADY, Ancona, Italy.

Jiang, T., Teng, J.G. (2007). "Analysis-oriented stress-strain models for FRP-confined concrete." *Eng. Struct.*, 29(11), 2968–2986.

Jiang, J.F., Wu, Y.F. (2012). "Identification of material parameters for Drucker–Prager plasticity model for FRP confined circular concrete columns." *Int. J. Solids Struct.*, 49(3-4), 445-456.

Kent, D.C., Park, R. (1971). "Flexural Members with Confined Concrete." *J. Struct. Div. ASCE*, 97(7), 1969-1990.

Karbhari, V.M., Gao, Y. (1997). "Composite jacketed concrete under uniaxial compression – verification of simple design equations." *J. Mater. Civ. Eng.*, 9(4),185-193.

Kshirsagar, S., Lopez-Anido, R.A., Gupta, R.K. (2000). "Environmental aging of fiber-reinforced polymer-wrapped concrete cylinders." *ACI Mater. J.*, 97(6), 703-712.

Karabinis, A.I., Rousakis, T.C. (2002). "Concrete confined by FRP material: a plasticity approach." *Eng. Struct.*, 24(7), 923-932.

Koksal, H.O., Doran, B., Turgay, T. (2009). "A practical approach for modeling FRP wrapped concrete columns." *Constr. Build. Mater.*, 23(3), 1429-1437.

Karthik, M.M., Mander, J.B. (2011). "Stress-Block parameters for unconfined and confined concrete based on a stress-strain model." *J. Struct. Eng. ASCE*, 137(2), 270-273.

Kupfer, H.B., Hilsdorf, H.D., Rusch, H. (1969). "Behavior of concrete under biaxial stresses." *ACI J.*, 659-666.

Lam, L., Teng, J.G. (2002c). "Strength Models for FRP-Confined Concrete." *J. Struct. Eng.*, 128(5), 612-623.

Lam, L., Teng, T.G. (2004). "Ultimate Condition of Fiber Reinforced Polymer-Confined Concrete", *J. Compos. Constr. ASCE*, 8, 539-548.

Lam, L., Teng, J.G., Cheung, C.H., Xiao, Y. (2006). "FRP-confined concrete under cyclic axial compression." *Cem. Concr. Compos.*, 28(10), 948–958.

Lim, J.C., Ozbakkaloglu, T. (2014). "Investigation of the Influence of the Application Path of Confining Pressure: Tests on Actively Confined and FRP-Confined Concretes." *J. Struct. Eng. ASCE*, 141(8), 04014203.

Lim, J.C., Ozbakkaloglu, T. (2015). "Lateral strain-to-axial strain relationship of confined concrete." *J. Struct. Eng. ASCE*, 141(5). DOI: 10.1061/(ASCE)ST.1943-541X.0001094.

Mander, J.B., Priestley, M.J., Park, R.N. (1988). "Theoretical Stress-Strain Model for Confined Concrete." *J. Struct. Eng. ASCE*, 114(8), 1804-1826.

Mirmiran, A., Shahawy, M., Samaan, M., El Echary, H. (1998). "Effect of Column Parameters on FRP-confined Concrete." *J. Compos. Constr.*, 2(4), 175-185.

McKenna, F., Fenves, G.L., Scott, M.H., Jeremic, B. (2000). "Open system for earthquake engineering simulation." Univ. of California, Berkeley, CA.

Mirmiran, A., Zagers, K., Yuan, W. (2000). "Nonlinear FE Modeling of Concrete Confined by Fiber Composites." *Finite Elem. Anal. Des.*, 35(1), 79-96.

Moran, D.A., Pantelides, C.P. (2002). "Stress-strain model for fiber-reinforced polymer-confined concrete." *J. Compos. Constr.*, 6(4), 233-240.

Malvar, L.J., Morrill, K.B., Crawford, J.E. (2004). "Numerical Modeling of Concrete Confined by Fiber-reinforced Composites." *J. Compos. Constr.*, 8(4), 315-322.

Montoya, E., Vecchio, F.J., Sheikh, S.A. (2004). "Numerical evaluation of the behaviour of steel- and FRP-confined concrete columns using compression field modeling." *Eng. Struct.*, 26(11), 1535-1545.

Monti, G., Nisticò, N. (2008). "Square and rectangular concrete columns confined by CFRP: Experimental and numerical investigation." *Mech. Compos. Mater.*, 44(3), 417-442.

Montuori, R., Piluso, V. (2009). "Reinforced concrete columns strengthened with angles and battens subjected to eccentric load." *Eng. Struct.*, 31(2), 539-550.

Morsy, A.M., El-Tony, M. (2012). "Repair of Pre-loaded R.C. Columns Using External CFRP Sheets and Embedded Longitudinal Steel Reinforcement." In: M.C. Forde (ed.) *14th International Conference Structural Faults and Repair*, 3rd-5th July. ECS Publications, Edinburgh, Scotland, UK.

Minafò, G. (2015). "A practical approach for the strength evaluation of RC columns reinforced with RC jackets." *Eng. Struct.*, 85, 162-169.

Ma, C.K, Apandi, N.M., Yung, S.C.S., Hau, N.J., Haur, L.W., Awang, A.Z., Omar, W. (2017). "Repair and rehabilitation of concrete structures using confinement: A review." *Constr. Build. Mater.*, 133, 502-515.

NTC. (2008). "Nuove Norme Tecniche per le Costruzioni." *D. M. II TT 14/01/2008*, Rome.

Nagaprasad, P., Sahoo, D.R., Rai, D.C. (2009). "Seismic strengthening of RC columns using external steel cage." *Earthquake Eng. Struct. Dyn.*, 38(4), 1563-1586.

Nisticò, N. (2014). "R.C. square sections confined by FRP: A numerical procedure for predicting stress–strain relationships." *Compos. B Eng.*, 59, 238-247.

Ozbakkaloglu, T., Lim, J.C., Vincent T. (2013). "FRP-confined concrete in circular sections: Review and assessment of stress–strain models." *Eng. Struct.*, 49, 1068-1088.

Popovics, S. (1973). "Numerical approach to complete stress-strain curve of concrete." *Cement and Concr. Res.*, 3(5), 583-599.

Parvin, A., Wang, W. (2001). "Behavior of FRP jacketed concrete columns under eccentric loading." *J. Compos. Constr.*, 5(3), 146-152.

Pessiki, S., Harries, K.A., Kestner, J.T., Sause, R., Ricles, J.M. (2001). "Axial behavior of reinforced concrete columns confined with FRP jackets." *J. Compos. Constr.*, 5(4), 237-245.

Pan, Y., Shuangyin, C., Denghu, J., Debao, C. (2009). "Test and analysis of the axial stress-strain relationship of square section concrete columns confined by CFRP under preload." *China Civ. Eng. J.*, 42(1), 23-29 (in Chinese).

Pan, Y., Shuangyin, C., Denghu, J., Zhao, S. (2011). "Experimental research on axially loaded circular concrete columns confined by CFRP under preload." *Adv. Mater. Res.*, 255-260, 694-698.

Pan, Y., Wan, L., Wu, X. (2015). "Analysis-Oriented Stress-Strain Model of CFRP Confined Concrete with Preload." *J. Southwest Jiaotong Univ.*, 50(3), 461-465 (in Chinese).

Pantazopoulou, S.J., Tastani, S.P., Thermou, G.E., Triantafillou, T., Monti, G., Bournas, D., Guadagnini, M. (2016). "Background to the European seismic design provisions for retrofitting RC elements using FRP materials." *Struct. Concr.*, 17(2), 1994-219.

Pan, Y., Guo, R., Li, H., Tang, H., Huang, J. (2017a). "Analysis-oriented stress-strain model for FRP-confined concrete with preload." *Compos. Struct.*, 166, 57-67.

Pan, Y., Rui, G., Li, H., Tang, H., Xu, L. (2017b) "Study on stress-strain relation of concrete confined by CFRP under preload." *Eng. Struct.*, 143, 52-63.

Richart, F.E., Brandtzaeg, A., Brown, R.L. (1928). "A study of the failure of concrete under combined compressive stresses." *Bulletin no. 185*, 20th November. Engineering Experiment Station, Champaign, University of Illinois, Urbana, 26(12), 1-104.

Rochette, P., Labossiere, P. (2000). "Axial testing of rectangular column models confined with composites." *J. Compos. Constr.*, 4(3), 129-136.

Rousakis, T., Tepfers, R. (2001). "Experimental Investigation of Concrete Cylinders Confined by Carbon FRP Sheets, under Monotonic and Cyclic Axial Compressive Load." Chalmers University of Technology, Division of Building Technology, 44, 87.

Rousakis, T., You, C.S., De Lorenzis, L., Tamužs, V., Tepfers, R. (2003). "Concrete cylinders confined by CFRP sheets subjected to cyclic axial compressive load." *Proceedings of the 6th International Symposium on FRP Reinforcement for Concrete Structures* (FRPRCS-6), 8th-10th July, World Scientific Publishing Co., Singapore, 571-580.

Rousakis, T., Karabinis, A., Kiousis, P. (2007). "FRP-confined concrete members: Axial compression experiments and plasticity modelling." *Eng. Struct.*, 29(7), 1343-1353.

Rocca, S., Galati, N., Nanni, A. (2008). "Review of design guidelines for FRP confinement of reinforced concrete columns of noncircular cross sections." *J. Compos. Constr.*, 12(1), 80-92.

Realfonzo, R., Napoli, A. (2011). "Concrete confined by FRP systems: confinement efficiency and design strength models." *Compos. Part B: Eng.*, 42, 736-755.

Spoelstra, M.R., Monti, G. (1999). "FRP-confined concrete model." *J. Compos. Constr.*, 3(3), 143-150.

Shahawy, M., Mirmiran, A., Beitelman, T. (2000). "Tests and modeling of carbon-wrapped concrete columns." *Compos. B Eng.*, 31(6-7), 471-480.

Santarosa, D., Filho, A.C., Beber, A.J., Campagnolo, J.L. (2001). "Concrete columns confined with CFRP sheets." In: J. G. Teng (ed.) *Proceedings of the International Conference of FRP Composites in Civil Engineering*, 12th-15th December, Elsevier Science Ltd., Hong Kong, China, 301-308.

Shehata, I.A.E.M., Carneiro, L.A.V., Shehata, L.C.D. (2002). "Strength of short concrete columns confined with CFRP sheets." *Mater. Struct.*, 35(1), 50-58.

Shrive, P.L., Azarnejad, A., Tadros, G., McWhinnie, C., Shrive, N.G. (2003). "Strengthening of concrete columns with carbon fibre reinforced polymer wrap." *Can. J. Civil Eng.*, 30(3), 543-554.

Shi, D., He, Z. (2009). "Short-Term Axial Behavior of Preloaded Concrete Columns Strengthened with Fiber Reinforced Polymer Laminate." *Comput. Struct. Eng.*, 1089-1098.

Samani, A.K., Attard, M.M. (2012). "A stress-strain model for uniaxial and confined concrete under compression." Eng. Struct., 41, 335-349.

Song, X., Gu, X., Li, Y., Chen, T., Zhang, W. (2013). "Mechanical behavior of FRP-strengthened concrete columns subjected to concentric and eccentric compression loading." *J. Compos. Constr.*, 17(3), 336-346.

Shafei, E., Rahmdel, J.M. (2017). "Plasticity constitutive modeling of partially confined concrete with steel jacketing." *J. Civ. Eng. KSCE*, 21(7), 2738-2750.

Thériault, M., Neale, K.W. (2000). "Design equations for axially loaded reinforced concrete columns strengthened with fibre reinforced polymer wraps." *Can. J. Civil Eng*., 27(5), 1011-1020.

Toutanji, H., Deng, Y. (2001). "Performance of concrete columns strengthened with fiber reinforced polymer composite sheets." *Adv. Compos. Mater.*, 10(2-3), 159-168.

Tan, K.H. (2002). "Strength enhancement of rectangular reinforced concrete columns using fiber-reinforced polymer." *J. Compos. Constr*., 6(3), 175-183.

Tsai, K.C., Lin, M.L. (2002). "Experimental axial load carrying performance of rectangular RC building columns retrofitted by steel or CFRP jacketing." *Technical report, National centre for research on earthquake engineering.* National Taiwan University, Taiwan.

Teng, J.G., Huang, Y.L., Lam, L., Ye, L. (2007). "Theoretical model for fiber reinforced polymer-confined concrete." *J. Compos. Constr.*, 11(2), 201-210.

Takeuti, A.R., de Hanay, J.B., Mirmiam, A. (2008). "Preloaded RC columns strengthened with high-strength concrete jackets under uniaxial compression." *Mater. Struct.*, 41(7), 1251-1262.

Teng, J.G., Xiao, Q.G., Yu, T., Lam, L. (2010). "Three-dimensional finite element analysis of reinforced concrete columns with FRP and/or steel confinement." *Eng. Struct.*, 97, 15-28.

Tarabia, A.M., Albakry, H.F. (2014). "Strengthening of RC columns by steel angles and strips." *Alexandria Eng. J.*, 53(3), 615-626.

William, K.J., Warnke, E.P. (1975). "Constitutive model for the triaxial behaviour of concrete." *Proceedings of the International Association for Bridge and Structural Engineering* (IABSE Zurich, Switzerland), 17th-19th May 1974. "Concrete Structures Subjected to Triaxial Stresses", E-Periodica, ISMES, Bergamo, Italy, 19(III), 1-30.

Wang, Y.C., Restrepo, J.I. (2001). "Investigation of concentrically loaded reinforced concrete columns confined with glass fiber-reinforced polymer jackets." *Struct. J.*, 98(3), 377-385.

Wu, Y.F., Wang, L. (2009). "Unified strength model for square and circular concrete columns confined by external jacket." *J. Struct. Eng.*, 135(3), 253-261.

Wu, H.L., Wang, Y.F., Yu, L., Li, X. R. (2009). "Experimental and Computational Studies on High-Strength Concrete Circular Columns Confined by Aramid Fiber-Reinforced Polymer Sheets." *J. Compos. Constr.*, 13(2), 125-134.

Xiao, Y., Wu, H. (2000). "Compressive behavior of concrete confined by carbon fiber composite jackets." *J. Mater. Civ. Eng.*, 12(2), 139-146.

Xiao, Q., Teng, J.G., Yu, T. (2010). "Behavior and modeling of confined high-strength concrete." *J. Compos. Constr.*, 14(3), 249–259.

Yang, X., Nanni, A., Chen, G. (2001). "Effect of Corner Radius on Performance of Externally Bonded FRP Reinforcement." *Proceedings of the 5th Conference on Non-Metallic Reinforcement for Concrete Structures* (FRPRCS-5), 16th-18th July. Cambridge, UK, 197-204.

Yu, T., Teng, J.G., Wong, Y.L., Dong, S.L. (2010). "Finite element modeling of confined concrete-I: Drucker–Prager type plasticity model." *Eng. Struct.*, 32, 665-679.

Yu, T., Teng, J.G., Wong, Y.L., Dong, S.L. (2010). "Finite element modeling of confined concrete-II: Plastic-damage model." *Eng. Struct.*, 32, 680-691.

Yang, Y.F., Zhang, Z.C., Fu F. (2015). "Experimental and numerical study on square RACFST members under lateral impact loading." *J. Constr. Steel Res.*, 111, 43-56.

Zhang, S., Ye, L., Mai, Y.W. (2000). "A study on Polymer Composites Strengthening Systems for Concrete Columns." *Appl. Compos. Mater.*, 7(2), 125-138.